The timing of high temperature metamorphism at the Snaefell magnetite deposit, South Australia

Thesis submitted in accordance with the requirements of the University of Adelaide for an Honours Degree in Geology

Kelly Macdonald

November 2020

THE UNIVERSITY of ADELAIDE

THE TIMING OF HIGH TEMPERATURE METAMORPHISM AT THE SNAEFELL MAGNETITE DEPOSIT, SOUTH AUSTRALIA

RUNNING TITLE: METAMORPHISM AT THE SNAEFELL MAGNETITE DEPOSIT

ABSTRACT

Zircon and monazite geochronology and trace elemental analysis provide the first constraints on the timing of high temperature metamorphism at the Snaefell magnetite deposit in the northern Gawler Craton, South Australia. The granulite facies rocks which host mineralisation at the Snaefell magnetite deposit yield zircon ages of 1749 ± 15 Ma and 1673 ± 16 Ma, as well as monazite ages of 1670 – 1660 Ma, 1590 – 1580 Ma and 1559 ± 10 Ma. The data indicates that the host sediments have a protolithic age of ca. 1750 Ma, consistent with depositional ages in the adjacent Mount Woods Inlier. The metasediments were exposed to high temperature granulite facies metamorphic conditions during the period 1670 – 1660 Ma. These ages are previously unrecognised in the northern Gawler Craton may indicate that the ca. 1720 – 1690 Ma Kimban Orogeny had a prolonged effect on the region. A second metamorphic event is recorded between 1590 and 1580 Ma saw the development of E-W-NE trending folds and is attributed to the 1570 – 1540 Ma Kararan Orogeny. Late deformation at 1559 ± 10 Ma caused north-dipping shear zones to crosscut the granulites and is associated second generation garnet growth. Possible hydrothermal zircon may indicate that magnetite is also of a hydrothermal source.

KEYWORDS

Geochronology, metamorphism, Mesoproterozoic, high temperature, magnetite, Snaefell, Gawler Craton

TABLE OF CONTENTS

LIST OF FIGURES AND TABLES

INTRODUCTION

The Gawler Craton (Figure 1) is a large Precambrian terrain with a complex geological evolution and tectonic history spanning more than 1 billion years (Hand, Reid & Jagodzinski, 2007). It is becoming increasingly recognised that the Gawler Craton was once a part of the North Australian Craton and rifted south between ca. 1470 and 1100 Ma to its current configuration (Armit et al., 2017; Betts et al., 2015; Betts & Giles, 2006; Giles, Betts & Lister, 2004; Morrissey, Barovich, Hand, Howard & Payne, 2019). The widespread nature of these tectonic events mean that their timing and systematics have a continental-scale context.

Although it is well understood that the Gawler Craton has been subject to prolonged tectonism, the timing of many of these events is still poorly constrained for extensive regions of the Gawler Craton (Armit et al., 2017; Dutch, Hand & Kelsey, 2010; Forbes et al., 2011; Forbes et al., 2012; Fraser, Reid & Stern, 2012; Hand et al., 2007; Howard, Hand, Barovich, Payne & Belousova, 2011; Payne, Hand, Barovich & Wade, 2008). The main factor preventing thorough research from occurring is the paucity of outcrop. Large regions of the craton are characterised by no outcrop at all. Therefore, knowledge of the basement geochronology relies heavily upon drill hole sampling and extrapolation from regional geophysical techniques.

Since the Gawler Craton has significant metal endowment, understanding the temporal evolution of the Gawler Craton is important in providing a framework for mineral exploration. Many of the deposits in the Gawler Craton are in the style of Iron-Oxide-Cu-Au (IOCG), as well as significant deposits of Au, Fe, Cu, U and Pb-Zn-Ag, and are attributed to the ca. 1595 – 1575 Ma magmatic Hiltaba Event (Budd, Wyborn & Bastrakova, 2001; Daly, 1998). The idea that most of the deposits formed during the

Hiltaba Event has informed much of the mineral systems work performed in the Gawler Craton. Gaining a deeper understanding of when and how these different deposits form is one way of narrowing down the broad region of prospectivity which is the Gawler Craton.

Snaefell, in the northern Gawler Craton, is a significant magnetite deposit hosted by granulite facies rocks in the northern Gawler Craton, and is an example of a deposit which has a poorly understood geochronological framework. It is located proximal to large Fe-oxide deposits Cairn Hill and Prominent Hill which are believed to have formed as a result of hydrothermal activity or magmatism (Bowden et al., 2017; Clark, 2014; Reid, 2019; Schlegel, Wagner, Wälle & Heinrich, 2018). Other Fe-oxide deposits in the Gawler Craton include Archean banded iron formations (BIFs) in the central/southern Gawler Craton and the Warramboo magnetite deposit in the southern Gawler Craton which was upgraded by granulite facies metamorphism (Davies & Twining, 2018; Lane, Jagodzinski, Dutch, Reid & Hand, 2015; Morrissey, Hand, Lane, Kelsey & Dutch, 2016).

Presently there is little understood about the Snaefell deposit, including the source of magnetite and the timing of metamorphism. This makes it difficult to attribute its formation to other Fe-oxide systems in the Gawler Craton. By understanding the timing of ore-forming processes at Snaefell, the deposit can potentially be linked to major metamorphic events in the Gawler Craton. Such information could also help inform the wider metamorphic framework of the northern Gawler Craton.

This study uses LA-ICP-MS U-Pb monazite and zircon geochronology, as well as trace elemental analysis to constrain the age of the protoliths and the timing of metamorphism in the Snaefell magnetite deposit. The new geochronology will be discussed in the

context of known metamorphic ages from the Gawler Craton. Detailed petrography and geochronology are also used to discuss possible sources of magnetite in the Snaefell deposit. The results of this study suggest that protolithic ages are equivalent to adjacent Mount Woods Inlier metasediments, that magnetite predates deformation and that the host rocks were metamorphosed during a previously unrecognised late-Kimban period, as well as during the later Hiltaba Event and Kararan Orogeny.

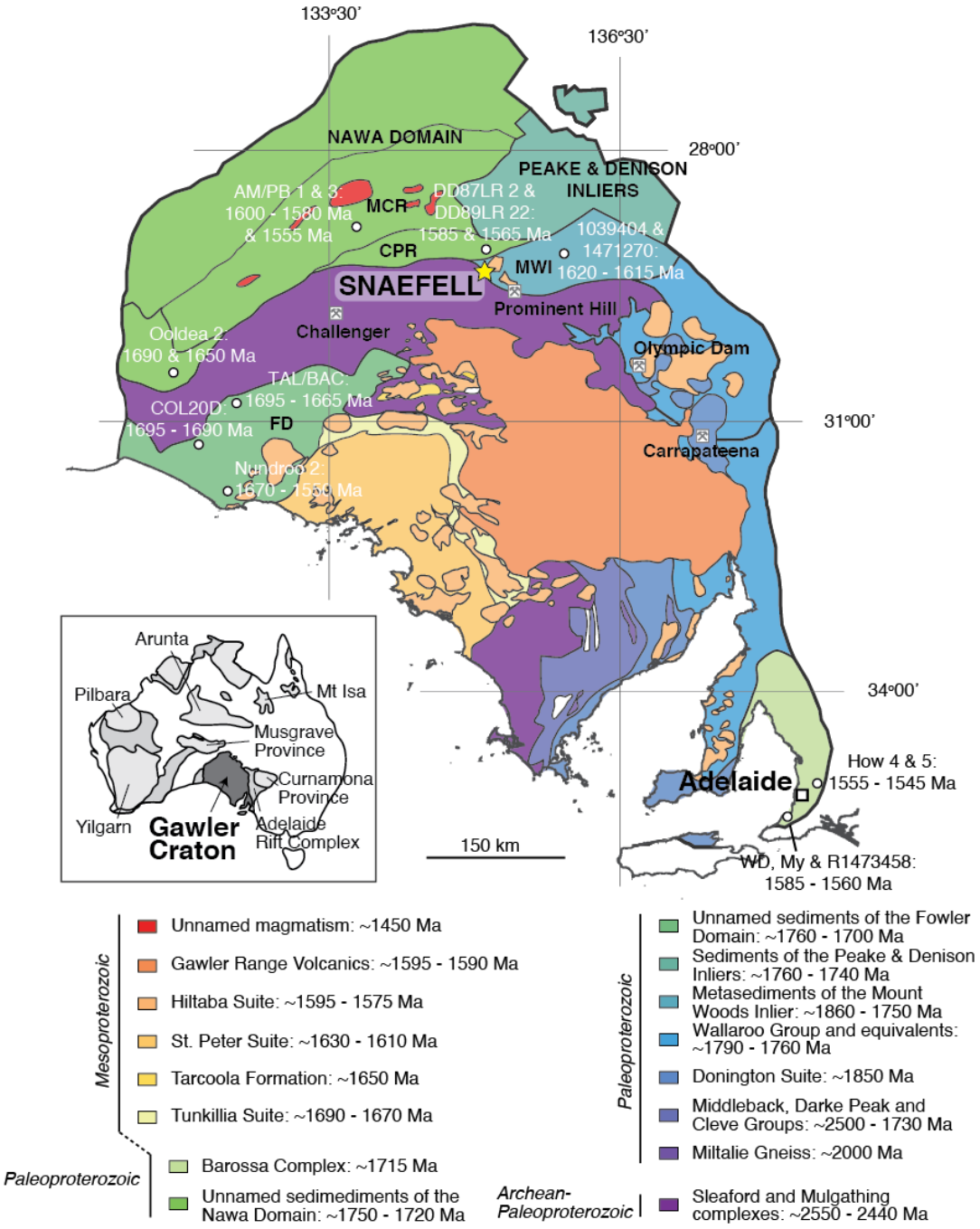

Figure 1: Geological map of the Gawler Craton. Snaefell (yellow star) is located in the northern Gawler Craton. Geological units are coloured by age. Major domains are labelled (MCR = Mabel Creek Ridge, CPR = Coober Pedy Ridge, MWI = Mount Woods Inlier and FD = Fowler Domain). Mines Prominent Hill, Challenger, Olympic Dam and Carrapateena are marked. White circles represent metamorphic zircon and monazite U-Pb geochronology from previous studies. Names of the samples and/or drill holes are provided for reference. Inset: Map of Australia, showing the location of the Gawler Craton. Geological map adapted from Hand et al. (2007). Geochronology from Cutts, Hand and Kelsey (2011); Forbes et al. (2011); Hand et al. (2007); Howard, Hand, Barovich, Payne and Belousova (2011); Howard, Hand, Barovich, Payne, Cutts, et al. (2011); Morrissey, Hand, Wade and Szpunar (2013); Payne et al. (2008); Reid, Halpin and Dutch (2019).

GEOLOGICAL BACKGROUND

Regional Geology of the Gawler Craton

The Gawler Craton constitutes a large portion of South Australia (Figure 1). Its long and complex geological evolution spans from the Mesoarchean to the Neoproterozoic (Hand et al., 2007; Reid & Hand, 2012). Its history involves rifting and the development of rift basins, interrupted by episodic orogenesis particularly on the eastern margin (Daly, 1998; Hand et al., 2007). The oldest rock package known to the Gawler Craton is a Mesoarchean (ca. 3150 Ma) granite (Fraser, McAvaney, Neumann, Szpunar & Reid, 2010).

During the late Archean (ca. 2560 – 2480 Ma), the Gawler Craton underwent syn-magmatic basin development (Hand et al., 2007; Reid, Jagodzinski, Fraser & Pawley, 2014). The Sleaford Complex (preserved in the southern Gawler Craton) and the Mulgathing Complex (preserved in the central western Gawler Craton) were formed during this time and are interpreted to be contiguous and underlie much of the Gawler Craton (Fanning, Reid & Teale, 2007; Reid, Jagodzinski, Fraser, et al., 2014; Swain et al., 2005). The Sleaford and the Mulgathing Complexes consist of aluminous metasediments, banded iron formations, carbonates, siliceous sediments and coeval volcanics (Daly, 1998; Drexel, Preiss & Parker, 1993). The volcanics are comprised of arc-like felsic and mafic to ultramafic successions, including ca. 2520 Ma komatiites, and are interpreted to have formed in an active subduction environment (Swain et al., 2005). From ca. 2520 to 2500 Ma the sedimentary successions were intruded by a series of arc-related magmas (Daly, 1998; Swain et al., 2005). Presence of a similarly aged (ca. 2525 Ma) magmatic gneiss in the northern Gawler Craton suggests that magmatism

of this time was more extensive than previously thought (Reid, Jagodzinski, Armit, et al., 2014).

During the earliest parts of the Paleoproterozoic (ca. 2480 – 2420 Ma), the southern Gawler Craton records metamorphism up to granulite facies, at conditions of 850°C and 5 – 7 kbar, during the Sleafordian Orogeny (Dutch et al., 2010; Halpin & Reid, 2016; Teasdale, 1997). There is a lack of evidence for geological events between 2400 – 2000 Ma, which has been interpreted to mean that the Sleafordian Orogeny was an intracontinental event (Halpin & Reid, 2016).

Magmatism is recorded at ca. 2000 Ma by the Miltalie Event. The resulting granodioritic Miltalie Gneiss crops out in the south-eastern Gawler Craton (Hand et al., 2007). Another orthogneiss, at ca. 1920 Ma, was also recently recognised in the Gawler Craton. It is proposed that this basement rock could be linked with similar events occurring in the Musgrave Province and Rudall Province of central-western Australia (Reid, Jagodzinski, Armit, et al., 2014).

Deposition of rift basin sediments occurred between ca. 2500 and 1690 Ma. These sediments include the ca. 2500 Ma Middleback and ca. 1865 – 1730 Ma Darke Peak and Cleve Groups (formerly the Hutchison Group) in the southern Gawler Craton (Daly, 1998; Ferris, Schwarz & Heithersay, 2002; Hand et al., 2007; Szpunar, Hand, Barovich, Jagodzinski & Belousova, 2011). Also of a similar age are unnamed sediments in the Nawa Domain (northern Gawler Craton) and Fowler Domain (western Gawler Craton), as well as the Skylark metasediments of the Mount Woods Inlier.

Coeval with sedimentation was a period of orogenesis (the Cornian Orogeny; Reid, Hand, Jagodzinski, Kelsey & Pearson, 2008) and bimodal magmatism of the ca. 1850 Ma Donington Suite in the eastern Gawler Craton (Daly, 1998; Reid, Curtis & Fraser,

2008). This event reached granulite facies conditions of 750°C and 6 kbar (Reid, Hand, et al., 2008).

Sedimentation at ca. 1760 – 1700 Ma is found in the Nawa Domain (Payne et al., 2008; Reid et al., 2019), Fowler Domain (Howard, Hand, Barovich, Payne, Cutts, et al., 2011), Mount Woods Inlier and Peake and Denison Inliers (Fanning, Flint, Parker, Ludwig & Blissett, 1988), as well as various locations in the southern Gawler Craton (Fanning et al., 1988; Jagodzinski, 2005).

From ca. 1730 to 1690 Ma, the Gawler Craton experienced magmatism, deformation and metamorphism in an event known as the Kimban Orogeny. Although magmatism of this age is well recognised throughout the Gawler Craton, metamorphism and deformation are only constrained in the south-east and sporadically in the north. In the south-eastern Gawler Craton, peak metamorphic conditions are documented at 800 – 850°C and 7 – 9 kbar (Drexel et al., 1993; Dutch et al., 2010; Morrissey et al., 2016; Tong, Wilson & Vassallo, 2004), and deformation is recorded by rocks within and surrounding the exposed Kalinjala Shear Zone (Vassallo & Wilson, 2002). Elsewhere in the Gawler Craton, the effects of the Kimban Orogeny are less understood. The northern Gawler Craton records upper amphibolite to granulite facies conditions, including crustal anatexis, between 1730 and 1690 Ma (Armit et al., 2017; Howard, Hand, Barovich, Payne, Cutts, et al., 2011; Payne et al., 2008; Reid et al., 2019). In the western Gawler Craton, granulite facies conditions are preserved in rocks with slightly younger metamorphic ages, at ca. 1690 – 1670 Ma (Howard, Hand, Barovich, Payne & Belousova, 2011). The ca. 1690 – 1670 Ma Tunkillia Suite is recognised in the central and western Gawler Craton, and interpreted as ‘late- to post-tectonic’ magmatism derived from the Kimban Orogeny (Payne, Ferris, Barovich & Hand, 2010).

Over the period ca. 1690 – 1665 Ma, the western Gawler Craton was subject to a high geothermal gradient and high temperature granulite facies conditions during the Ooldean Event (Cutts, Kelsey & Hand, 2013; Hand et al., 2007; Teasdale, 1997). High temperature metamorphism during the Ooldean Event was coeval with deposition of the ca. 1650 Ma Tarcoola Formation preserved in the central Gawler Craton. The Tarcoola Formation contains fluvial to marine sediments including clastic units, dolomites and carbonaceous shales, as well as volcanic tuffs (Budd, 2006; Daly, 1998; Howard, Hand, Barovich & Belousova, 2011).

Magmatism of the ca. 1630 – 1610 Ma St Peter Suite appears in the south-western to central Gawler Craton and is attributed to a continental magmatic arc setting (Reid et al., 2020).

The ca. 1595 – 1575 Ma Hiltaba magmatic suite and related ca. 1595 – 1590 Ma Gawler Range Volcanics are widespread throughout the Gawler Craton. The Hiltaba magmatic event is credited for regional IOCG-style mineralisation in the eastern Gawler Craton, and significant Au mineralisation in the central Gawler Craton (Belperio, Flint & Freeman, 2007; Bowden et al., 2017; Daly, 1998; Ferris et al., 2002; Reid, 2019; Schlegel et al., 2018; Skirrow et al., 2007; Tunnadine, 2017).

Metamorphism coeval with magmatism during the interval 1600 – 1550 Ma is observed in the northern and south-eastern Gawler Craton. Ultrahigh temperature metamorphism at conditions of 925°C and 6.5 kbar were achieved at ca. 1590 Ma in the Coober Pedy and Mabel Creek Domains of the northern Gawler Craton (Cutts et al., 2011), as well as conditions of 800°C and 7 kbar in the western Gawler Craton (Reid et al., 2019). The Mount Woods Inlier records conditions of 750°C and 5 kbar (Forbes et al., 2011). In the Barossa Complex in the south-eastern Gawler Craton, peak metamorphism at 1600 –

1550 Ma occurred at conditions of 850°C and 7 kbar (Morrissey et al., 2013). In a recent study, it is proposed that a metamorphic core complex developed in the Mount Woods Inlier over the period ca. 1600 – 1580 Ma (Tiddy et al., 2020). During this time, extensive deformation and fault reactivation occurred throughout in the Gawler Craton (Hand et al., 2007). In the nearby Curnamona Province of southern Australia, the Olarian Orogeny records compressional deformation of a similar age (Fricke, Preiss & Neumann, 2010; Rutherford, Hand & Barovich, 2007), and thus observations from the Gawler Craton and Curnamona Province suggest that there may be one large-scale overriding tectonic system (Hand et al., 2007; Payne et al., 2008).

The Kararan Orogeny, ca. 1570 – 1540 Ma (Hand et al., 2007), is associated with widespread deformation and metamorphism in the western, central and northern Gawler Craton (Daly, 1998; Fanning et al., 2007; Teasdale, 1997). Spread of metamorphic ages suggests that the Kararan Orogeny may be a case of late deformation related to the Hiltaba Suite (Hand et al., 2007). In the western Gawler Craton, metamorphism of this age is represented by granulites and metapelites which reached peak conditions of 800°C and 10 kbar (Teasdale, 1997). Subsequent cooling of ~300°C is recorded in rocks of the northern Gawler Craton and is interpreted to be due to the termination of magmatism and exhumation across shear zones (Forbes et al., 2012; Tiddy et al., 2020).

The period ca. 1470 – 1450 Ma is characterised by large-scale reactivation of shear systems and cooling, as well as localised magmatism (Fraser & Lyons, 2006; Fraser et al., 2012; Hand et al., 2007; Morrissey et al., 2019). In the northern Gawler Craton, magmatism of this age is associated with a high geothermal gradient where metamorphism peaked at 750 – 850°C and 3 – 5.5 kbar (Morrissey et al., 2019). This is

interpreted as a period of rifting between Proterozoic Australia and supercontinent Laurentia (Morrissey et al., 2019).

Geology of the Mount Woods Inlier

Little is known about the geology of the Snaefell deposit. However, it is located adjacent to the Mount Woods Inlier (Figure 2), which has been the subject of a handful of studies. The basement geology of the Mount Woods Inlier is sparsely outcropping and consists of late Paleoproterozoic to early Mesoproterozoic sediments and intrusives. The Mount Woods Metamorphics and Skylark Metasediments yield maximum depositional ages of ca. 1860 Ma (Tiddy et al., 2020) and ca. 1750 Ma (Chalmers, 2007; Jagodzinski et al., 2007), respectively. The Coodnambana Metaconglomerate overlies the Skylark Metasediments but does not have a known protolith age.

Early metamorphism is recorded by the Skylark Metasediments, at 1736 ± 14 Ma (Daly, 1998; Fanning, 1993; Finlay, 1993), and attributed to the 1730 – 1690 Ma Kimban Orogeny (Daly, 1998; Fanning, 1993; Finlay, 1993). Kimban-aged deformation in the Mount Woods Inlier includes fold and foliation development, as well as movement along the north-dipping Southern Overthrust (Betts, Valenta & Finlay, 2003; Forbes et al., 2012; Harris, Murphy, Funk & Betts, 2013). At ca. 1692 Ma, the late-Kimban Engenina Adamellite intruded the Skylark Metasediments (Daly, 1998; Fanning, 1993; Finlay, 1993) and further deformation saw the thrusting of the western region of the Mount Woods Inlier over central and southern regions, across the Panorama Fault Zone (Betts et al., 2003). A younger metamorphic zircon age of 1641 ± 23 Ma is also reported for the Skylark Metasediments (Tiddy et al., 2020).

At ca. 1590 Ma, metamorphism and localised crustal anatexis in the Mount Woods Inlier are attributed to the emplacement of the ca. 1584 Ma Balta Granite (Chalmers,

2007; Daly, 1998; Finlay, 1993), a Hiltaba Suite equivalent (Creaser & Cooper, 1993; Daly, 1998; Fanning et al., 1988). Zircon rims within the Coodnambana Metaconglomerate yield a metamorphic age of ca. 1590 Ma (Chalmers, 2007; Holm, 2004; Jagodzinski, 2005; Jagodzinski et al., 2007; O'Sullivan, 2010) and conditions at this time are constrained at 750°C and 5 kbar (Forbes et al., 2011). Other metamorphic and magmatic ages of this time are recorded for the interval 1590 – 1580 Ma (Holm, 2004).

Cooling is recorded at ca. 1560 Ma in the Mount Woods Metamorphics (Tiddy et al., 2020) and ca. 1540 Ma in the younger Skylark Metasediments (Forbes et al., 2012; Tiddy et al., 2020), and is attributed to exhumation along the Southern Overthrust. Conversely, ages of ca. 1560 Ma obtained from monazites within the Coodnambana Metaconglomerate are interpreted as hydrothermal activity (O'Sullivan, 2010).

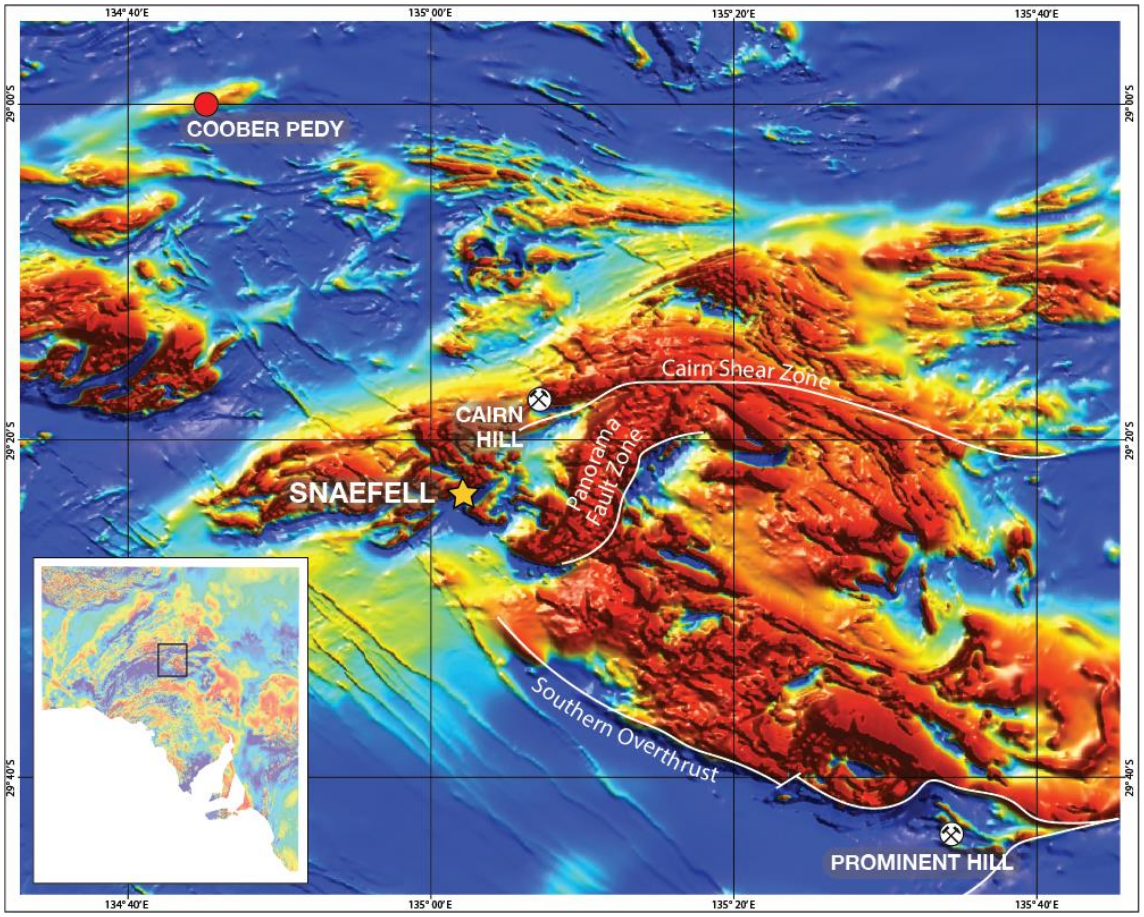

Figure 2: Total magnetic intensity (TMI) image of the Mount Woods Inlier. The large magnetic high (red) in the centre-east of the image is the Mount Woods Inlier. Snaefell is in the west of the Mount Woods Inlier. Other nearby deposits include Cairn Hill and Prominent Hill. Major faults, the Cairn Shear Zone, Panorama Fault Zone and the Southern Overthrust, are marked. Inset: TMI of South Australia showing location of the Mount Woods Inlier. Images after SARIG (2020) and faults obtained from Tiddy et al. (2020).

SAMPLE SELECTION AND PETROGRAPHY

The samples analysed in this study were selected from diamond drill holes SFD001 (Figure 3a) and SFD015 (Figure 3b) which are located in the centre and northeast of the Snaefell deposit, respectively. Precise locations of the drillholes and sample drillhole depths are provided in Appendix A.

The samples consist of a variety of granulite-facies gneisses. Four of the seven samples contain porphyroblastic garnet of one to two generations whereas the others do not contain garnet. Magnetite ± hematite is present in all samples with varying abundance. Petrographic descriptions are provided below for each sample.

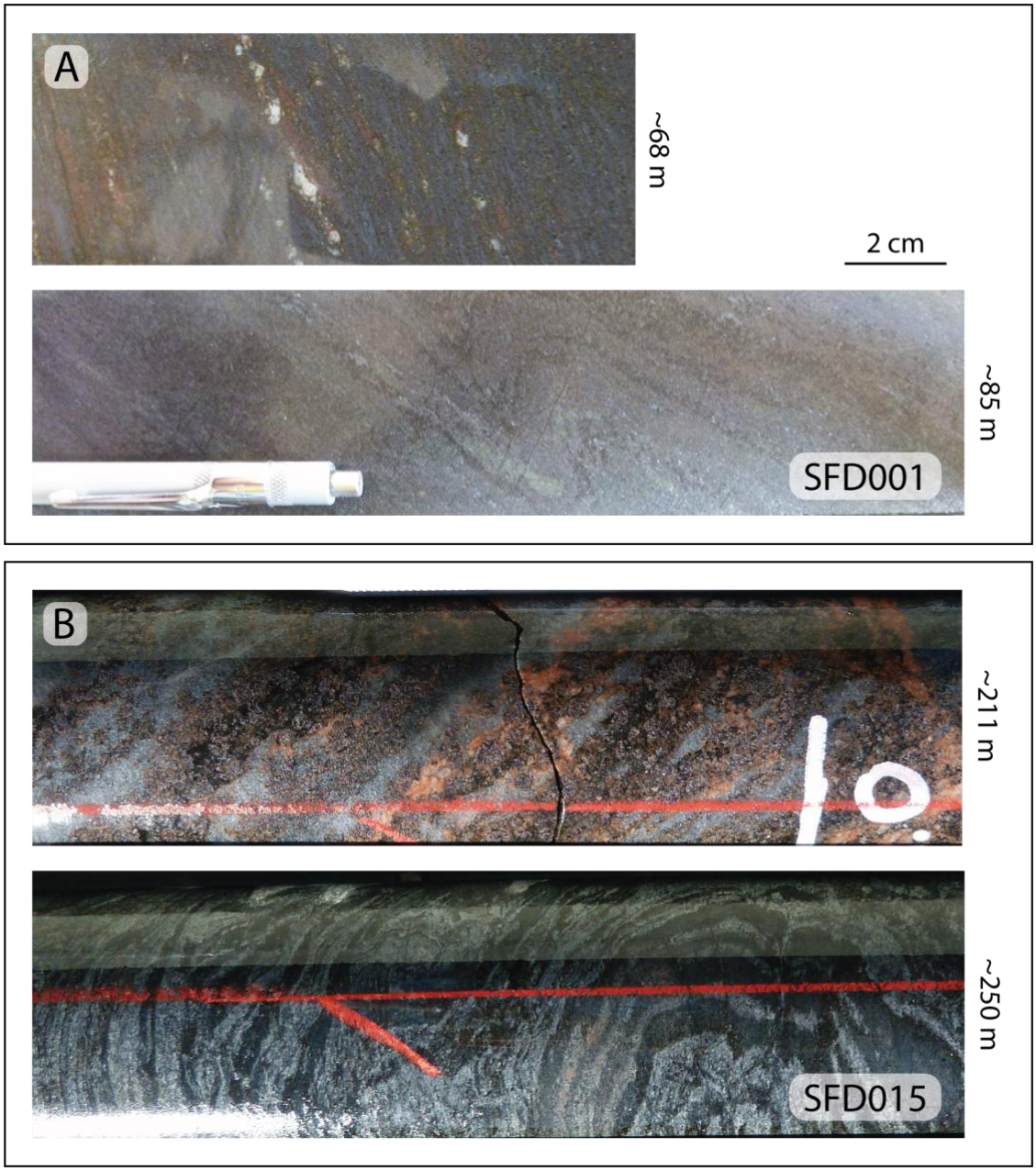

Figure 3: Images of core for drill holes SFD001 (a) and SFD015 (b). The rocks are strongly foliated and preserve a variety of deformation textures and mineral assemblages.

Magnetite-rich gneisses

SFDD01-03

Sample SFDD01-03 contains garnet, magnetite, quartz and biotite. At hand sample scale, it contains a gneissic fabric defined by alternating pale quartz + garnet ± magnetite layers and dark layers containing biotite + magnetite + quartz + garnet (Figure 4a). In the pale layers, porphyroblastic garnet (up to 5 mm) is fractured and anhedral and forms lobate grain boundaries where it is in contact with coarse-grained quartz (up to 2 mm). Magnetite (up to 1 mm) occurs adjacent to garnet or as finer-grained inclusions within garnet. In the darker layers, biotite and coarse-grained, deformed quartz and magnetite (up to 1 mm) define a foliation (Figure 4b) which wraps porphyroblastic garnet. Magnetite, biotite and quartz commonly occur finely intergrown within the foliation. Rare coarse-grained biotite (up to 1 mm) is located in garnet strain shadows. Garnet in the darker layers contains abundant inclusions of fine-grained quartz, magnetite and minor biotite. Often, the inclusions are more common in the cores of the grains. Chalcopyrite and pyrite occur in trace amounts. The peak assemblage is interpreted to be garnet + quartz + biotite + magnetite.

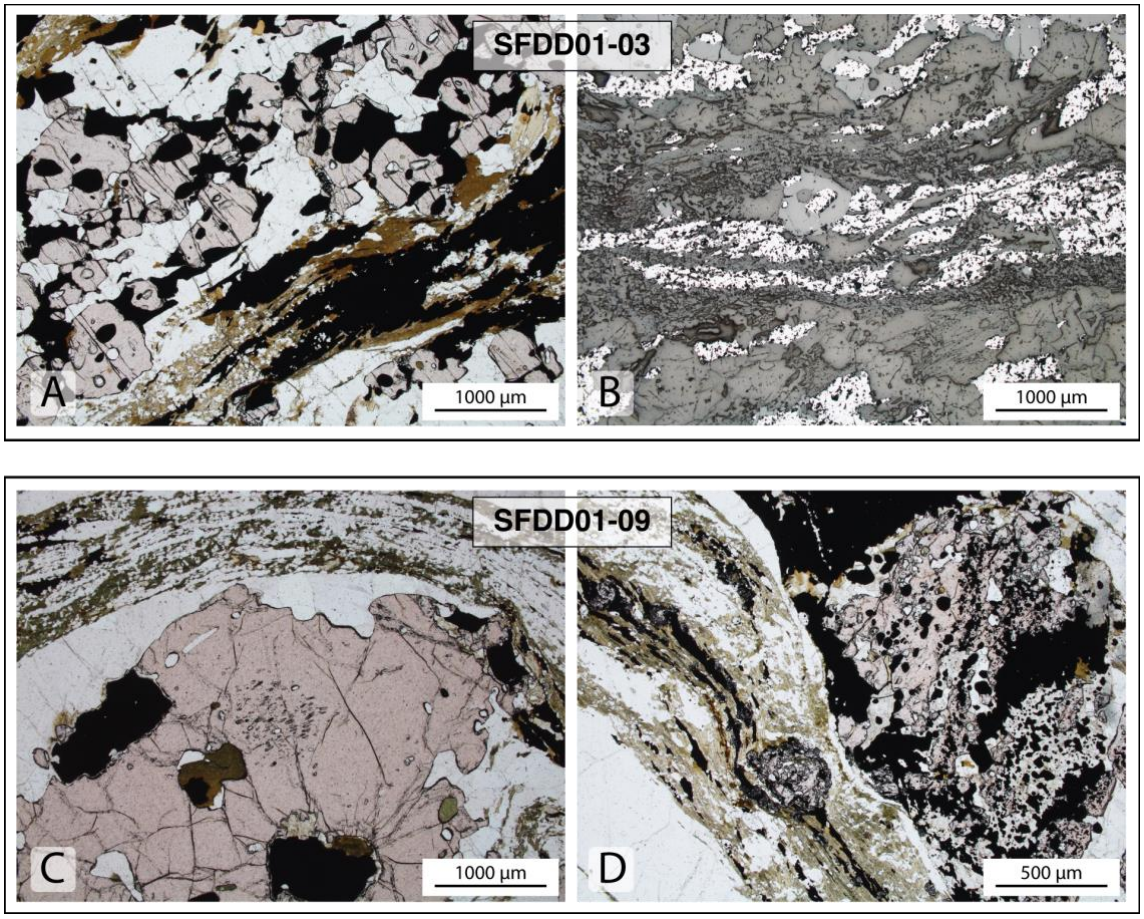

Figure 4: Thin section photomicrographs for magnetite-rich gneiss samples SFDD01-03 and SFDD01-09. (a) Transmitted light image of sample SFDD01-03. Gneissic layering is defined by pale quartz + garnet ± magnetite layers (top left) and foliated biotite + magnetite + quartz + garnet layers (bottom right). (b) Reflected light image of samples SFDD01-03. Deformed magnetite (white) occurs within the foliation. (c) Transmitted light image of sample SFDD01-09. Gneissic layering (top) wraps porphyroblastic garnet (bottom centre). (d) Transmitted light image of sample SFDD01-09. Finer-grained garnet (left) occurs within the foliated layering.

SFDD01-09

Sample SFDD01-09 contains garnet, quartz, magnetite and biotite. At hand sample scale, it has a strong mylonitic fabric in which alternating translucent and dark layers wrap around large garnet porphyroblasts (Figure 4c). Translucent layers are 1 – 3 mm thick and consist only of coarse-grained, deformed quartz (up to 2mm). Dark layers are up to 10 mm thick and contain quartz, biotite, magnetite and garnet. Quartz occurs finely intergrown with biotite and magnetite. Biotite occurs either coarsely (up to 1 mm) and elongated in the direction of foliation, or intergrown with quartz ± magnetite.

Magnetite (up to 2 mm) is coarse-grained and elongate or found as fine-grained intergrowths with quartz ± biotite. Garnet porphyroblasts (up to 5 mm) are heavily fractured and range from inclusion-poor to poikioblastic, with inclusions consisting of quartz, biotite and magnetite. Fine-grained garnet (up to 500 μm) also occurs in the dark layers and is commonly poikioblastic with magnetite inclusions (Figure 4d). Fine-grained muscovite pseudomorphs (up to 1 mm) are interpreted as the retrograde breakdown of plagioclase. Such grains commonly occur adjacent to garnet or wrapped by the foliation in the layering. The peak assemblage is interpreted as garnet + quartz + biotite + plagioclase + magnetite. Garnet in the foliation is interpreted as a separate (older) generation to garnet which is wrapped by the foliation.

SFDD01-12

Sample SFDD01-12 contains garnet, biotite, quartz, K-feldspar, magnetite and plagioclase. At hand sample scale, a fabric is defined by biotite wrapping garnet porphyroblasts (Figure 5a). The rest of the sample consists of coarse-grained quartz, K-feldspar, magnetite and plagioclase. Garnet (up to 2 cm) is highly fractured and contains coarse-grained inclusions of quartz and biotite, as well as inclusions of fine-grained magnetite at the rims and abundant fine-grained monazites (Figure 5b). Biotite occurs as inclusions in garnet and also in the matrix, defining a strong foliation which wraps around garnet grains. Biotite (up to 1 mm) in the matrix occurs in two orientations. This is interpretated as a feature of thin section orientation, and thus the two orientations are considered unigenerational. Abundant quartz (up to 2 mm) is coarse and deformed. It commonly occurs elongated in the direction of the foliation and may contain aligned fine-grained biotite and magnetite. Quartz may also be found intergrown with biotite

and plagioclase (myrmekite) in domains (up to 5 mm). Hematite-stained K-feldspar (up to 3 mm) occurs in clusters in the matrix. Hematite-stained plagioclase (up to 1 mm) occurs in the matrix and often exhibits a mymerkitic texture (intergrown with quartz). Partial to intense sericitic alteration commonly occurs along fracture and cleavage surfaces of both K-feldspar and plagioclase. Magnetite (up to 2 mm) is deformed and elongated in the direction of foliation. The peak assemblage is interpreted as garnet + biotite + K-feldspar + quartz + plagioclase + magnetite.

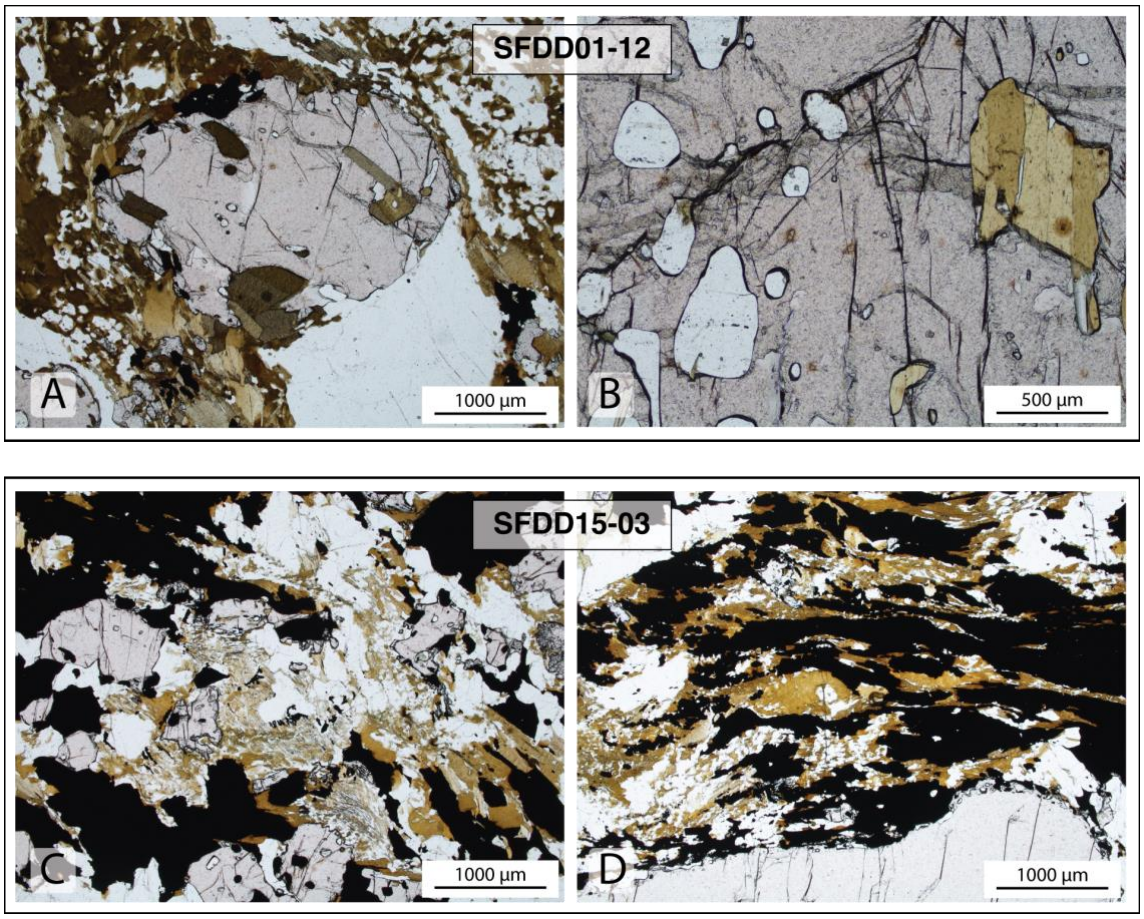

Figure 5: Transmitted light thin section photomicrographs for magnetite-rich gneiss samples SFDD01-12 and SFDD15-03. (a) Sample SFDD01-12. Biotite defines a foliation which wraps around porphyroblastic garnet. (b) Sample SFDD01-12. Garnet (pink) contains inclusions of quartz, biotite, monazite and magnetite (not pictured). (c) Sample SFDD15-03. Biotite is commonly intergrown with quartz (centre). (d) Sample SFDD15-03. Deformed magnetite (black) occurs within the foliation.

SFDD15-03

Sample SFDD15-03 is comprised of garnet, biotite, quartz, K-feldspar and magnetite. At hand sample scale, a gneissic fabric is defined by alternating quartz + K-feldspar + garnet ± magnetite leucosomes and finer-grained layers containing quartz, magnetite, biotite and garnet. In the leucosomes, garnet (up to 7 mm) occurs as fractured porphyroblasts. It contains inclusions of quartz and minor biotite. Quartz (up to 1 mm) exhibits lobate grain edges. Magnetite occurs in some leucosomes and lacks distinct elongation. Minor anhedral K-feldspar (up to 500 μm) occurs as perthite within these domains and is partially to strongly hematite-stained. In the fine-grained layers, quartz, magnetite and biotite define a foliation which wraps garnet. Garnet (up to 3 mm) contains magnetite inclusions. Quartz (up to 500 μm) may be found in deformed clusters wrapping garnet, or finely intergrown with biotite (Figure 5c). Biotite may also be found as coarse, elongate grains (up to 3 mm) in the foliation. Opaques consist of magnetite, as well as trace chalcopyrite and pyrite. Magnetite commonly occurs elongated in the foliation (Figure 5d), or as fine inclusions in garnet. The peak assemblage is interpreted to be garnet + biotite + quartz + K-feldspar + magnetite.

Magnetite-poor gneisses

SFDD01-04

Samples SFDD01-04A and SFDD01-04B contain K-feldspar, quartz, plagioclase, biotite, cordierite, magnetite and hematite. Sample SFDD01-04A contains a weak foliation defined by oxides within a pale matrix. The matrix consists of abundant quartz, K-feldspar, cordierite (altered to amorphous clay), biotite and minor plagioclase. Oxides (up to 1 mm) comprise ~5% of the matrix and consist of magnetite and hematite. They occur elongated and define the foliation (Figure 6a). Fine-grained oxides can be found as inclusions in quartz and K-feldspar. Quartz (up to 2mm) occurs abundantly in the matrix, often forming lobate grain boundaries. K-Feldspar (up to 2 mm) is less abundant, found as perthite or microcline and is pervasively hematite-stained. Moderate sericitisation of K-feldspar is common. Rare myrmekite (up to 500 μm) occurs adjacent to K-feldspar and quartz. Large domains (up to 5 mm) of pale green, amorphous clay (Figure 6b) are interpreted as altered cordierite. Rare sillimanite (up to 500 μm) only occurs within cordierite and is elongated in the direction of foliation. Oxides and quartz also occur as inclusions in cordierite domains. Pale green biotite (up to 1 mm) with high birefringence is interpreted to be phlogopite. Rare sericitised plagioclase (up to 500 μm) occurs dispersed in the matrix. Sample SFDD01-04B is finer-grained and has a weak foliation defined by phlogopite (Figure 6c). The matrix consists of sub-equant K-feldspar, oxides and minor quartz, as well as rare plagioclase and clays. Phlogopite (up to up to 500 μm) is dispersed throughout the matrix. Its elongation orientation defines a weak foliation. Abundant K-feldspar (up to 500 μm) occurs as perthite and microcline. It is partially to strongly hematite-stained and contains inclusions of fine-grained, rounded quartz. Oxides comprise ~2% of the matrix and consist of magnetite and

hematite. Most occur as equant grains, but some are elongated in the direction of foliation. Coarse quartz (up to 500 μm) forms lobate grain boundaries in the matrix. Rare plagioclase (up to 200 μm) occurs dispersed throughout the matrix. Pale green, amorphous clay, also interpreted as cordierite, occurs in domains (50 – 500 μm). Rare clusters of fine-grained, elongate sillimanite (up to 100 μm) may occur within clay domains (Figure 6d). The peak assemblage in both samples is interpreted as K-feldspar + quartz + magnetite + hematite + plagioclase + biotite ± cordierite.

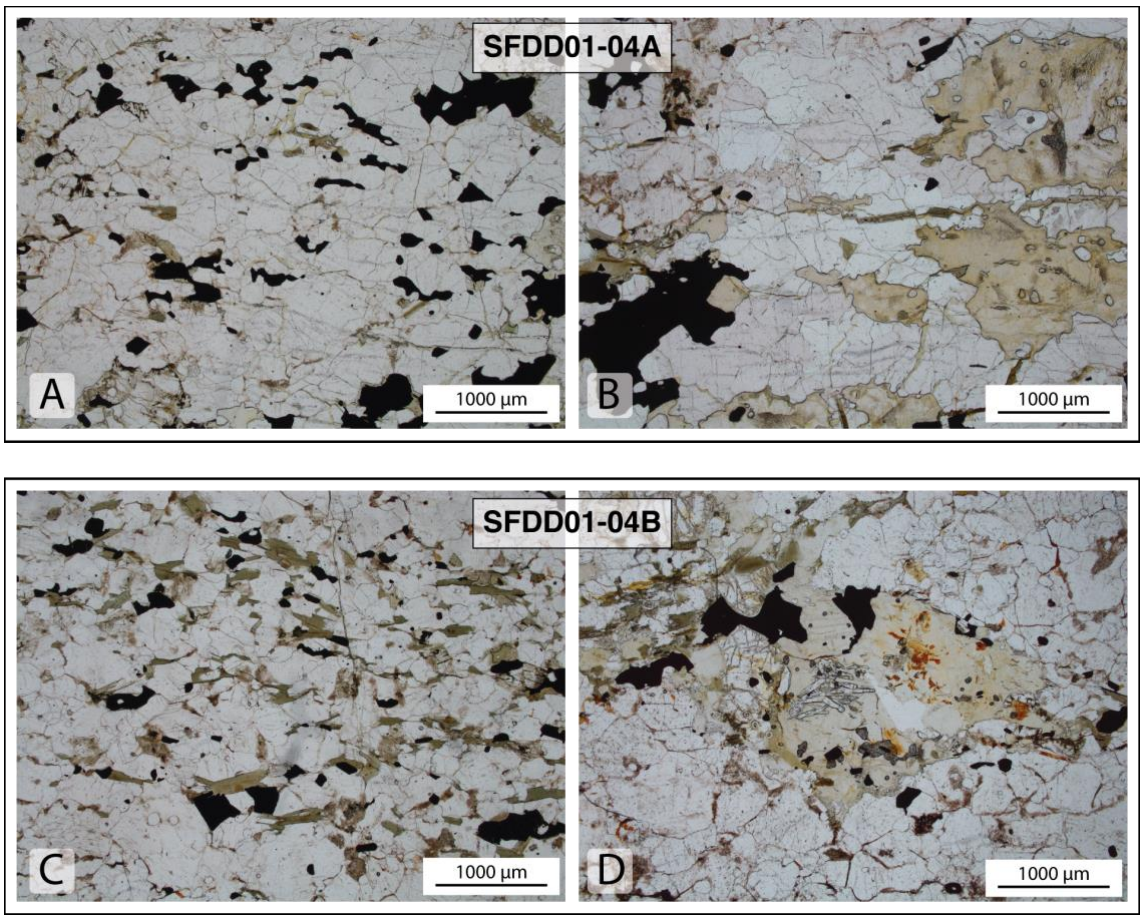

Figure 6: Transmitted light thin section photomicrographs for magnetite-poor gneiss samples SFDD01-04A and SFDD01-04B. (a) Sample SFDD01-04A. Magnetite (black) defines a weak foliation. (b) Sample SFDD01-04A. Large domains of amorphous clay are interpreted as areas of cordierite alteration. (c) Sample SFDD01-04B. Phlogopite (brown/green) is more abundant than in sample SFDD01-04A and defines a weak foliation. (d) Sample SFDD01-04B. Rare sillimanite occurs in amorphous clay domains (interpreted as cordierite).

SFDD01-17

Sample SFDD01-17 is comprised of biotite, sillimanite, quartz, K-feldspar and cordierite. At hand sample scale, a gneissic fabric is defined by alternating quartzofeldspathic and biotite-sillimanite-rich layers. The quartzofeldspathic layers are dominated by elongate quartz (up to 1 mm) but also contain elongate, partially sericitised and hematite-stained K-feldspar (up to 1 mm) and minor biotite (Figure 7b). The biotite-sillimanite-rich layers consist of a matrix of cordierite, K-feldspar, biotite and sillimanite accompanied by elongate layer-parallel clusters of biotite and sillimanite. Partially sericitised K-feldspar (up to 1 mm) is commonly perthitic, hematite-stained and sericitised. Coarse-grained, anhedral biotite (up to 400 μm) and coarse-grained, euhedral sillimanite (up to 5 mm) form a strong layer-parallel foliation (Figure 7a). Longer sillimanite grains show fractures which are perpendicular to their elongation. Sillimanite also commonly occurs perpendicular to the thin section, displaying a prefect euhedral cubic shape. Finer-grained biotite and sillimanite (up to 400 μm) also occur elongated in the direction of foliation. Fine-grained opaques are low in abundance and consist of magnetite and rare chalcopyrite. The peak assemblage is interpreted to be quartz + K-feldspar + biotite + sillimanite + cordierite.

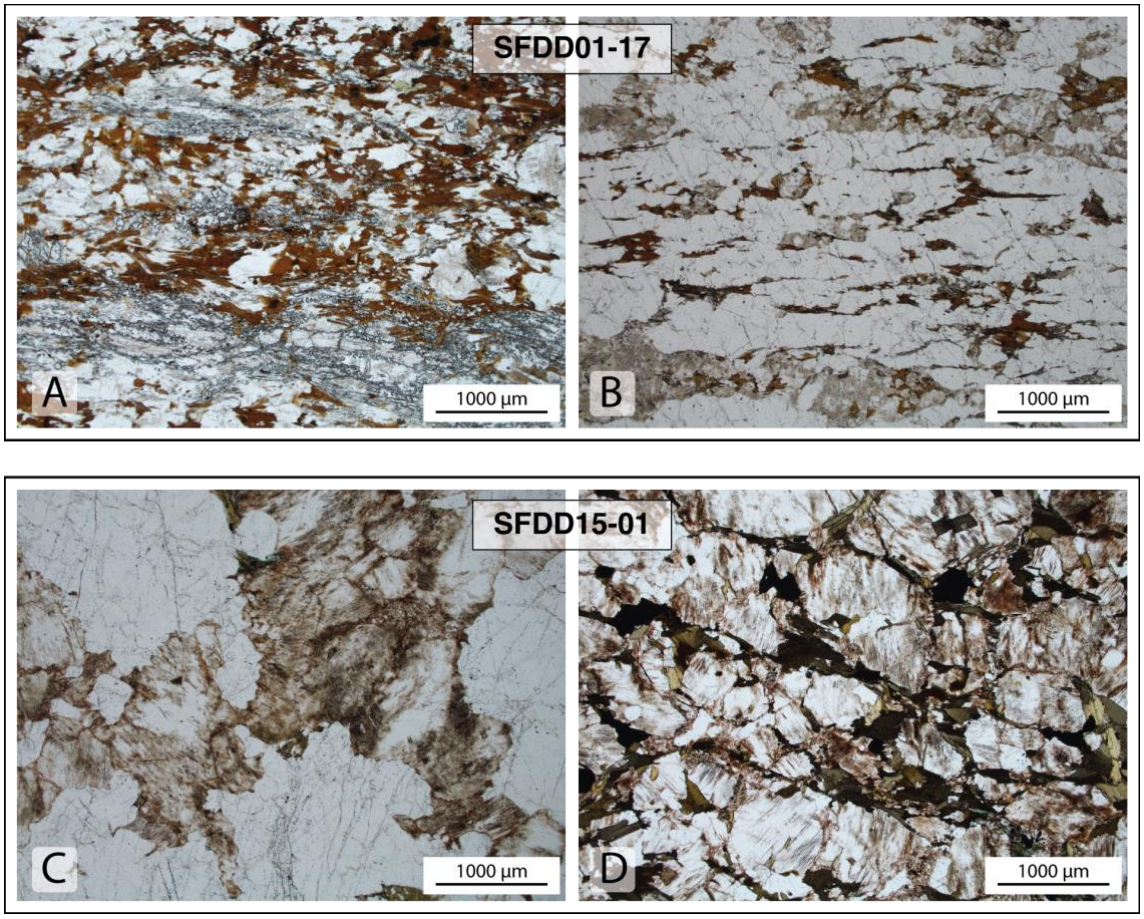

Figure 7: Transmitted light thin section photomicrographs for magnetite-poor gneiss samples SFDD01-17 and SFDD15-01. (a) Sample SFDD01-17. A strong foliation is defined by sillimanite (pale blue) and biotite (brown). (b) Sample SFDD01-17. Quartzofeldspathic leucosomes contain abundant deformed quartz (clear), K-feldspar (pinkish-grey) and elongated biotite (brick red). (c) Sample SFDD15-01. Quartzofeldspathic leucosomes contain coarse-grained anhedral quartz and hematite-stained K-feldspar. (d) Sample SFDD15-01. The matrix consists of abundant hematite-stained K-feldspar, biotite, magnetite and minor quartz.

SFDD15-01

Sample SFDD15-01 consists of K-feldspar, biotite, quartz and magnetite. At hand sample scale, a weak foliation is defined by biotite between quartzofeldspathic leucosomes. Leucosomes are comprised of coarse-grained quartz and K-feldspar (Figure 7c), whereas the matrix contains more abundant, finer-grained K-feldspar, biotite, magnetite and minor quartz (Figure 7d). In the leucosomes, quartz (up to 2 mm) has lobate grain boundaries. Anhedral K-feldspar (up to 2 mm) is hematite-stained. It contains small fine-grained inclusions of rounded quartz. In the matrix, K-feldspar (up

to 1 mm) is strongly hematite-stained and contains fine-grained inclusions of quartz, biotite and magnetite. Subhedral biotite (up to 500 μm) occurs in clusters and defines a weak foliation sub-parallel to leucosome orientation. Opaques (up to 500 μm) are present in the matrix and consist of magnetite and hematite. Wavy quartz-chlorite veins (up to 100 μm thick) crosscut the foliation at a low angle. The peak assemblage is interpreted as K-feldspar + biotite + quartz + magnetite + hematite.

METHODS

Zircon and monazite LA-ICP-MS

Zircon and monazite U-Pb and trace element data was acquired for seven samples using Laser Ablation – Inductively Coupled Plasma – Mass Spectrometry (LA-ICP-MS). The instrument used was a RESOlution LR 193nm Excimer laser system with an Agilent 7900x ICP-MS at Adelaide Microscopy, University of Adelaide.

Initially four samples were analysed as grain mounted zircon and monazite separates to collect reconnaissance data. A second *in situ* batch was then collected in order to observe any trend between age and textural location of the grains. During this analysis, one sample was repeated, along with three new samples.

Data processing and reduction was performed in *Iolite 4* software (Hellstrom, Paton, Woodhead & Hergt, 2008; Paton, Hellstrom, Paul, Woodhead & Hergt, 2011).

Extended LA-ICP-MS methods are provided in Appendix B. U-Pb data is presented in Appendix C, and trace element data is presented in Appendix D.

Whole-rock Geochemistry

Whole-rock geochemistry was obtained for six samples from Bureau Veritas, Adelaide. Samples were crushed, dried and cast to glass beads. The major elements were analysed by X-Ray Fluorescence (XRF) and trace elements were obtained by LA-ICP-MS. Fluorine concentrations were measured using a specific ion electrode after combining the samples with sodium carbonate. Whole-rock geochemical data is provided in Appendix E.

RESULTS

Zircon LA-ICP-MS

U-Pb geochronology and trace elements were analysed on zircon in grain mounts from four samples: SFDD01-03, SFDD01-12, SFDD15-01 and SFDD15-03. U-Pb age data is presented on Terra-Wasserburg concordia plots. Trace element data is presented for samples SFDD01-03 and SFDD15-03 on rare earth element (REE) spider plots. For samples SFDD01-12 and SFDD15-01, trace element data is excluded due to lack of concordant analyses. All presented ages are $^{207}Pb/^{206}Pb$ ages. Trace element data is given in units of ppm / chondrite (after McDonough & Sun, 1995). The Ce anomaly (Ce*) in zircon is measured using the equation $Ce^* = Ce_{(n)}/(Nd_{(n)}^2 * Sm_{(n)})$, where $_{(n)}$ denotes composition normalised to chondrite (Loader, Wilkinson & Armstrong, 2017). Individual spot ages for the samples and standards can be found in Appendix C. Trace element data is provided in Appendix D.

Zircons in the samples preserve a range of zoning and morphology (Figure 8) and are generally on the scale of 70 – 240 μm in diameter. Sample SFDD01-03 contains zircons which are rounded to subhedral and preserve fine concentric zoning (individual rims up to 20 μm thick). For samples SFDD01-12, SFDD15-01 and SFDD15-03, zircons are rounded, smaller and have more irregular zoning. The zircons are overall comparatively dark.

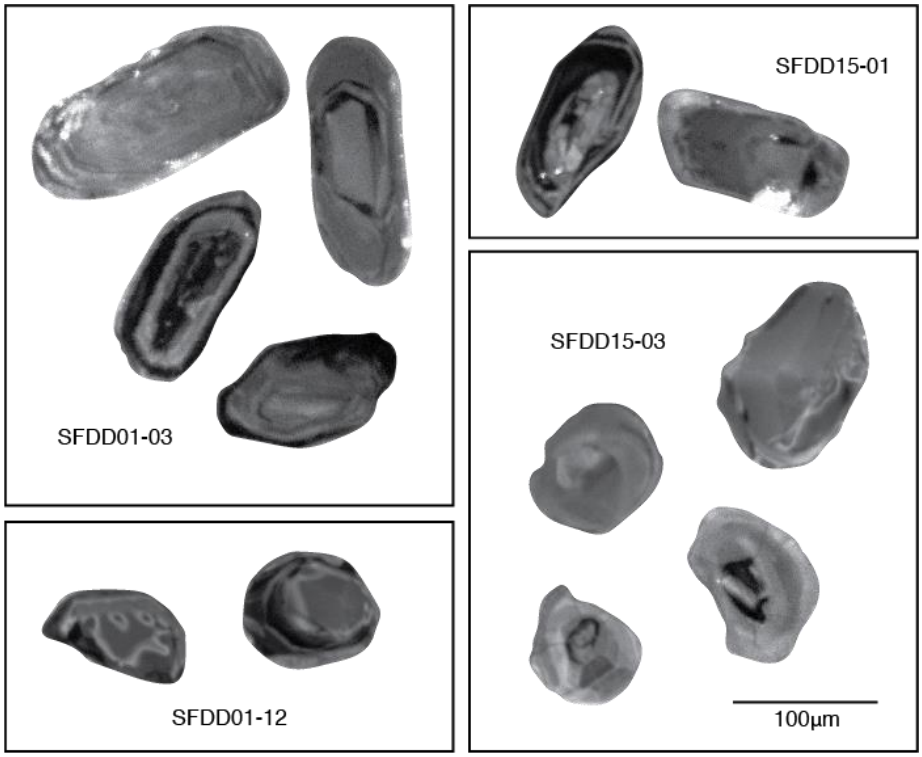

Figure 8: Zircon cathodoluminescence (CL) images for samples SFDD01-03, SFDD01-12, SFDD15-01 and SFDD15-03. Zircons are 70 – 240 µm in size. They are subhedral to rounded and display concentric to irregular zoning. Some zoning is comparatively dark.

SFDD01-03

Geochronology and trace element data for sample SFDD01-03 was calculated for 34 analyses. Many of the analyses returned discordant ages, toward Pb loss values (Figure 9a). However, a concordant population consisting of nine analyses is present at 1749 ± 15 Ma (MSWD = 2.87; Figure 9b). In comparison to recognised igneous zircon compositions (Belousova, Griffin, O'Reilly & Fisher, 2002), zircons for SFDD01-03 are enriched in light rare earth elements (LREEs; Figure 9c). The Ce anomaly is not significantly pronounced, with Ce* on the scale of 10^{-6} to 10^{-3}.

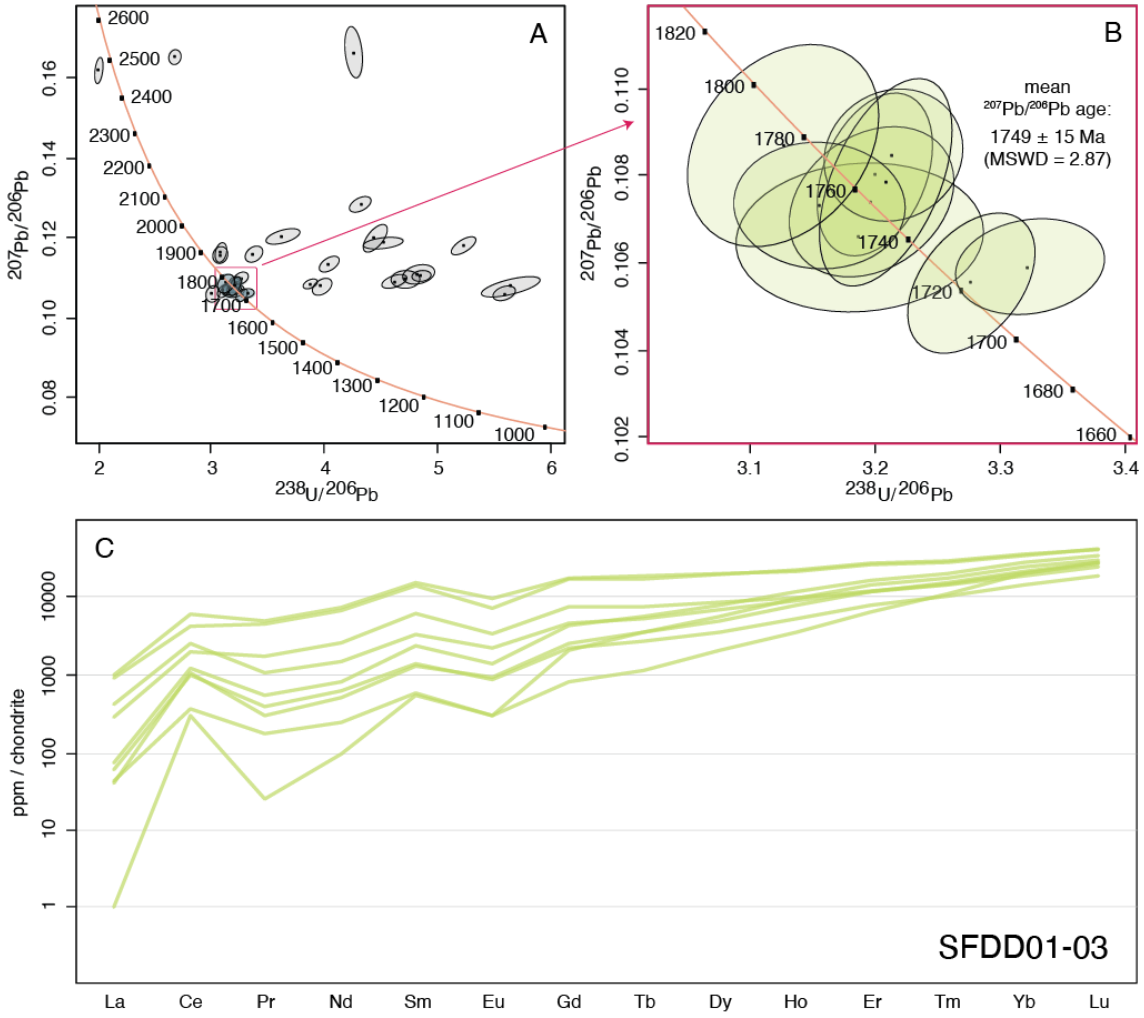

Figure 9: Zircon LA-ICP-MS results for sample SFDD01-03. (a) Terra-Wasserburg concordia plot with 2 sigma error ellipses. Ages are given in Ma. Discordant data is greyed out. (b) Concordant data shows a population at 1749 ± 15 Ma (MSWD = 2.87). (c) REE spider plot of concordant analyses showing LREE enrichment.

SFDD01-12

10 analyses were performed on grain mounted zircon for sample SFDD01-12. A single concordant analysis yielded an age of 1664 ± 22 Ma, whilst all other analyses were discordant (Figure 10a). Discordance is in the direction of Pb loss.

SFDD15-01

Geochronology for sample SFDD15-01 was analysed from 11 spots. A single concordant analysis was obtained at 1691 ± 17 Ma. All other analyses were discordant (Figure 10b). Discordance is in the direction of Pb loss.

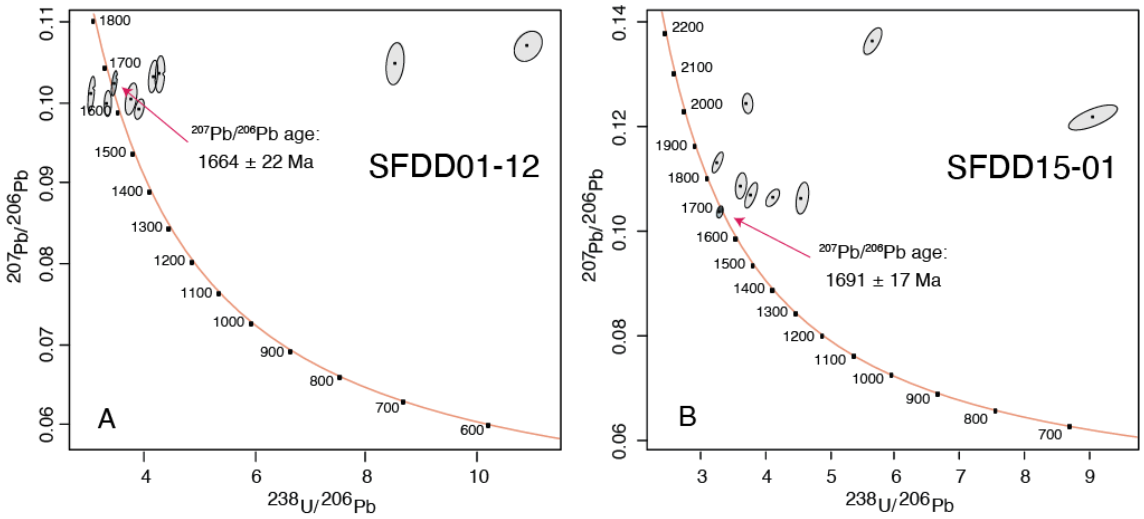

Figure 10: Zircon LA-ICP-MS results for samples SFDD01-12 and SFDD15-01. Terra-Wasserburg concordia plots with 2 sigma error ellipses. Ages are given in Ma. Discordant data is greyed out. (a) Sample SFDD01-12 has one concordant analysis at 1664 ± 22 Ma. (b) Sample SFDD15-01 has one concordant analysis at 1691 ± 17 Ma.

SFDD15-03

Geochronology for sample SFDD15-03 was obtained 21 analyses. The analyses yielded mostly concordant data – a population consisting of eight analyses, as well as one younger analysis (Figure 11a). The concordant population yields an age of 1673 ± 16 Ma (MSWD = 2.75) whilst the younger analysis gives an age of 1612 ± 23 Ma (Figure 11b). Abundances of the LREEs result in two distinct compositional groups (Figure 11c). Samples relatively depleted in LREEs have a prominent Ce anomaly with Ce* values between 10^{-2} and 10^{1}. The Ce anomaly is not as pronounced for samples that have a relatively flat REE pattern with Ce* on the scale of 10^{-6} to 10^{-2}.

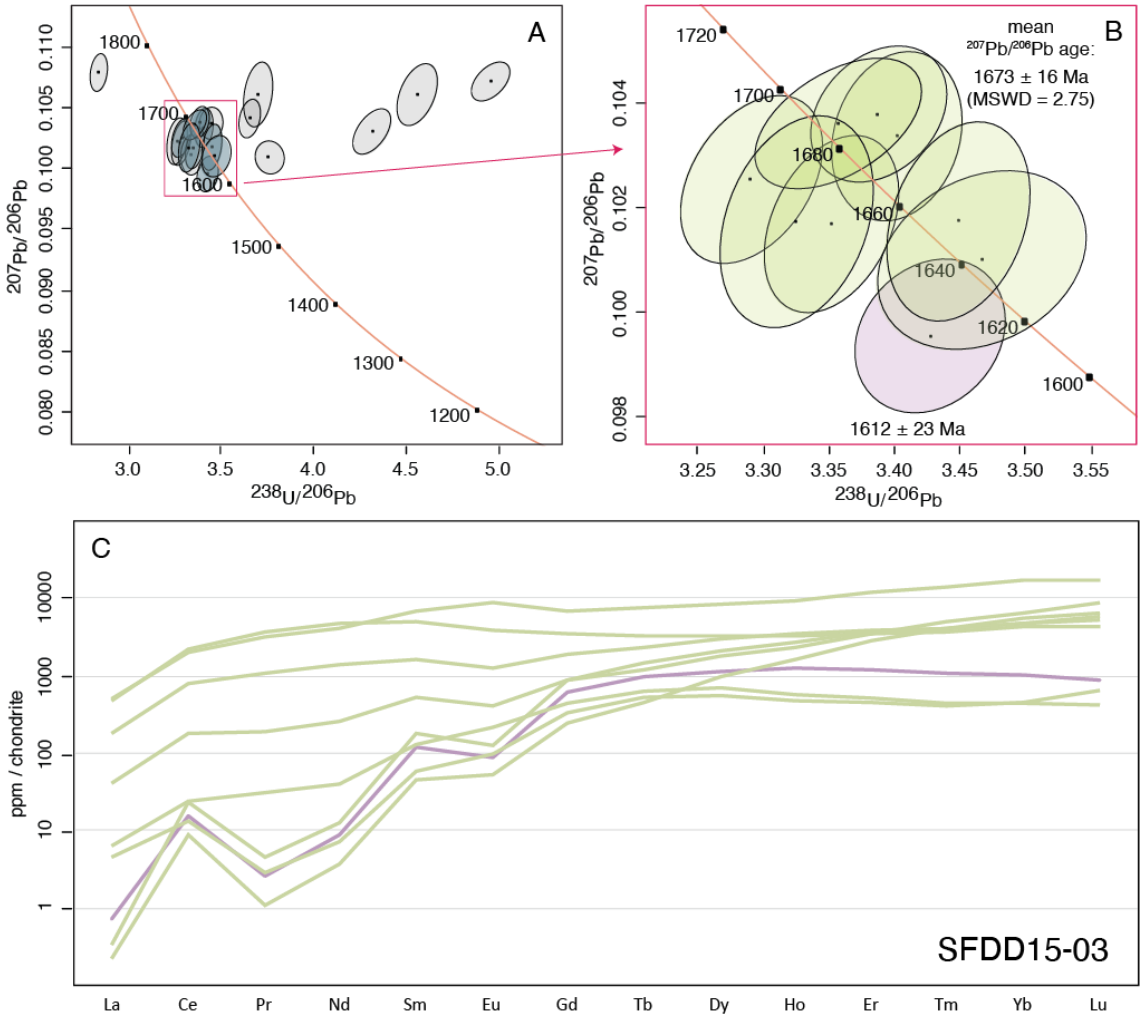

Figure 11: Zircon LA-ICP-MS results for sample SFDD15-03. (a) Terra-Wasserburg concordia plot with 2 sigma error ellipses. Ages are given in Ma. Discordant data is greyed out. (b) Concordant data shows a population at 1673 ± 16 Ma (MSWD = 2.75) and one analysis at 1612 ± 23 Ma. (c) REE spider plot of concordant analyses. Variance within LREE abundance and patterns suggests there are two distinct compositional groups.

Monazite LA-ICP-MS

U-Pb geochronology and trace element abundances were collected for seven samples. Samples SFDD01-03, SFDD01-12, SFDD15-01 and SFDD15-03 were analysed from monazites in a grain mount. *In situ* analysis was carried out on monazite grains in thin sections of samples SFDD01-04A, SFDD01-09, SFDD01-12 (repeat) and SFDD01-17. The Gd/Yb ratio is used as a measure of the slope of the line from middle to heavy rare earth elements (M – HREEs). This ratio quantifies the partitioning of HREE into monazite during crystallisation. For samples in this study, a Gd/Yb ratio of > 100 is considered depleted in HREEs, whilst a Gd/Yb ratio << 100 is enriched in HREEs. The Eu anomaly (Eu*) is measured using the equation $Eu^* = Eu_{(n)}/(Sm_{(n)}^2 * Tb_{(n)})^{1/3}$ (after Lawrence & Kamber, 2006). An Eu* value of ~ 1 means that there is no Eu anomaly, whilst an Eu* value < 1 indicates a negative Eu anomaly.

The data is presented on Terra-Wasserburg concordia plots, weighted mean age plots, REE spider plots and on plots of Gd/Yb vs age, as appropriate. All presented ages are $^{207}Pb/^{206}Pb$ ages. Trace element data is given in units of ppm / chondrite (after McDonough & Sun, 1995). Individual spot ages for the samples and standards can be found in Appendix C, whilst trace element results are provided in Appendix D.

Backscattered electron images (Figure 12) were collected for monazite in samples SFDD01-03, SFDD01-12, SFDD15-01 and SFDD15-03, which were analysed in a grain mount. The monazite grains preserve a range of zoning and are commonly rounded. They are generally on the scale of 70 – 240 μm in diameter. In some cases, a clear compositional or geochronological trend is observed across the zoning. Such cases are reported in the text below.

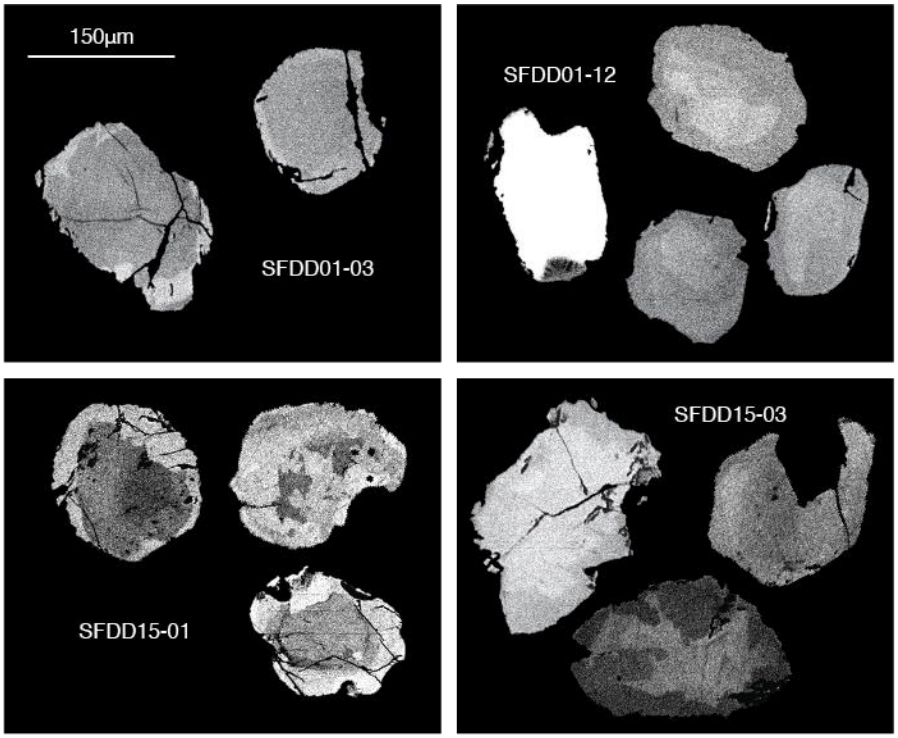

Figure 12: Monazite backscattered electron (BSE) images for grain mounted samples SFDD01-03, SFDD01-12, SFDD15-01 and SFDD15-03. Monazites are 60 – 240 µm in size. They are rounded and display zoning which ranges from rim-only to irregular.

SFDD01-03

Mounted monazites for sample SFDD01-03 were analysed from 42 spots.

Geochronology yielded ages of 1580 – 1710 Ma with one large concordant population and several younger spots (Figure 13a). The population, consisting of 36 analyses, gave a weighted mean age of 1665 ± 4 Ma (MSWD = 1.03). Younger analyses resulted in ages of 1609 ± 40 Ma, 1601 ± 44 Ma and 1582 ± 26 Ma. Monazite in this sample is typically enriched in HREEs in comparison to other samples (Gd/Yb << 100; Figure 13b, c). Monazites younger than 1650 Ma have compositions which are more depleted in HREEs than the 1665 Ma population and tend to have more prominent negative Eu anomalies (Eu* ~ 0.35).

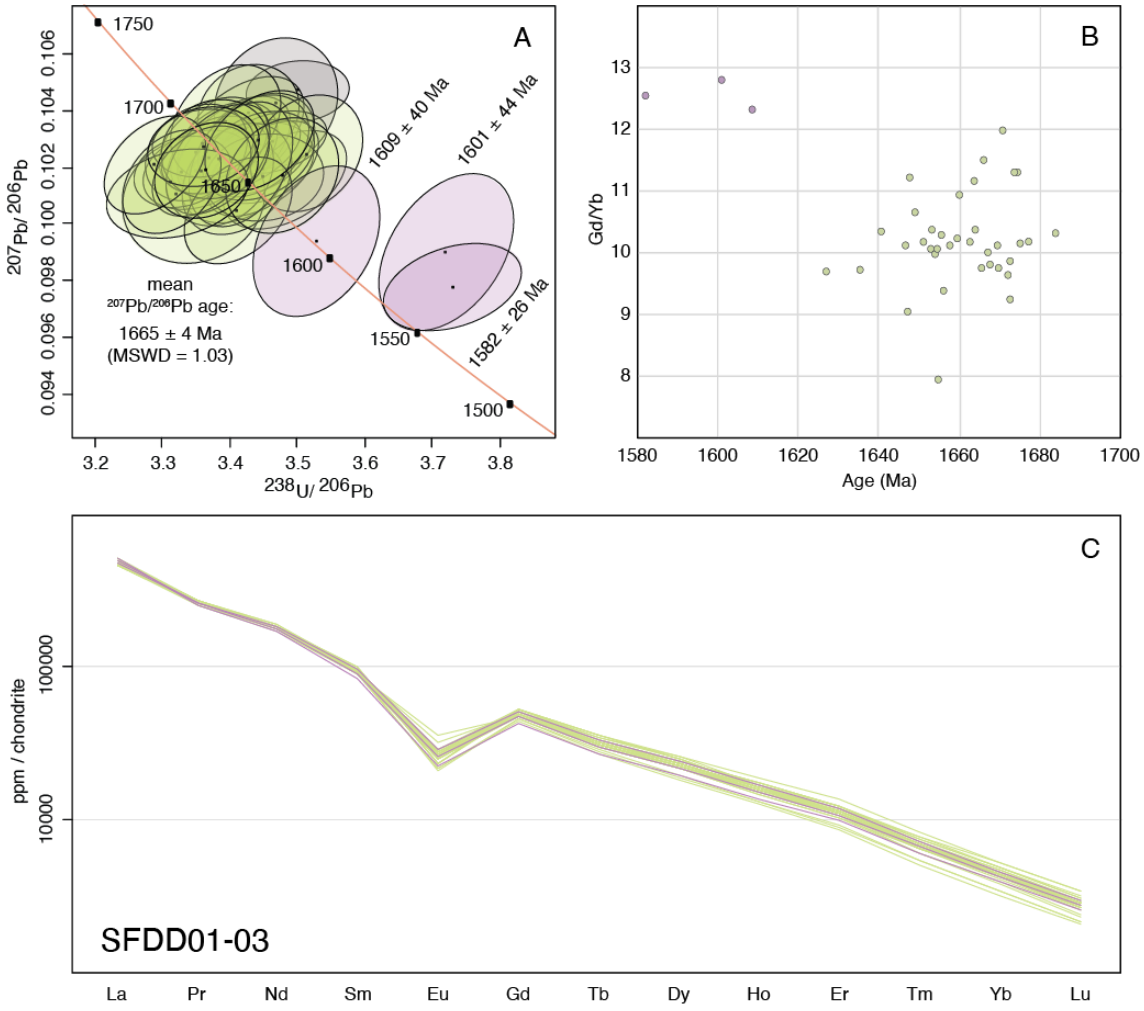

Figure 13: Monazite LA-ICP-MS results for sample SFDD01-03. (a) Terra-Wasserburg concordia plot with 2 sigma error ellipses. Ages are given in Ma. Discordant data is greyed out. Concordant data yields a population at 1665 ± 4 Ma (MSWD = 1.03), as well as younger analyses with ages of 1609 ± 40 Ma, 1601 ± 44 Ma and 15852 ± 26 Ma. (b) Gd/Yb ratios for concordant analyses show that HREEs are more depleted in the younger samples. (c) REE spider plot of concordant analyses showing an enrichment of HREEs relative to the other samples.

SFDD01-09

For sample SFDD01-09, analysis was performed on *in situ* monazite grains, 20 – 90 μm in size. 24 analyses were collected from 16 grains. All of the grains were located within a quartz-biotite-hematite mylonitic fabric. ~30% of the grains displayed a foliation-parallel elongation (e.g. Figure 14c). Spot locations were chosen carefully to avoid commonly occurring small, dark inclusions. The analyses range in age from 1525 to 1595 Ma and yield a weighted mean age of 1559 ± 10 Ma (MSWD = 0.85; Figure 14a,

b). In comparison to other samples, monazite in this sample is depleted in HREEs (Figure 14d). Eu anomalies (Eu*) are reasonably flat, varying from 0.4 to 0.8. Alignment of grains relative to the foliation did not yield distinct ages or compositions.

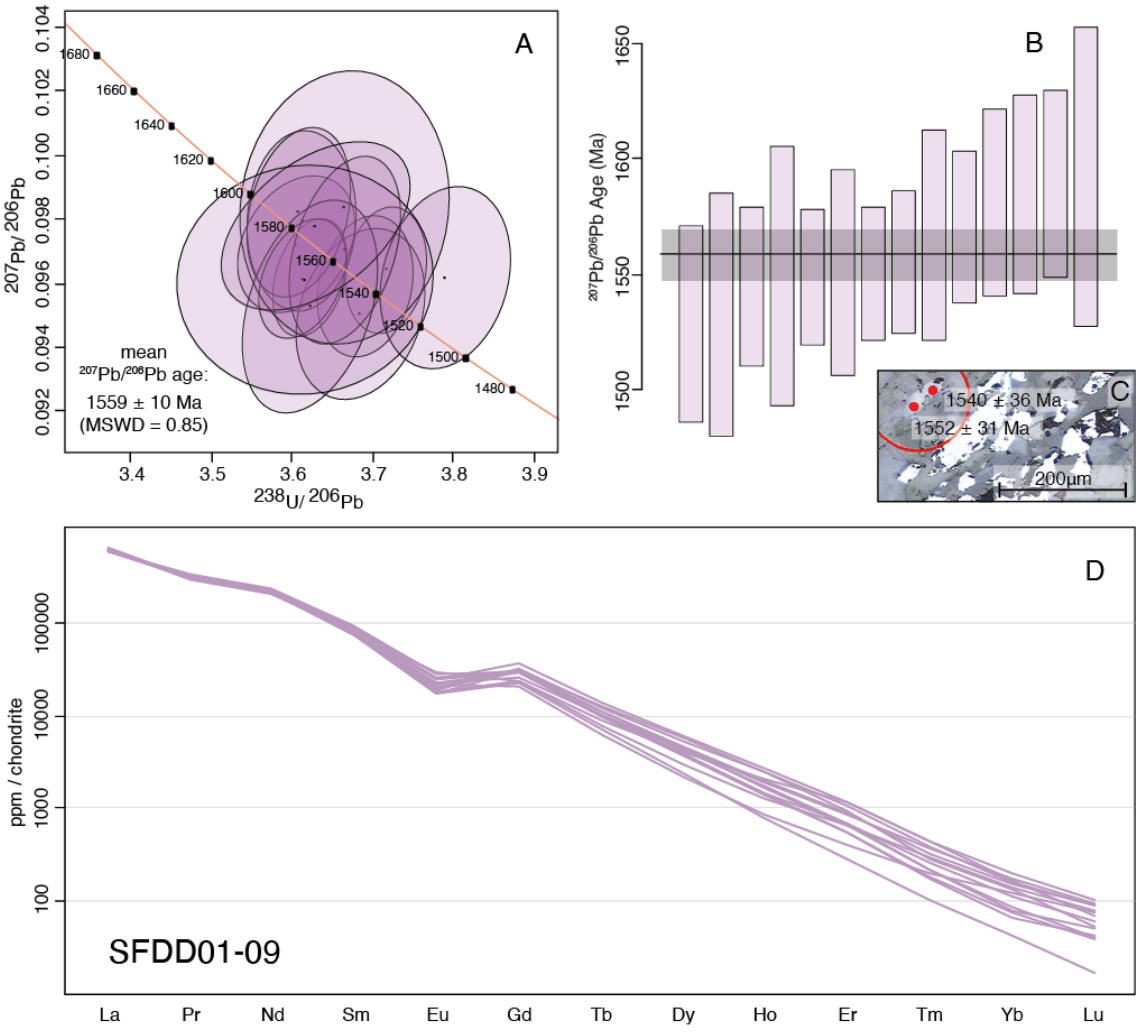

Figure 14: Monazite LA-ICP-MS results for sample SFDD01-09. (a) Terra-Wasserburg concordia plot with 2 sigma error ellipses. Ages are given in Ma. The population yields a mean age of 1559 ± 10 Ma (MSWD = 0.85). (b) Weighted mean age plot illustrating the coherence of the given age. (c) Reflected light image of a monazite grain which is parallel to the foliation. The grain yields ages which are young in comparison to the mean age. (d) REE spider plot of concordant analyses showing the depletion of HREEs relative to the other samples.

SFDD01-12

For sample SFDD01-12, monazite grains were analysed both *in situ* and in a grain mount. 56 analyses were obtained from 36 *in situ* monazites, ranging in size from 20 to

160 μm. They occur as inclusions in garnet or within a foliated matrix of biotite, magnetite, quartz, K-feldspar and plagioclase. Spot locations were chosen carefully to avoid inclusions. 42 analyses were performed on 25 mounted monazite grains which are 80 – 200 μm in size. The grains are commonly rounded and preserve varying amounts of zoning (e.g. Figure 15a). Monazites located within garnet returned ages of 1560 – 1710 Ma, whilst monazites in the matrix range in age from 1540 to 1670 Ma. Mounted monazite grains returned similar ages of 1545 – 1700 Ma (Figure 15a). The unmix function in isoplot (Ludwig, 2012) yields two distinct ages from the combined grain mounted monazite and *in situ* monazite analyses. The two populations have mean ages of 1579 ± 4 Ma and 1669 ± 5 Ma with a relative misfit of 0.535. Monazites found in garnet are typically more enriched in HREEs than monazites in the matrix and in the grain mount. The mounted monazites are commonly more depleted in HREEs than in situ monazites (Figure 15b, c). Negative Eu anomalies vary from flat (Eu* = 0.95) to strongly pronounced (Eu* = 0.25).

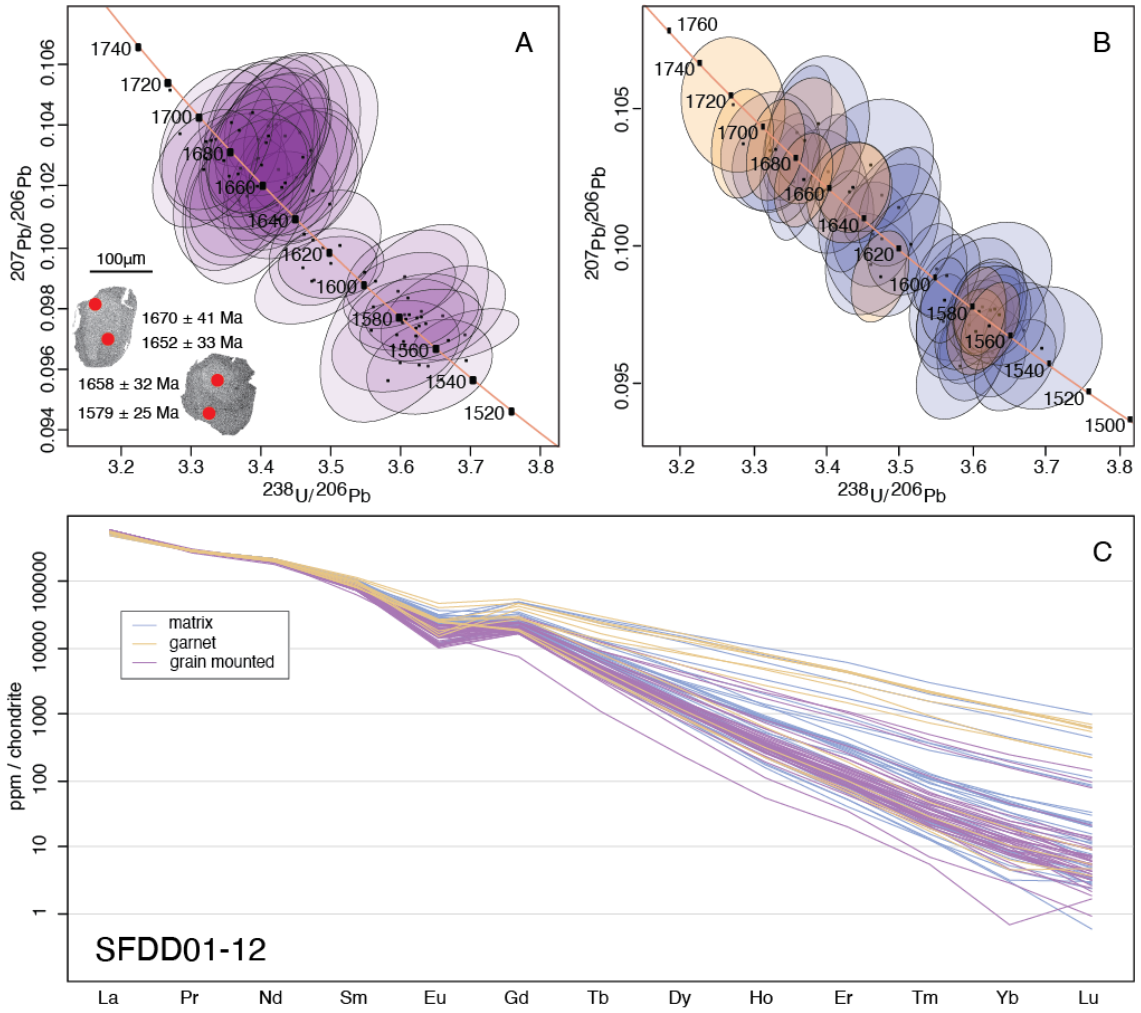

Figure 15: Monazite LA-ICP-MS results for sample SFDD01-12. (a) Terra-Wasserburg concordia plot of grain mounted data with 2 sigma error ellipses. Ages are given in Ma. Grain mounted data is in purple. Bottom left: BSE images of zoned monazites in the grain mount. Lighter zones (cores) are generally older than darker zones (rims). (b) Terra-Wasserburg concordia plot of *in situ* data with 2 sigma error ellipses. Ages are given in Ma. Monazites occurring in garnet are orange and matrix monazites are blue. The ages of *in situ* monazite have more spread over the interval 1710 – 1540 Ma. The combined data yields two ages of 1669 ± 5 Ma and 1579 ± 4 Ma with a relative misfit of 0.535. (c) REE spider plot of concordant analyses of both in situ (matrix-hosted = blue; garnet-hosted = orange) and grain mounted (purple) monazites. Grains hosted in garnet are typically more enriched in HREEs, whilst monazites occurring in the matrix have a range in HREE compositions. Grain mounted analyses are comparatively depleted in HREEs.

SFDD15-03

Monazites for sample SFDD15-03 were analysed in a grain mount. 46 analyses were collected from 29 grains ranging in size from 90 to 240 µm. Monazite grains are rounded and commonly contain zoning (e.g. Figure 16a). Individual spot ages for this sample range from 1570 to 1690 Ma and plot on concordia as two populations (Figure

16a). The unmix function in isoplot (Ludwig, 2012) yields ages of 1582 ± 9 Ma and 1668 ± 4 Ma for the two populations, with a relative misfit of 0.599. Monazites for this sample have a range in trace element compositions (Figure 16 c, d). Monazites of the younger population (< 1610 Ma) are typically more depleted in HREEs (Gd/Yb = 10 – 400) when compared to older monazites (> 1630 Ma), which have a Gd/Yb ratio ranging from 30 to 5000. Eu* is also generally higher in the younger analyses (0.40 – 0.75) with respect to the older analyses (0.15 – 0.45).

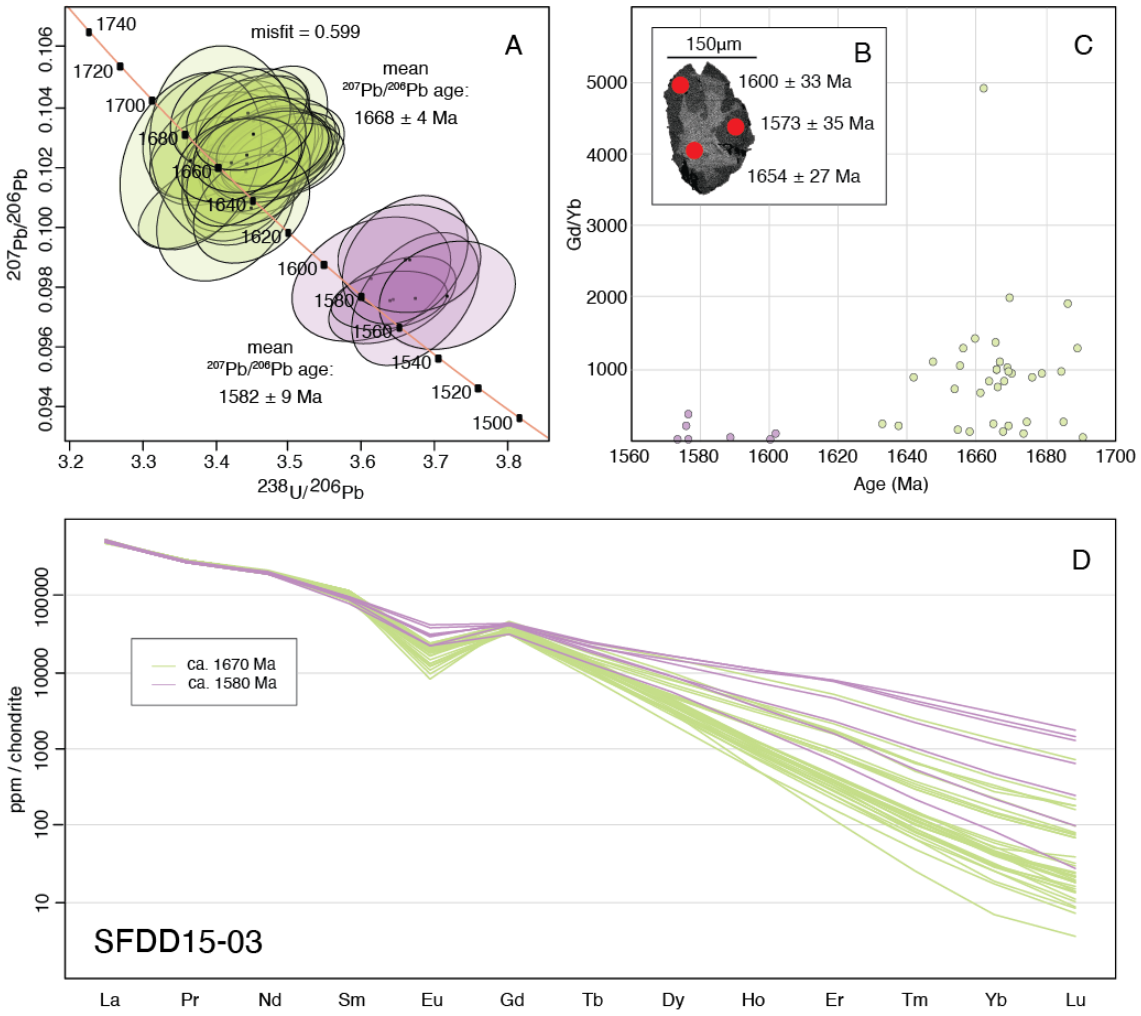

Figure 16: Monazite LA-ICP-MS results for sample SFDD15-03. (a) Terra-Wasserburg concordia plot with 2 sigma error ellipses. Ages are given in Ma. Concordant data yields two ages of 1668 ± 4 Ma and 1582 ± 9 Ma with a relative misfit of 0.599. The spots are coloured by age population. (b) BSE image of a monazite grain. The grain has an older core with a younger rim. (c) Gd/Yb ratios for concordant analyses show that the younger analyses are comparatively enriched in HREEs

whilst older analyses show more variation. (d) REE spider plot of concordant analyses illustrates that the younger analyses are more enriched in HREEs than the older analyses. The younger analyses also have a less prominent Eu anomaly.

SFDD01-04

In situ monazites analysed for sample SFDD01-04A were generally 20 to 100 μm in diameter, with one larger 180μm grain. 20 grains were ablated for a total of 31 analyses. Of the 20 grains, nine occur in quartz and are adjacent to either magnetite or clay (cordierite) inclusions. Three grains exist in clay domains and five grains occur within feldspars and have a corona of clay. The remaining three grains are hosted by magnetite, biotite or K-feldspar. Ages of 1585 – 1685 Ma were obtained, showing one large concordant population and one younger spot (Figure 17a). Some discordant analyses occur adjacent to the population. The population, consisting of 15 analyses, yielded a weighted mean age of 1662 ± 8 Ma (MSWD = 1.08). The younger spot resulted in an age of 1586 ± 31 Ma. For this sample, monazite hosted in quartz generally yields younger ages (1585 – 1670 Ma) than monazites hosted in other minerals (1655 – 1685 Ma; Figure 17a). Monazites are enriched in HREEs in comparison to other samples (Gd/Yb << 100; Figure 17b, c). The 1585 Ma grain is amongst the most enriched in HREEs. One other grain is particularly enriched in Nd, Sm, Eu and Gd. Eu anomalies (Eu*) for this sample vary from 0.35 to 0.7.

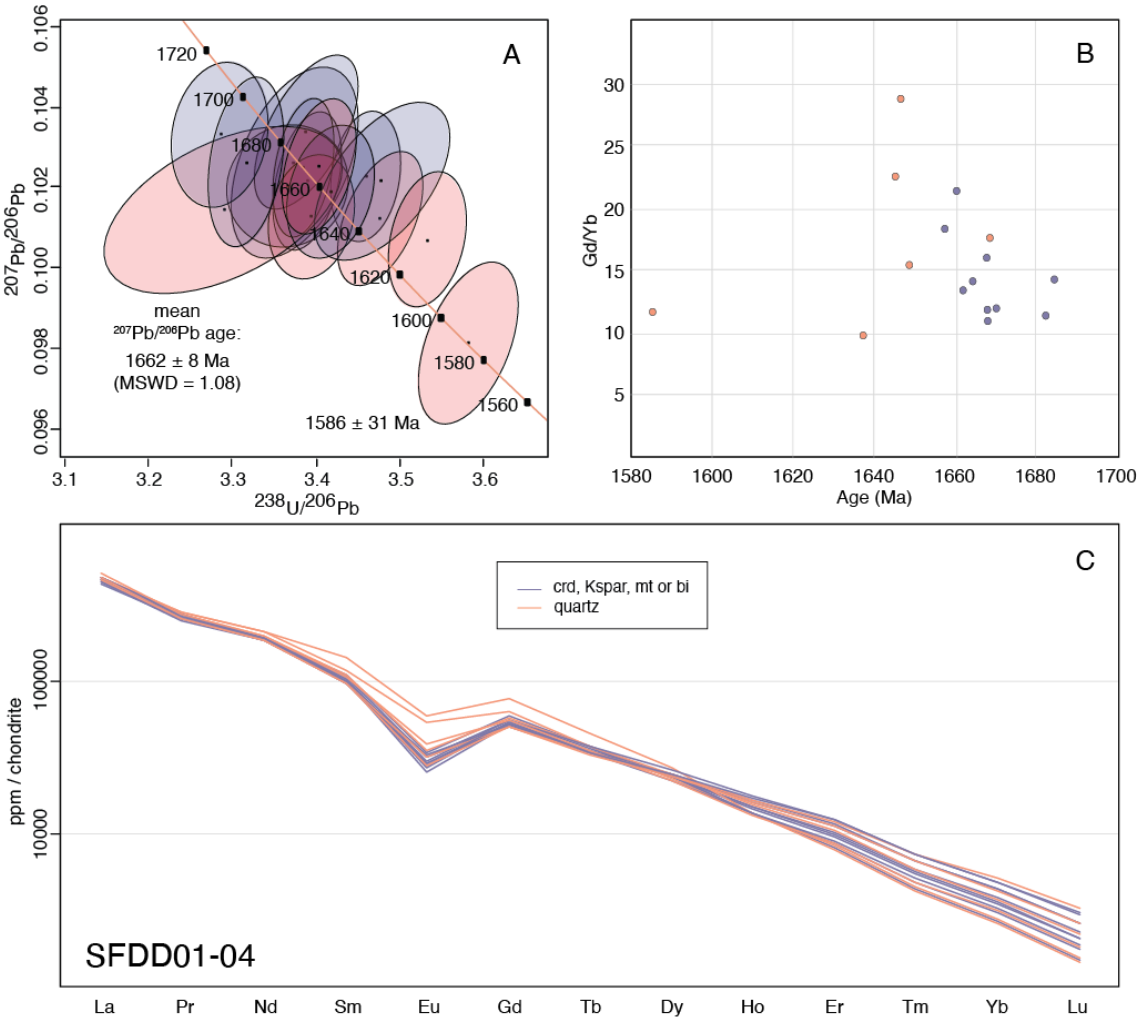

Figure 17: Monazite LA-ICP-MS results for sample SFDD01-04. (a) Terra-Wasserburg concordia plot with 2 sigma error ellipses. Ages are given in Ma. Concordant data is coloured by textural location – red analyses occur in quartz and blue analyses are hosted in cordierite, K-feldspar, magnetite or biotite. A population is present at 1662 ± 8 Ma (MSWD = 1.08) and a younger spot exists at 1586 ± 31 Ma. (b) Gd/Yb ratios for concordant analyses show the range of HREE compositions. The youngest spot is one of the most enriched in HREEs. (c) REE spider plot of concordant analyses shows that differences in grain location does not necessarily affect trace element composition. One grain (represented by two analyses) has high abundances of Nd, Sm, Eu and Gd.

SFDD01-17

28 analyses for sample SFDD01-17 were performed on 16 *in situ* monazites ranging in size from 30 to 120 μm. 13 of the grains occur in strongly foliated domains of biotite and sillimanite, whilst the remaining grains occur in a weakly foliated matrix of quartz, K-feldspar, cordierite and biotite. Four of the grains are elongated in the direction of

foliation (e.g. Figure 18a). Individual analysis ages for this sample range from 1570 – 1680 Ma and plot on concordia as two populations (Figure 18a). The unmix function in isoplot (Ludwig, 2012) yields ages of 1590 ± 10 Ma and 1662 ± 7 Ma for the two populations with a relative misfit of 0.566. Monazites are enriched in HREEs in comparison to other samples (Gd/Yb << 100; Figure 18b, c) and tend to show an inverse relationship between HREE enrichment and age. Eu anomalies for this sample are relatively prominent. Monazites of the ca. 1660 Ma population yield Eu* values from 0.08 to 0.18, whilst the younger population has higher Eu* values of 0.15 – 0.23.

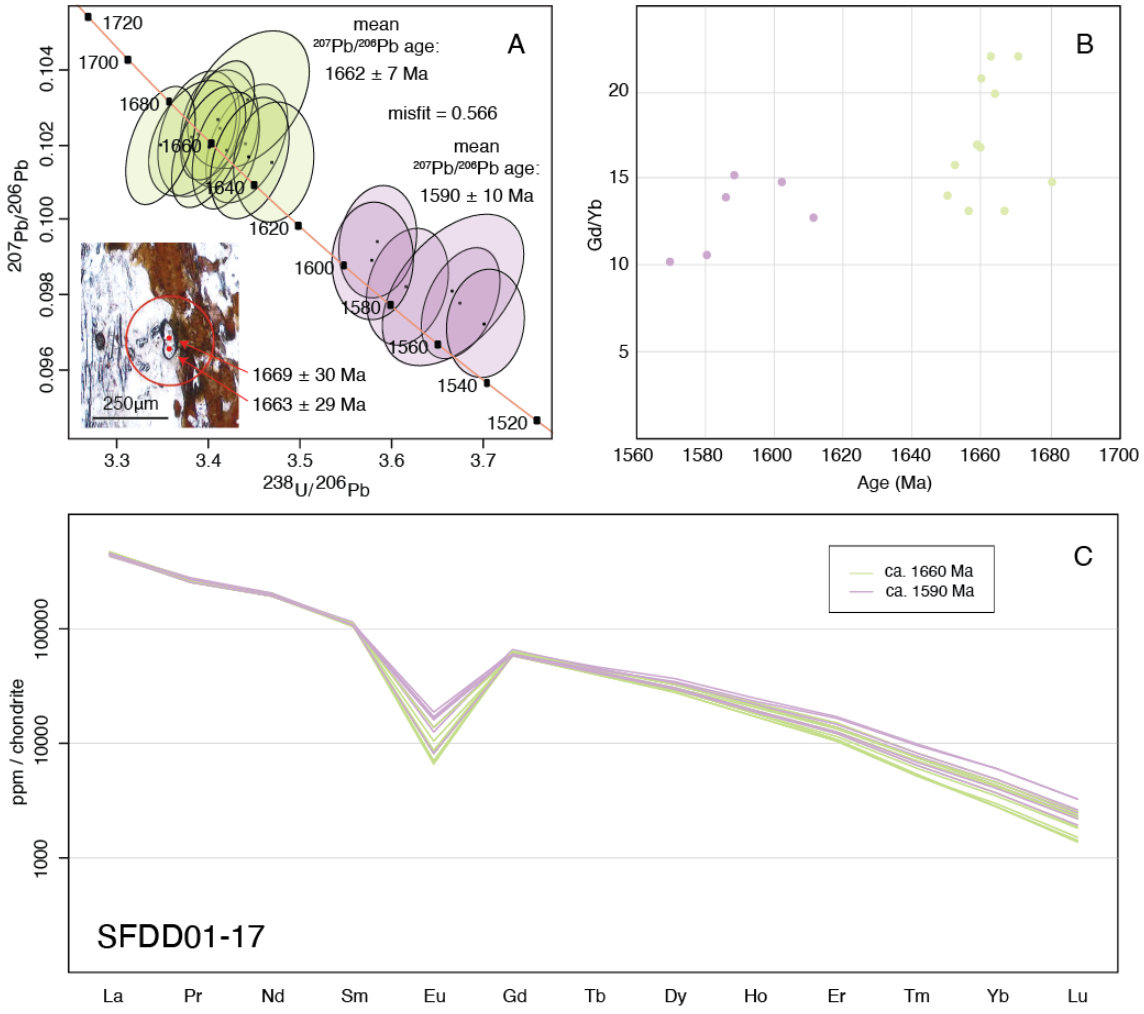

Figure 18: Monazite LA-ICP-MS results for sample SFDD01-17. (a) Terra-Wasserburg concordia plot with 2 sigma error ellipses. Ages are given in Ma. Concordant data is coloured by age population. The two populations yield ages of 1662 ± 7 Ma and 1590 ± 10 Ma with a relative misfit

of 0.566. Bottom left: transmitted light photomicrograph of a monazite grain parallel to the foliation. The grain yields ages of the older population. (b) Gd/Yb ratios for concordant analyses show that the younger grains are more enriched in HREEs than the older grains. (c) REE spider plot of concordant analyses showing an enrichment of HREEs compared to other samples.

SFDD15-01

Monazite grains for sample SFDD15-01 were analysed in a grain mount. 45 analyses were performed on 27 grains, 60 – 160 μm in size. Monazite grains are rounded and commonly contain zoning from a dark core to a light rim (Figure 19a). Geochronology returned ages a of spread between 1550 and 1690 Ma (Figure 19b). The unmix function in isoplot (Ludwig, 2012) yields two distinct ages of 1585 ± 6 Ma and 1664 ± 6 Ma with a relative misfit of 0.538. In comparison to other samples, monazite in SFDD15-01 is enriched in HREEs (Gd/Yb << 100; Figure 19c). Younger monazites is this sample commonly have a less pronounced Eu anomaly (Eu* 0.25 – 0.55) than older samples (Eu* 0.10 – 0.30, as well as two analyses ~ 0.50).

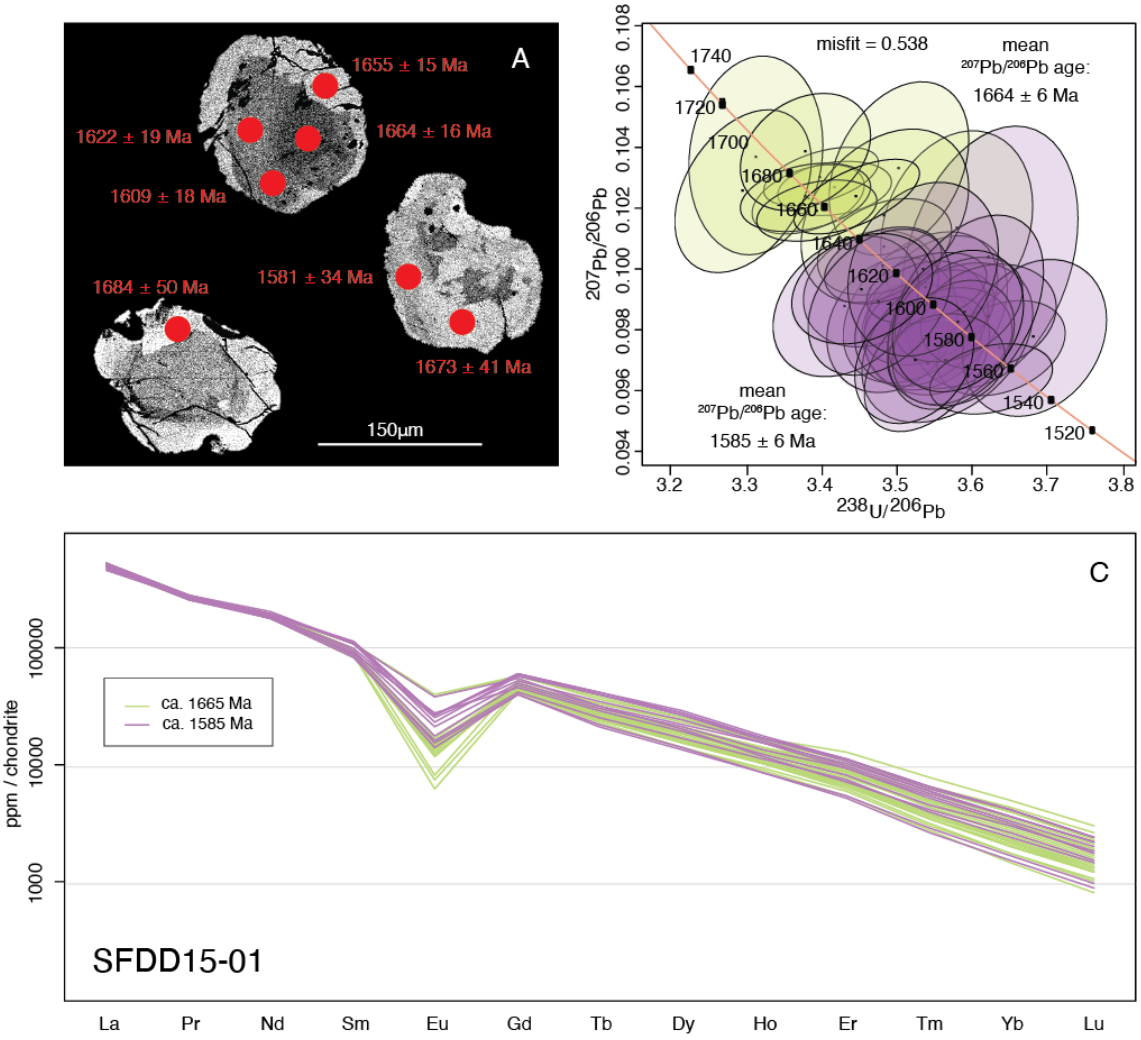

Figure 19: Monazite LA-ICP-MS results for sample SFDD15-01. (a) BSE image of three monazite grains. The grains are zoned and have ages which vary with the zoning. (b) Terra-Wasserburg concordia plot with 2 sigma error ellipses. Ages are given in Ma. Two populations are present: 1664 ± 6 Ma and 1585 ± 6 Ma, with a relative misfit of 0.538. (c) REE spider plot of concordant analyses coloured by isoplot age population (1664 Ma = green; 1585 Ma = purple). Younger analyses typically have a less pronounced Eu anomaly.

Whole-rock Geochemistry

Whole-rock geochemistry was obtained for six samples: SFDD01-09, SFDD01-12, SFDD01-13, SFDD01-14, SFDD01-17 and SFDD15-03. A suite of major oxides and trace elements was collected and is presented here. Further results are provided in Appendix E.

Fe_2O_3 is present in a range of abundances, from 2.9 wt% (SFDD01-17) to 58.5 wt% (SFDD01-14). SiO_2 ranges from 37 wt% (SFDD01-14) to 74.7 wt% (SFDD01-17). SiO_2 concentration is inversely proportional to Fe_2O_3 (Figure 20a). Al_2O_3 ranges from 2.5 wt% (SFDD01-14) to 17.4 wt% (SFDD01-13) and is also inversely proportional to Fe_2O_3 abundances (Figure 20a). Fe-poor sample SFDD01-17 is the most enriched in LREEs and is comparatively depleted in HREEs (Figure 20b). It also has the highest Gd/Yb ratio of 5.6.

SFDD01-09

Sample SFDD01-09 is a magnetite-rich, garnet-bearing gneiss with an overprinting mylonitic fabric. It has high iron content, 44.9 wt% Fe_2O_3 and contains 44.7 wt% SiO_2, 6.99 wt% Al_2O_3 and 2.52 wt% MgO.

SFDD01-12

Sample SFDD01-12 is a magnetite-rich, garnet-bearing gneiss. It contains less iron than SFDD01-09, at 32.9 wt% Fe_2O_3. It has a similar silica content, 44.9 wt% SiO_2, but contains more Al_2O_3 and MgO, at 14.9 wt% and 3.9 wt%, respectively.

SFDD01-17

Sample SFDD01-17 is a magnetite-poor, bi-sill-qtz-kspar-crd gneiss. It contains significantly less iron – only 2.9 wt% Fe_2O_3. Silica and aluminium are high, at 74.7 wt% SiO_2 and 14.1 wt% Al_2O_3. MgO comprises just 2.3 wt% of the sample.

SFDD15-03

Sample SFDD15-03 is a magnetite-rich, garnet-bearing gneiss. It contains abundant iron, at 42.5 wt% Fe_2O_3. It also has 44.0 wt% SiO_2, 9.5 wt% Al_2O_3 and 2.8 wt% MgO.

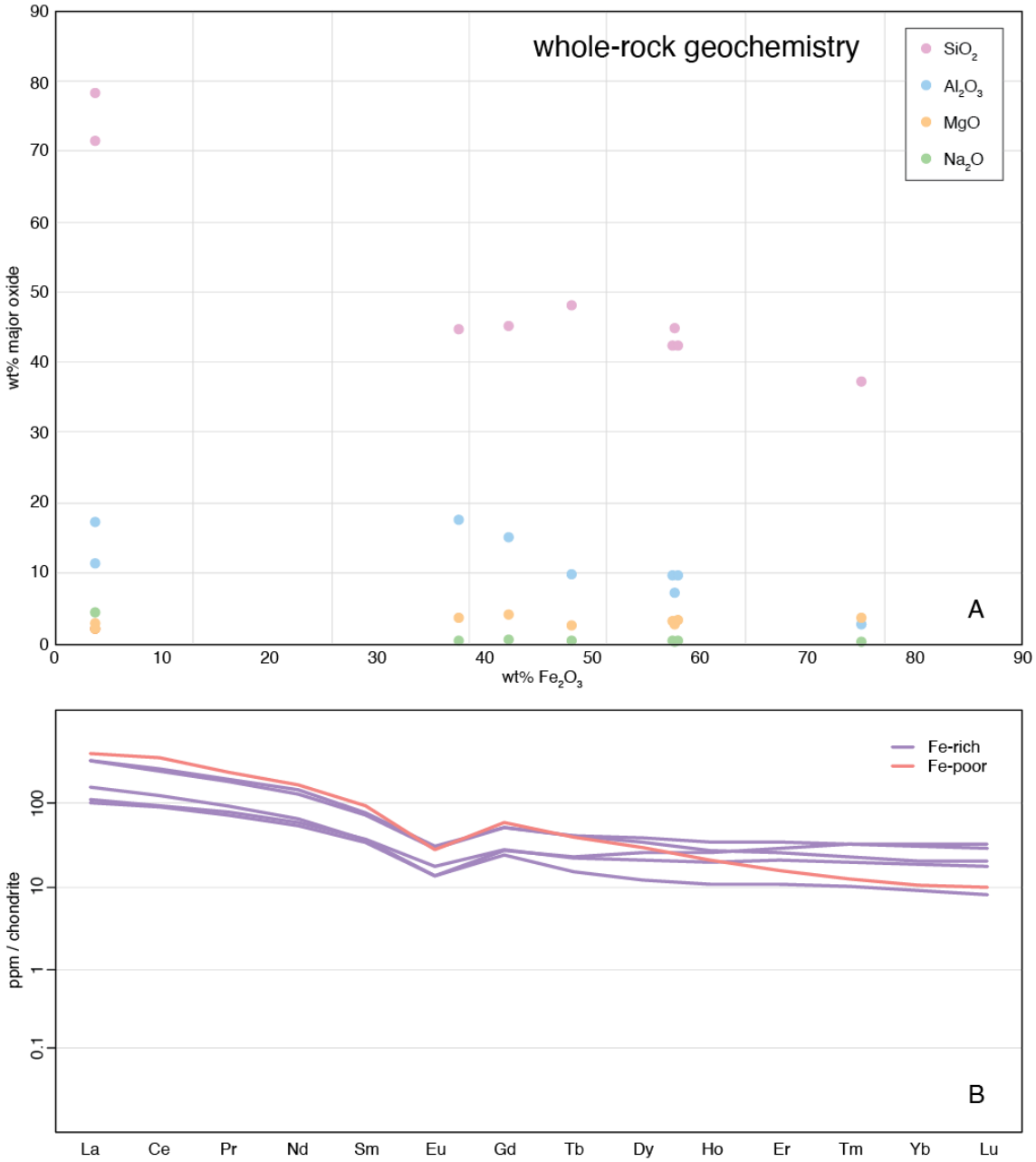

Figure 20: Summary of whole-rock geochemistry results. (a) Plot showing abundances of major oxides SiO_2 (pink), Al_2O_3 (blue), MgO (yellow) and Na_2O (green) against Fe_2O_3 abundance. Concentrations given in wt%. Strong trends are observed between SiO_2 and Fe_2O_3, as well as Al_2O_3 and Fe_2O_3. (b) REE spider plot showing trace element abundances for the whole-rock samples. Fe-poor sample SFDD01-17 (orange) is more enriched in LREEs and depleted in HREEs than Fe-rich samples (purple).

DISCUSSION

Style of metamorphism

The rocks which host the magnetite mineralisation in the Snaefell deposit are granulite facies metasediments. The mineral assemblages are characterised by garnet + quartz + biotite + magnetite ± K-feldspar ± plagioclase and quartz + K-feldspar + biotite + magnetite ± plagioclase ± cordierite ± sillimanite. The presence of cordierite-bearing mineral assemblages suggests metamorphic conditions were of comparatively low pressures (Sorcar, Joshi, Oliveira, Tomson & Nandakumar, 2020; Yin, Zhao & Sun, 2015). P-T calculations performed on similar mineral assemblages in rocks of broadly similar compositions suggest these assemblages formed under conditions of 700 – 800°C and 4 – 6 kbar (White, Powell & Clarke, 2003). Preservation of granulite facies assemblages implies that these rocks underwent significant amounts of melt loss (White & Powell, 2002).

The granulites are foliated and define a regional E-W-NE structural trend (Figure 21). In some cases, granulite facies assemblages have seen secondary garnet growth and are crosscut by mylonitic shear zones. It is interpreted that deformation was a multi-stage process. The first stage involved folding to a broad, shallowly plunging synform (F2; Figure 21). The second stage of folding oriented the units into an E-W-NE structure. A possible third stage saw the development of north dipping D3 shear zones (Figure 21) and is associated with secondary garnet growth.

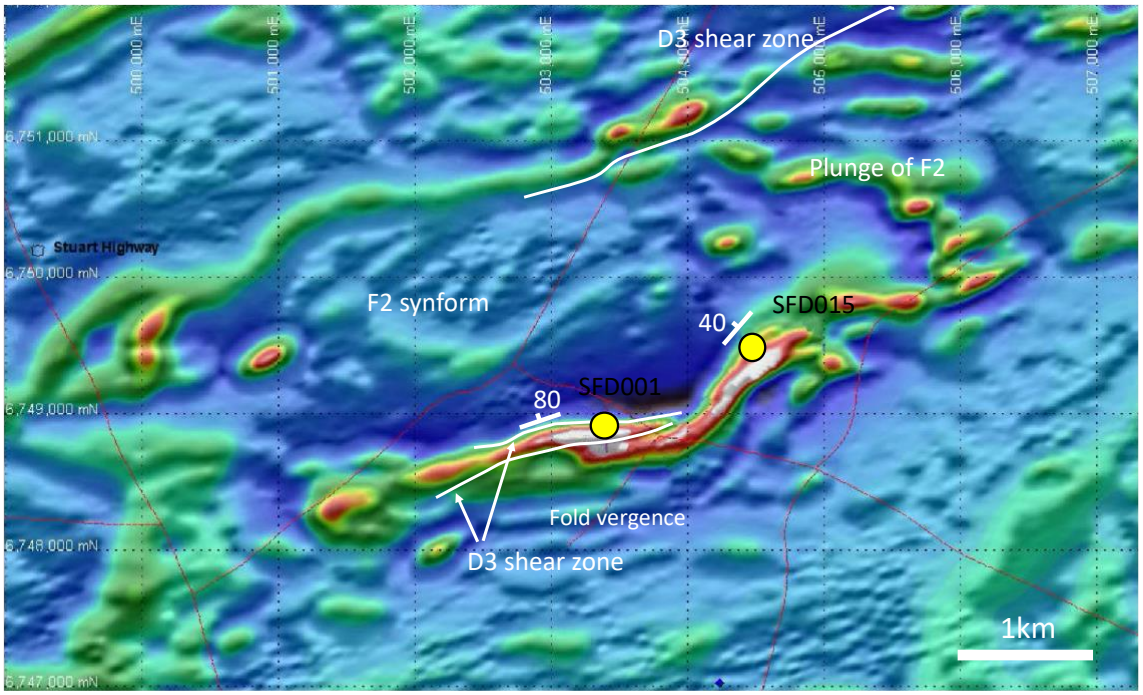

Figure 21: Structural interpretation of the Snaefell deposit (after Fahey, 2011). Base map is a total magnetite intensity (TMI) image. Snaefell makes up the highly magnetitic (red and white) E-W-NE trending elongate structure in the centre. Beds in the SW of the magnetic body are more steeply dipping than in the NE. The F2 synform (dashed white line) is defined by a composite S0/S1 surface. North dipping D3 shear zones (solid white lines) are approximately parallel to the structure of the magnetitic body.

Zircon geochronology

Zircons from this study yield $^{207}Pb/^{206}Pb$ population ages of 1749 ± 15 Ma and 1673 ± 16 Ma. One other concordant analysis produced a $^{207}Pb/^{206}Pb$ age 1612 ± 23 Ma. Trace elemental analysis reveals at least two distinct compositional groups within the samples: those which are relatively enriched in LREEs and those which are relatively depleted in LREEs. The two compositions are present in both the 1749 Ma and 1673 Ma zircons. Zircons of the population 1749 ± 15 Ma are interpreted to represent the protolithic age of the metasediments. The population 1673 ± 16 Ma is interpreted to represent metamorphic zircon growth. The single concordant zircon analysis at 1612 Ma is interpreted as an older zircon which has been partially reset during later metamorphism.

The compositions which have flat REE patterns and 'murky' CL images may be indicate of a hydrothermal origin (Hoskin, 2005; Vetrin & Skublov, 2016; Yang et al., 2014). If the zircons in this study are hydrothermal, they must have grown in the absence of monazite or during the break down of monazite due to the partitioning of LREEs into monazite (Stepanov, Hermann, Rubatto & Rapp, 2012).

Monazite geochronology

Monazites from this study yielded three $^{207}Pb/^{206}Pb$ age populations: 1670 – 1660 Ma, 1590 – 1580 Ma and 1559 ± 10 Ma (Figure 22). The 1673 ± 16 Ma zircons are within error of the 1670 – 1660 Ma monazite group and are therefore considered a product of the same period of mineral growth. Single monazite analyses of the ages 1610 – 1580 Ma are considered to belong to the 1670 – 1660 Ma population and have been partially reset during metamorphism. The three stages of metamorphic monazite growth are consistent with the three-stage interpretation of deformation.

The LREE (La to Sm) compositions of monazites throughout this study are quite similar, ranging from 10^6 to 10^5 ppm / chondrite. The concentrations of Eu and the HREEs are more variable. Eu anomalies (Eu*) range from 0.10 to 0.95. The presence of plagioclase in some samples may be responsible for more pronounced Eu anomalies (Rubatto, 2002; Schaltegger et al., 1999). In addition to this, monazite aged 1670 – 1660 Ma tends to be more depleted in Eu relative to monazite aged 1590 – 1580 Ma. The HREEs are comparatively depleted in garnet-bearing assemblages. This depletion is interpreted to be an effect of partitioning of the HREEs into garnet (Hickmott, Shimizu, Spear & Selverstone, 1987; Warren et al., 2019; Zhu & O'Nions, 1999).

In situ monazite occurring as inclusions in porphyroblastic garnet generally returned ages of 1670 – 1660 Ma and compositions which are enriched in the HREEs. Hence, it

is interpreted that monazite growth during the period 1670 – 1660 Ma was in the absence of garnet and that garnet likely grew during metamorphism of the age 1590 – 1580 Ma. Secondary garnet growth was coeval with the development of the ca. 1560 Ma mylonitic fabric.

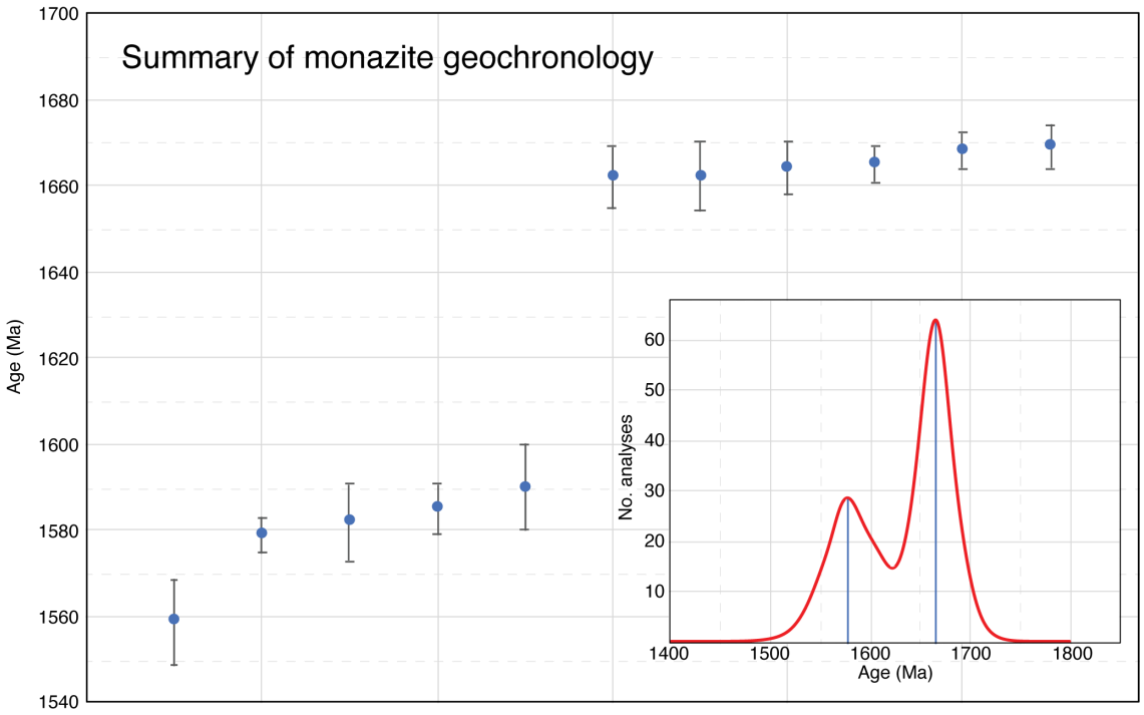

Figure 22: Summary of monazite geochronology from this study. Mean ages from the geochronological populations in the samples are plotted in age order with 2σ error bars. Two distinct ages are present at ca. 1670 – 1660 Ma and ca. 1590 – 1580 Ma. Sample SFDD01-09 yields a younger mean age at 1559 Ma. Inset: age probability plot highlighting the statistical significance of the two older ages.

New constraints on mineralisation

Fe-oxides at the Snaefell deposit are, in general, abundant and highly deformed. In garnet-bearing gneisses, Fe-oxide grains are typically coarse and deformed in a strongly foliated pelitic layering. In the garnet-absent gneisses, Fe-oxides occur in the matrix and may be elongated in the direction of foliation. Significant deformation of Fe-oxide

grains within the samples suggests that Fe-oxides were present before the occurrence of deformation.

The gneisses analysed in this study have a composition which varies on the scale of millimetres to metres. It is likely that the abundance of Fe-oxides, which ranges from 2 to 60 % Fe_2O_3 between samples, is controlled by the amount of melt loss experienced during high temperature metamorphism. This hypothesis is supported by the whole-rock geochemistry which shows that Fe_2O_3 concentration is inversely proportional to SiO_2 and Al_2O_3. Therefore, as SiO_2 was lost, Fe_2O_3 increased in concentration. This process is also documented at the Warramboo magnetite deposit and related Price Metasediments (Morrissey et al., 2016).

The possible presence of hydrothermal zircon may indicate that magnetite is also of a hydrothermal source which predate metamorphism. The commonality of U-Pb concordia-discordant and LREE-enriched zircon across the Gawler Craton may represent a previously unaccounted for widespread hydrothermal event during the late Paleoproterozoic to early Mesoproterozoic.

Regional significance of metamorphism

The new geochronology yields a protolithic age of 1749 ± 15 Ma which is consistent with protolithic ages of the Mount Woods Inlier (Chalmers, 2007; Jagodzinski et al., 2007; O'Sullivan, 2010).

New monazite geochronology yields a metamorphic age of 1670 – 1660 Ma. Metamorphism of this age has not previously been reported for the Mount Woods Inlier, however, some similar ages are obtained in the Western Gawler Craton. Howard, Hand, Barovich, Payne and Belousova (2011), Payne et al. (2008) and (Teasdale, 1997) relate metamorphic ages of 1720 – 1660 Ma and ca. 1690 Ma to the Kimban Orogeny. Payne

et al. (2008) suggests metamorphism of the age ca. 1660 Ma indicates the presence of a slightly younger, unknown event. In a more recent paper, Cutts et al. (2013) relates metamorphic ages of the period ca. 1690 – 1665 Ma to the ultrahigh temperature Ooldean event. This new geochronology may indicate the presence of Ooldean-aged metamorphism in the northern Gawler Craton, or that orogenesis related to the Kimban occurred in the northern Gawler Craton for longer than the accepted 1730 – 1690 Ma time period.

New 1590 – 1580 Ma metamorphic ages are consistent with ca. 1600 – 1585 Ma Hiltaba Event metamorphic and magmatic ages obtained in the northern and south-eastern Gawler Craton, including within the Mount Woods Inlier (Chalmers, 2007; Cutts et al., 2011; Holm, 2004; Jagodzinski, 2005; Jagodzinski et al., 2007; Morrissey et al., 2013). The new monazite geochronology of age 1590 – 1580 Ma is interpreted as metamorphism due to magmatism of the Hiltaba Event.

The new monazite age of 1559 ± 10 Ma corresponds to metamorphic ages of the Kararan Orogeny in the northern and western Gawler Craton (Fanning et al., 2007; Hand et al., 2007; Payne, Barovich & Hand, 2006; Payne et al., 2008). Within the Mount Woods Inlier, O'Sullivan (2010) suggests that ages of 1558 ± 9 Ma represent hydrothermal activity and Tiddy et al. (2020) attributes $^{40}Ar/^{39}Ar$ biotite cooling ages of 1560 Ma and 1540 Ma to exhumation along the Southern Overthrust.

CONCLUSIONS

1. The rocks which host magnetite mineralisation were metamorphosed to granulite facies conditions – possibly to 700 – 800°C and 4 – 6 kbar. Three phases of

metamorphic mineral growth occurred. Deformation occurred during all three phases.

2. New zircon geochronology 1749 ± 15 Ma represents protolith age and is consistent with ca. 1750 Ma protolithic ages across the Mount Woods Inlier.
3. New geochronology yields three distinct metamorphic ages:
    (a) Zircon ages of 1673 ± 16 Ma and monazite ages of 1670 – 1660 Ma are considered equivalent and represent previously unrecognised ages in the northern Gawler Craton. These ages may indicate that the ca. 1720 – 1690 Ma Kimban Orogeny was longer-lasting than previous literature states, or that the 1690 – 1665 Ma Ooldean event in the western Gawler Craton also affected parts of the northern Gawler Craton.
    (b) Monazites which yield ages 1590 – 1580 Ma represent metamorphism which occurred during the magmatic Hiltaba Event.
    (c) 1559 ± 10 Ma monazite ages are attributed to the Kararan Orogeny.
4. Magnetite mineralisation predates deformation. The possible presence of hydrothermal zircons suggests a period of hydrothermal activity before or during high grade metamorphism. Magnetite may have been sourced from hydrothermal fluids.

ACKNOWLEDGMENTS

I would like to acknowledge and thank my supervisors, Prof. Martin Hand and Dr Laura Morrissey, for their tireless support over the course of this project. Special thanks are also given to the Geological Society of Australia – South Australia Division, Playford Trust and MinEx-CRC for funding this project.
Thank you to Dr Sarah Gilbert for her assistance with data acquisition and processing. Lastly, thank you to the honours cohort of 2020, and particularly to Samantha March for her persistent encouragement throughout the year.

REFERENCES

ARMIT, R., BETTS, P., SCHAEFER, B., YI, K., KIM, Y., DUTCH, R. A., .REID, A., JAGODZINSKI, L., GILES, D. & AILLERES, L. 2017. Late Palaeoproterozoic evolution of the buried northern Gawler Craton. *Precambrian Research* **291**, 178-201.

BELOUSOVA, E., GRIFFIN, W. L., O'REILLY, S. Y. & FISHER, N. 2002. Igneous zircon: trace element composition as an indicator of source rock type. *Contributions to Mineralogy and Petrology* **143**, 602-622.

BELPERIO, A., FLINT, R. & FREEMAN, H. 2007. Prominent Hill: A hematite-dominated, iron oxide copper-gold system. *Economic Geology* **102**, 1499-1510.

BETTS, P. G., ARMIT, R., STEWART, J., AITKEN, A., AILLERES, L., DONCHAK, P., HUTTON, L., WITHNALL, I & GILES, D. 2015. Australia and Nuna. *Geological Society London Special Publications* **424**.

BETTS, P. G. & GILES, D. 2006. The 1800–1100 Ma tectonic evolution of Australia. *Precambrian Research* **144**, 92-125.

BETTS, P. G., VALENTA, R. K. & FINLAY, J. 2003. Evolution of the Mount Woods Inlier, northern Gawler Craton, Southern Australia: an integrated structural and aeromagnetic analysis. *Tectonophysics* **366**, 83-111.

BOWDEN, B., FRASER, G., DAVIDSON, G. J., MEFFRE, S., SKIRROW, R., BULL, S. & THOMPSON, J. 2017. Age constraints on the hydrothermal history of the Prominent Hill iron oxide copper-gold deposit, South Australia. *Mineralium Deposita* **52**, 863-881.

BUDD, A. 2006. *The Tarcoola Goldfield of the Central Gawler Gold Province, and the Hiltaba Association Granites, Gawler Craton, South Australia.* (Doctor of Philosophy). Australian National University, Canberra.

BUDD, A., WYBORN, L. & BASTRAKOVA, I. 2001. *The metallogenic potential of Australian Proterozoic granites*. Geoscience Australia Record 2001/12.

CHALMERS, N. 2007. *Mount Woods domain: Proterozoic metasediments and intrusives*. South Australia. Department of Primary Industries and Resources. Report Book 20.

CLARK, J. 2014. Defining the style of mineralisation at the Cairn Hill magnetite-sulphide deposit, Mount Woods Inlier, Gawler Craton, South Australia. Honours Thesis, University of Adelaide, South Australia.

CREASER, R. A. & COOPER, J. A. 1993. U-Pb geochronology of middle Proterozoic felsic magmatism surrounding the Olympic Dam Cu-U-Au-Ag and Moonta Cu-Au-Ag deposits, South Australia. *Economic Geology* **88**, 186-197.

CUTTS, K., HAND, M. & KELSEY, D. 2011. Evidence for early Mesoproterozoic (ca. 1590 Ma) ultrahigh-temperature metamorphism in southern Australia. *Lithos* **124,** 1-16.

CUTTS, K., KELSEY, D. & HAND, M. 2013. Evidence for late Paleoproterozoic (ca 1690–1665 Ma) high-to ultrahigh-temperature metamorphism in southern Australia: implications for Proterozoic supercontinent models. *Gondwana Research* **23**, 617-640.

DALY, S. 1998. Tectonic evolution and exploration potential of the Gawler Craton, South Australia. *AGSO Journal of Australian Geology and Geophysics* **17**, 145-168.

DAVIES, M. & TWINING, M. 2018. Magnetite: South Australia's potential. *MESA Journal* **86**, 30-44.

DREXEL, J. F., PREISS, W. V. & PARKER, A. J. 1993. *The Geology of South Australia*. Geological Survey of South Australia.

DUTCH, R., HAND, M. & KELSEY, D. 2010. Unravelling the tectonothermal evolution of reworked Archean granulite facies metapelites using in situ geochronology: an example from the Gawler Craton, Australia. *Journal of Metamorphic Geology* **28**, 293-316.

FAHEY, I. 2011, December. [Snaefell resource notes, 2nd resource model (core zone and Barrule)].

FANNING, C. 1993. Ion-microprobe *U–Pb zircon dating of the Mount Woods Inlier, Preliminary Results (Unpublished)*. Research School of Earth Sciences, Australian National University.

FANNING, C., FLINT, R., PARKER, A., LUDWIG, K. & BLISSETT, A. 1988. Refined Proterozoic evolution of the Gawler Craton, South Australia, through U-Pb zircon geochronology. *Precambrian Research* **40-41**, 363-386.

FANNING, C., REID, A. & TEALE, G. 2007. *A geochronological framework for the Gawler Craton, South Australia*. Geological Survey of South Australia Bulletin 55.

FERRIS, G. M., SCHWARZ, M. P. & HEITHERSAY, P. 2002. The geological framework, distribution and controls of Fe-oxide Cu-Au mineralisation in the Gawler Craton, South Australia. Part I–Geological and tectonic framework. *Hydrothermal iron oxide copper-gold and related deposits: A global perspective* 2, 9-31.

FINLAY, J. 1993. Structural interpretation in the Mount Woods Inlier. Honours Thesis, Monash University, Melbourne.

FORBES, C., GILES, D., HAND, M., BETTS, P. G., SUZUKI, K., CHALMERS, N., & DUTCH, R. 2011. Using P–T paths to interpret the tectonothermal setting of prograde metamorphism: An example from the northeastern Gawler Craton, South Australia. *Precambrian Research* **185**, 65-85.

FORBES, C., GILES, D., JOURDAN, F., SATO, K., OMORI, S. & BUNCH, M. 2012. Cooling and exhumation history of the northeastern Gawler Craton, South Australia. *Precambrian Research* **200**, 209-238.

FRASER, G. & LYONS, P. 2006. Timing of Mesoproterozoic tectonic activity in the northwestern Gawler Craton constrained by 40Ar/39Ar geochronology. *Precambrian Research* **151**, 160-184.

FRASER, G., MCAVANEY, S., NEUMANN, N., SZPUNAR, M. & REID, A. 2010. Discovery of early Mesoarchean crust in the eastern Gawler Craton, South Australia. *Precambrian Research* **179**, 1-21.

FRASER, G., REID, A. & STERN, R. 2012. Timing of deformation and exhumation across the Karari Shear Zone, north-western Gawler Craton, South Australia. *Australian Journal of Earth Sciences* **59**, 547-570.

FRICKE, C., PREISS, W. & NEUMANN, N. 2010. *Curnamona Province: a Paleo-to Mesoproterozoic time slice.* Paper presented at the South Australian Seismic and MT Workshop 2010.

GILES, D., BETTS, P. G. & LISTER, G. S. 2004. 1.8–1.5-Ga links between the north and south Australian cratons and the early–middle Proterozoic configuration of Australia. *Tectonophysics* **380**, 27-41.

HALPIN, J. A. & REID, A. J. 2016. Earliest Paleoproterozoic high-grade metamorphism and orogenesis in the Gawler Craton, South Australia: The southern cousin in the Rae family? *Precambrian Research* **276**, 123-144.

HAND, M., REID, A. & JAGODZINSKI, L. 2007. Tectonic Framework and Evolution of the Gawler Craton, Southern Australia. *Economic geology and the bulletin of the Society of Economic Geologists* **102**, 1377-1395.

HARRIS, T., MURPHY, F., FUNK, C. & BETTS, P. 2013. *Mt Woods 2D seismic reflection survey, Gawler craton, South Australia: An intergrated minerals exploration case study*. ASEG-PESA 23rd International Geophysical Conference and Exhibition. CSIRO Publishing, Melbourne.

HELLSTROM, J., PATON, C., WOODHEAD, J. & HERGT, J. 2008. Iolite: software for spatially resolved LA-(quad and MC) ICPMS analysis. *Mineralogical Association of Canada short course series* **40**, 343–348.

HICKMOTT, D., SHIMIZU, N., SPEAR, F. S. & SELVERSTONE, J. 1987. Trace-element zoning in a metamorphic garnet. *Geology* **15**, 573-576.

HOLM, O. 2004. *New geochronology of the Mount Woods Inlier and the central Gawler gold province*. Paper presented at the Gawler craton: State of play conference, Adelaide.

HOSKIN, P. W. 2005. Trace-element composition of hydrothermal zircon and the alteration of Hadean zircon from the Jack Hills, Australia. *Geochimica et Cosmochimica Acta* **69**, 637-648.

HOWARD, K., HAND, M., BAROVICH, K. & BELOUSOVA, E. 2011. Provenance of late Paleoproterozoic cover sequences in the central Gawler Craton: exploring stratigraphic correlations in eastern Proterozoic Australia using detrital zircon ages, Hf and Nd isotopic data. *Australian Journal of Earth Sciences* **58**, 475-500.

HOWARD, K., HAND, M., BAROVICH, K., PAYNE, J. & BELOUSOVA, E. 2011. U–Pb, Lu–Hf and Sm–Nd isotopic constraints on provenance and depositional timing of metasedimentary rocks in the western Gawler Craton: Implications for Proterozoic reconstruction models. *Precambrian Research* **184**, 43-62.

HOWARD, K., HAND, M., BAROVICH, K., PAYNE, J., CUTTS, K. & BELOUSOVA, E. 2011. U–Pb zircon, zircon Hf and whole-rock Sm–Nd isotopic constraints on the evolution of Paleoproterozoic rocks in the northern Gawler Craton. *Australian Journal of Earth Sciences* **58**, 615-638.

JACKSON, S. E., PEARSON, N. J., GRIFFIN, W. L. & BELOUSOVA, E. A. 2004. The application of laser ablation-inductively coupled plasma-mass spectrometry to in situ U–Pb zircon geochronology. *Chemical geology* **211**, 47-69.

JAGODZINSKI, E. 2005. *Compilation of SHRIMP U-Pb geochronological data, Olympic Domain, Gawler Craton, South Australia, 2001-2003*. Geoscience Australia Record 20.

JAGODZINSKI, E., REID, A., CHALMERS, N., SWAIN, G., FREW, R. & FOUDOULIS, C. 2007. *Compilation of SHRIMP U-Pb geochronological data for the Gawler craton, South Australia, 2007*. Primary Industries and Resources South Australia.

LANE, K., JAGODZINSKI, E., DUTCH, R., REID, A. & HAND, M. 2015. Age constraints on the timing of iron ore mineralisation in the southeastern Gawler Craton. *Australian Journal of Earth Sciences* **62**, 55-75.

LAWRENCE, M. G. & KAMBER, B. S. 2006. The behaviour of the rare earth elements during estuarine mixing—revisited. *Marine Chemistry* **100**, 147-161.

LOADER, M. A., WILKINSON, J. J. & ARMSTRONG, R. N. 2017. The effect of titanite crystallisation on Eu and Ce anomalies in zircon and its implications for the assessment of porphyry Cu deposit fertility. *Earth and Planetary Science Letters* **472**, 107-119.

LUDWIG, K. 2012. *Isoplot 3.75: A Geochronological toolkit for Microsoft Excel*. Berkeley Geochronology Center Special Publication 5.

MAIDMENT, D. W. 2005. Palaeozoic high-grade metamorphism within the Centralian Superbasin, Harts Range region, central Australia. PhD Thesis, Australian National University, Canberra.

MCDONOUGH, W. F. & SUN, S.-S. 1995. The composition of the Earth. *Chemical geology* **120**, 223-253.

MORRISSEY, L., BAROVICH, K., HAND, M., HOWARD, K. & PAYNE, J. 2019. Magmatism and metamorphism at ca.1.45 Ga in the northern Gawler Craton: The Australian record of rifting within Nuna (Columbia). *Geoscience Frontiers* **10,** 175-194.

MORRISSEY, L., HAND, M., LANE, K., KELSEY, D. & DUTCH, R. 2016. Upgrading iron-ore deposits by melt loss during granulite facies metamorphism. *Ore geology reviews* **74**, 101-121.

MORRISSEY, L., HAND, M., WADE, B. & SZPUNAR, M. 2013. Early Mesoproterozoic metamorphism in the Barossa Complex, South Australia: links with the eastern margin of Proterozoic Australia. *Australian Journal of Earth Sciences* **60**, 769-795.

O'SULLIVAN, S. 2010. The Depositional and Clast Provenance Age of the Coodnambana Metaconglomerate, Mount Woods Inlier. Honours Thesis, University of Adelaide, South Australia.

PATON, C., HELLSTROM, J., PAUL, B., WOODHEAD, J. & HERGT, J. 2011. Iolite: Freeware for the visualisation and processing of mass spectrometric data. *Journal of Analytical Atomic Spectrometry* **26**, 2508-2518. doi:10.1039/C1JA10172B

PAYNE, J. L., BAROVICH, K. M. & HAND, M. 2006. Provenance of metasedimentary rocks in the northern Gawler Craton, Australia: Implications for Palaeoproterozoic reconstructions. *Precambrian Research* **148**, 275-291.

PAYNE, J. L., FERRIS, G., BAROVICH, K. M. & HAND, M. 2010. Pitfalls of classifying ancient magmatic suites with tectonic discrimination diagrams: An example from the Paleoproterozoic Tunkillia Suite, southern Australia. *Precambrian Research* **177**, 227-240.

PAYNE, J. L., HAND, M., BAROVICH, K. M. & WADE, B. 2008. Temporal constraints on the timing of high-grade metamorphism in the northern Gawler Craton: implications for assembly of the Australian Proterozoic. *Australian Journal of Earth Sciences* **55**, 623-640.

REID, A. 2019. The Olympic Cu-Au Province, Gawler Craton: A Review of the Lithospheric Architecture, Geodynamic Setting, Alteration Systems, Cover Successions and Prospectivity. *Minerals* **9**, 371.

REID, A., CURTIS, S. & FRASER, G. 2008. Nature of the Kimban Orogeny across northern Eyre Peninsula. *MESA Journal* **51**, 25-34.

REID, A., HALPIN, J. & DUTCH, R. 2019. Timing and style of high-temperature metamorphism across the Western Gawler Craton during the Paleo-to Mesoproterozoic. *Australian Journal of Earth Sciences* **66**, 1085-1111.

REID, A. & HAND, M. 2012. Mesoarchean to mesoproterozoic evolution of the southern Gawler Craton, South Australia. *Episodes* **35**, 216-225.

REID, A., HAND, M., JAGODZINSKI, E., KELSEY, D. & PEARSON, N. 2008. Paleoproterozoic orogenesis in the southeastern Gawler Craton, South Australia. *Australian Journal of Earth Sciences* **55**, 449-471.

REID, A., JAGODZINSKI, E., ARMIT, R., DUTCH, R., KIRKLAND, C., BETTS, P. & SCHAEFER, B. 2014. U-Pb and Hf isotopic evidence for Neoarchean and Paleoproterozoic basement in the buried northern Gawler Craton, South Australia. *Precambrian Research* **250**, 127-142.

REID, A., JAGODZINSKI, E., FRASER, G. & PAWLEY, M. 2014. SHRIMP U–Pb zircon age constraints on the tectonics of the Neoarchean to early Paleoproterozoic transition within the Mulgathing Complex, Gawler Craton, South Australia. *Precambrian Research* **250**, 27-49.

REID, A., PAWLEY, M., WADE, C., JAGODZINSKI, E., DUTCH, R. & ARMSTRONG, R. 2020. Resolving tectonic settings of ancient magmatic suites using structural, geochemical and isotopic constraints: the example of the St Peter Suite, southern Australia. *Australian Journal of Earth Sciences* **67**, 31-58.

RUBATTO, D. 2002. Zircon trace element geochemistry: partitioning with garnet and the link between U–Pb ages and metamorphism. *Chemical Geology* **184**, 123-138.

RUTHERFORD, L., HAND, M. & BAROVICH, K. 2007. Timing of Proterozoic metamorphism in the southern Curnamona Province: implications for tectonic models and continental reconstructions. *Australian Journal of Earth Sciences* **54**, 65-81.

SCHALTEGGER, U., FANNING, C. M., GÜNTHER, D., MAURIN, J. C., SCHULMANN, K. & GEBAUER, D. 1999. Growth, annealing and recrystallization of zircon and preservation of monazite in high-grade metamorphism: conventional and in-situ U-Pb isotope, cathodoluminescence and microchemical evidence. *Contributions to Mineralogy and Petrology* **134**, 186-201.

SCHLEGEL, T. U., WAGNER, T., WÄLLE, M. & HEINRICH, C. A. 2018. Hematite breccia-hosted iron oxide copper-gold deposits require magmatic fluid components exposed to atmospheric oxidation: evidence from Prominent Hill, Gawler Craton, South Australia. *Economic Geology* **113**, 597-644.

SKIRROW, R., BASTRAKOV, E., BAROVICH, K., FRASER, G., CREASER, R., FANNING, C., RAYMOND, C. & DAVIDSON, G. 2007. Timing of Iron Oxide Cu-Au-(U) Hydrothermal Activity and Nd Isotope Constraints on Metal Sources in the Gawler Craton, South Australia. *Economic Geology* **102**, 1441-1470.

SLÁMA, J., KOŠLER, J., CONDON, D. J., CROWLEY, J. L., GERDES, A., HANCHAR, J. M., HORSTWOOD, M., MORRIS, G.A., NASDALA, L. & NORBERG, N. 2008. Plešovice zircon—a new natural reference material for U–Pb and Hf isotopic microanalysis. *Chemical Geology* **249**, 1-35.

SORCAR, N., JOSHI, K. B., OLIVEIRA, E. P., TOMSON, J. & NANDAKUMAR, V. 2020. Characterization of partial melting events in garnet-cordierite gneiss from the Kerala Khondalite Belt, India. *Geoscience Frontiers* **11**, 597-611.

STEPANOV, A. S., HERMANN, J., RUBATTO, D. & RAPP, R. P. 2012. Experimental study of monazite/melt partitioning with implications for the REE, Th and U geochemistry of crustal rocks. *Chemical Geology* **300**, 200-220.

SWAIN, G., WOODHOUSE, A., HAND, M., BAROVICH, K., SCHWARZ, M. & FANNING, C. 2005. Provenance and tectonic development of the late Archaean Gawler Craton, Australia; U–Pb zircon, geochemical and Sm–Nd isotopic implications. *Precambrian Research* **141**, 106-136.

SZPUNAR, M., HAND, M., BAROVICH, K., JAGODZINSKI, E. & BELOUSOVA, E. 2011. Isotopic and geochemical constraints on the Paleoproterozoic Hutchison Group, southern Australia: Implications for Paleoproterozoic continental reconstructions. *Precambrian Research* **187**, 99-126.

TEASDALE, J. 1997. Methods for understanding poorly exposed terranes: the interpretive geology and tectonothermal evolution of the western Gawler Craton. PhD Thesis, University of Adelaide, South Australia.

TIDDY, C. J., BETTS, P. G., NEUMANN, M. R., MURPHY, F. C., STEWART, J., GILES, D., SAWYER, M., FREEMAN, H. & JOURDAN, F. 2020. Interpretation of a ca. 1600–1580 Ma metamorphic core complex in the northern Gawler Craton, Australia. *Gondwana Research* **85**, 263-290.

TONG, L., WILSON, C. J. L. & VASSALLO, J. J. 2004. Metamorphic evolution and reworking of the Sleaford Complex metapelites in the southern Eyre Peninsula, South Australia. *Australian Journal of Earth Sciences* **51**, 571-589.

TUNNADINE, A. 2017. *Fingerprinting the source of mineralising fluids in IOCG systems, Mount Woods Inlier.* Masters Thesis, Macquarie University, New South Wales.

VASSALLO, J. J. & WILSON, C. J. L. 2002. Palaeoproterozoic regional-scale non-coaxial deformation: an example from eastern Eyre Peninsula, South Australia. *Journal of Structural Geology* **24**, 1-24.

VETRIN, V. & SKUBLOV, S. 2016. Trace elements in various genetic types of zircon from syenite of the Sakharjok massif, Kola Peninsula. *Geology of Ore Deposits* **58**, 542-550.

WARREN, C. J., GREENWOOD, L. V., ARGLES, T. W., ROBERTS, N. M., PARRISH, R. R. & HARRIS, N. B. 2019. *Garnet–monazite rare earth element relationships in sub-solidus metapelites: a case study from Bhutan*. Geological Society of London, Special Publication 478.

WHITE, R. & POWELL, R. 2002. Melt loss and the preservation of granulite facies mineral assemblages. *Journal of Metamorphic Geology* **20**, 621-632.

WHITE, R., POWELL, R. & CLARKE, G. 2003. Prograde Metamorphic Assemblage Evolution during Partial Melting of Metasedimentary Rocks at Low Pressures: Migmatites from Mt Stafford, Central Australia. *Journal of Petrology* **44**, 1937-1960.

WIEDENBECK, M., ALLE, P., CORFU, F., GRIFFIN, W., MEIER, M., OBERLI, F., QUADT, A., RODDICK, J. C. & SPIEGEL, W. 1995. Three natural zircon standards for U-Th-Pb, Lu-Hf, trace element and REE analyses. *Geostandards newsletter* **19**, 1-23.

YANG, W.-B., NIU, H.-C., SHAN, Q., SUN, W.-D., ZHANG, H., LI, N.-B., JIANG, Y.-H. & YU, X.-Y. 2014. Geochemistry of magmatic and hydrothermal zircon from the highly evolved Baerzhe alkaline granite: implications for Zr–REE–Nb mineralization. *Mineralium Deposita* **49**, 451-470.

YIN, C., ZHAO, G. & SUN, M. 2015. High-pressure pelitic granulites from the Helanshan Complex in the Khondalite Belt, North China Craton: Metamorphic Pt path and tectonic implications. *American Journal of Science* **315**, 846-879.

ZHU, X. K. & O'NIONS, R. K. 1999. Monazite chemical composition: some implications for monazite geochronology. *Contributions to Mineralogy and Petrology* **137**, 351-363.

APPENDIX A: SAMPLE LOCATIONS

			MGA94 (Zone 53)			
Drill hole name	Type	Max. Depth (m)	Easting	Northing	Drilled by	Location in deposit
SFD001	DDH	394.6	503418.75	6748929.57	IMX Resources Ltd	Centre
SFD015	DDH_MET	279.8	504481.15	6749526.88	IMX Resources Ltd	North-east

Sample Name	Drill hole	Depth from (m)	Depth to (m)
SFDD01-03	SFD001	162.43	162.85
SFDD01-04	SFD001	120.5	120.77
SFDD01-09	SFD001	168.3	168.4
SFDD01-12	SFD001	195.86	196.13
SFDD01-17	SFD001	217.9	218.55
SFDD15-01	SFD015	154.15	154.8
SFDD15-03	SFD015	162.43	162.85

APPENDIX B: EXTENDED LA-ICP-MS METHODS

Mineral Separate Preparation

Zircon and monazite separates were collected using standard crushing, sieving and panning procedures. Grains were hand-picked from each sample and mounted on the base of a 2.5 cm mould. The mould was filled with epoxy resin and later polished to expose the grains. Mounted monazite grains were imaged before analysis using a back-scattered electron (BSE) detector on a FEI Quanta 600 MLA Scanning Electron Microscope (SEM) to determine the presence of compositional zoning. Zircon grains were imaged using a Gatan Cathodoluminescence detector attached to the SEM.

Identification of *in situ* Monazite

Monazite grains were identified in thin sections using a standard petrographic microscope. After marking each thin section, the grains were imaged in reflected light. These images were used to record the location of ablation spots and for ease of identification during Laser Ablation – Inductively Coupled Plasma – Mass Spectrometry (LA-ICP-MS).

LA-ICP-MS Analysis

U-Pb isotopic and trace element data were collected at Adelaide Microscopy, University of Adelaide using a RESOlution LR 193nm Excimer laser system with an Agilent 7900x ICP-MS. Zircon and monazite were ablated using a He-laser with a frequency of 5 Hz. Spot sizes of 13 μm for monazite (both mounted grains and *in situ*) and 29 μm for zircon were used. Total acquisition time for all analyses was 60 seconds, which included 30 seconds of background measurement followed by 30 seconds of sample ablation and measurement.

Standards

For zircon U-Pb analysis, primary standard *GJ* was used, as well as secondary standards *Plešovice* and *91500*. *GJ* has accepted ages of $^{206}Pb/^{238}U$ age = 600.7 ± 1.1 Ma, $^{207}Pb/^{235}U$ age = 602 ± 1.0 Ma and $^{207}Pb/^{206}Pb$ age = 607.7 ± 4.3 Ma (Jackson, Pearson, Griffin & Belousova, 2004). *Plešovice* has accepted ages of $^{206}Pb/^{238}U$ age = 337.13 ± 0.37 Ma, $^{207}Pb/^{235}U$ age = 337.27 ± 0.11 Ma and $^{207}Pb/^{206}Pb$ age = 339.22 ± 0.25 Ma (Sláma et al., 2008). *91500* has accepted ages of $^{206}Pb/^{238}U$ age = 1062.4 ± 0.4 Ma, $^{207}Pb/^{235}U$ age = 1061 ± 0.3 Ma and $^{207}Pb/^{206}Pb$ age = 1065.4 ± 0.2 Ma (Wiedenbeck et al., 1995). Throughout the course of this study, repeated analysis of *Plešovice* yielded a $^{206}Pb/^{238}U$ age of 336.3 ± 6.5 Ma (MSWD = 1.86; n = 14) and *91500* yielded a $^{207}Pb/^{206}Pb$ age of 1032 ± 91 Ma (MSWD = 1.39; n = 14).
For monazite U-Pb analysis, primary standard *MAdel* was used, as well as secondary standards *Ambat* and *222*. *MAdel* has accepted ages of $^{206}Pb/^{238}U$ age = 517.9 ± 2.6 Ma, $^{207}Pb/^{235}U$ age = 513.13 ± 0.2 Ma and $^{207}Pb/^{206}Pb$ age = 492.01 ± 0.77 Ma (Payne et al., 2008). *Ambat* has an accepted $^{206}Pb/^{238}U$ age of 520-525 Ma and *222* has an accepted

$^{206}Pb/^{238}U$ age of 450.2 ± 3.4 Ma (Maidment, 2005). This study yielded $^{206}Pb/^{238}U$ ages of 514.1 ± 7.9 Ma (MSWD = 0.692; n = 9) and 527 ± 44 Ma (MSWD = 42.3; n = 16) for *Ambat* and 446 ± 15 Ma (MSWD = 2.13; n = 20) and 451.4 ± 8.1 Ma (MSWD = 2.65; n = 16) for *222*.
For trace element analysis, *NIST610* was used as the primary standard for both zircon and monazite. Secondary standards *NIST612* and *NIST610* (43µm) were used for zircon and monazite, respectively. Internal element standards of Zr = 43.14% for zircon and Ce = 20% for monazite were used for data processing in *Iolite*.

Data Processing and Reduction

The data was processed and reduced in *Iolite* version 4 software (Hellstrom et al., 2008; Paton et al., 2011). The software uses a data reduction scheme (DRS) to correct data for instrument drift and downhole fractionation, whilst allowing the user to choose the best fit. The DRS calculates time-dependant $^{206}Pb/^{238}U$, $^{207}Pb/^{235}U$ and $^{207}Pb/^{206}Pb$ ages, as well as trace element compositional data.
Signals (time-explicit compositional and age data) are bracketed to improve the quality of the result. This is done by removing spikes in the signal or discarding signals reflecting compositions of minerals other than zircon and monazite. Such modifications must be practiced with caution so as to not deliberately manipulate the result.
After exporting, monazite trace element data was corrected for variance from the standard Ce = 20% value using an in-house spreadsheet that renormalises the data.

APPENDIX C: U-PB LA-ICP-MS RESULTS

Sample	$^{206}Pb/^{238}U$	$^{206}Pb/^{238}U$ age	$^{207}Pb/^{235}U$	$^{207}Pb/^{235}U$ age	$^{207}Pb/^{206}Pb$	$^{207}Pb/^{206}Pb$ age
Grain mounted zircon & standards						
SFDD01-03						
1	0.316 ± 0.0074	1770.6 ± 36.4	4.612 ± 0.156	1747.4 ± 28.9	0.107 ± 0.0014	1738 ± 24
2	0.232 ± 0.0041	1343.8 ± 21.6	4.082 ± 0.1043	1652.6 ± 22.9	0.128 ± 0.0016	2077.4 ± 20.2
3	0.278 ± 0.009	1580.9 ± 45.5	4.631 ± 0.1595	1752.9 ± 29	0.12 ± 0.0016	1965.7 ± 27.8
4	0.305 ± 0.0039	1718 ± 19.2	4.449 ± 0.111	1720.9 ± 20.7	0.106 ± 0.0013	1721.1 ± 23
5	0.312 ± 0.0041	1751 ± 20	4.644 ± 0.1211	1756.4 ± 21.7	0.108 ± 0.0015	1762.5 ± 25.7
6	0.258 ± 0.0034	1480.8 ± 17.5	3.856 ± 0.0925	1604 ± 19.3	0.108 ± 0.001	1766.6 ± 17
7	0.206 ± 0.003	1208.4 ± 15.8	3.143 ± 0.0835	1442.7 ± 20.5	0.11 ± 0.0011	1805.8 ± 18.3
8	0.326 ± 0.0058	1817.9 ± 28	5.175 ± 0.1529	1846.6 ± 25	0.116 ± 0.0017	1884.2 ± 26.7
9	0.225 ± 0.0044	1310.6 ± 23.4	3.717 ± 0.1067	1574.5 ± 22.6	0.12 ± 0.0028	1949.6 ± 41.5
11	0.314 ± 0.0052	1758.8 ± 25.7	4.607 ± 0.1229	1749.2 ± 22.1	0.107 ± 0.0014	1751.5 ± 24
12	0.302 ± 0.0043	1698.6 ± 21.6	4.381 ± 0.1108	1708 ± 20.9	0.106 ± 0.0009	1727.7 ± 15.8
13	0.311 ± 0.0046	1745.6 ± 22.7	4.633 ± 0.123	1754.1 ± 22.2	0.108 ± 0.0012	1770.6 ± 20.9
14	0.248 ± 0.0044	1429.9 ± 22.8	3.874 ± 0.1029	1607.5 ± 21.5	0.113 ± 0.0016	1851.1 ± 25.8
15	0.318 ± 0.0056	1779.3 ± 27.4	4.692 ± 0.1285	1764.3 ± 22.8	0.107 ± 0.0012	1754.7 ± 21.5
16	0.374 ± 0.0062	2049.9 ± 28.9	8.498 ± 0.2311	2284.3 ± 24.8	0.165 ± 0.0015	2508.1 ± 15.4
17	0.323 ± 0.0043	1803 ± 21.1	4.755 ± 0.1191	1776.1 ± 21	0.107 ± 0.0013	1741.8 ± 22.1
18	0.213 ± 0.0046	1243.9 ± 24.5	3.223 ± 0.1066	1461.1 ± 26	0.11 ± 0.0018	1790.6 ± 30.1
19	0.224 ± 0.0069	1302.7 ± 36.5	3.714 ± 0.1275	1570.7 ± 28.2	0.119 ± 0.0012	1937.3 ± 18.7
20	0.307 ± 0.005	1723.8 ± 24.5	4.677 ± 0.1218	1762.2 ± 22.1	0.11 ± 0.0013	1789.3 ± 20.9
21	0.235 ± 0.0035	1359.9 ± 18.5	5.451 ± 0.2316	1889 ± 36.5	0.166 ± 0.0053	2511.6 ± 54.4
22	0.498 ± 0.0079	2605.1 ± 34.4	11.121 ± 0.2936	2532.4 ± 24.8	0.162 ± 0.0027	2471.7 ± 27.4
24	0.253 ± 0.0044	1451.1 ± 22.7	3.78 ± 0.1038	1587.6 ± 22	0.108 ± 0.0017	1761.1 ± 29.6
25	0.312 ± 0.0041	1749.5 ± 20.4	4.649 ± 0.1266	1757.3 ± 23	0.108 ± 0.0019	1759.6 ± 33.3
26	0.179 ± 0.0026	1061.4 ± 14	2.623 ± 0.0692	1306.5 ± 19.3	0.106 ± 0.0015	1726 ± 26
27	0.178 ± 0.0064	1056.3 ± 35.2	2.677 ± 0.0934	1321.1 ± 25.9	0.108 ± 0.0021	1760.7 ± 34.8
28	0.208 ± 0.0047	1216.7 ± 25.4	3.221 ± 0.1034	1461.6 ± 25.3	0.111 ± 0.002	1810.1 ± 33.4
29	0.326 ± 0.0044	1816.3 ± 21.5	5.292 ± 0.1481	1865.8 ± 23.7	0.116 ± 0.002	1893.7 ± 30.4
30	0.297 ± 0.0056	1676.3 ± 27.9	4.84 ± 0.1366	1791.5 ± 23.8	0.116 ± 0.0017	1891.9 ± 25.7
31	0.321 ± 0.0064	1792.1 ± 31.2	4.881 ± 0.1472	1797.7 ± 25.6	0.109 ± 0.0019	1773.9 ± 31.4
32	0.217 ± 0.0043	1267.9 ± 22.8	3.325 ± 0.0899	1485.7 ± 21.1	0.109 ± 0.0014	1776.5 ± 23.8
33	0.191 ± 0.0032	1128.7 ± 17.5	3.18 ± 0.0804	1452.1 ± 19.6	0.118 ± 0.0018	1923.1 ± 27.9
34	0.333 ± 0.0052	1851.1 ± 25.1	4.983 ± 0.1439	1814.4 ± 24.4	0.106 ± 0.0017	1727.2 ± 29.1
SFDD01-12						
1	0.117 ± 0.0018	714.5 ± 10.5	1.68 ± 0.0513	1000.5 ± 19.5	0.105 ± 0.0021	1708.9 ± 37.4
2	0.091 ± 0.002	563.5 ± 11.6	1.336 ± 0.0404	861.1 ± 17.5	0.107 ± 0.0015	1748.2 ± 26
4	0.267 ± 0.0059	1527.1 ± 30.2	3.696 ± 0.1135	1569.6 ± 24.7	0.1 ± 0.0016	1629.5 ± 30.1
	0.331 ± 0.0054	1841.8 ± 26.3	4.57 ± 0.1322	1742.9 ± 23.7	0.101 ± 0.0018	1649.6 ± 37.2

Sample	$^{206}Pb/^{238}U$	$^{206}Pb/^{238}U$ age	$^{207}Pb/^{235}U$	$^{207}Pb/^{235}U$ age	$^{207}Pb/^{206}Pb$	$^{207}Pb/^{206}Pb$ age
5	0.303 ± 0.0047	1703.7 ± 23.5	4.113 ± 0.1163	1655.1 ± 23.3	0.1 ± 0.0013	1617.2 ± 24.7
6	0.29 ± 0.0036	1643.2 ± 18	4.054 ± 0.0992	1644.5 ± 20	0.102 ± 0.0013	1663.9 ± 22.6
8	0.256 ± 0.0051	1466.5 ± 26.4	3.476 ± 0.0947	1521.1 ± 21.7	0.099 ± 0.001	1606.7 ± 19.3
9	0.235 ± 0.0039	1358 ± 20.4	3.339 ± 0.1015	1489.5 ± 23.8	0.104 ± 0.0019	1685.3 ± 33
10	0.24 ± 0.0039	1389.1 ± 20.1	3.414 ± 0.0932	1506.9 ± 21.4	0.103 ± 0.0016	1679.6 ± 29.4
SFDD15-01						
1	0.277 ± 0.0052	1577.9 ± 26.1	4.257 ± 0.1364	1683.5 ± 26.5	0.109 ± 0.002	1775 ± 34.2
2	0.22 ± 0.0039	1282.1 ± 20.6	3.34 ± 0.1065	1489.4 ± 24.7	0.106 ± 0.0025	1732.1 ± 42.4
3	0.306 ± 0.0036	1718.5 ± 17.6	4.56 ± 0.111	1741.3 ± 20.3	0.104 ± 0.0009	1690.8 ± 16.7
4	0.266 ± 0.0054	1518.3 ± 27.7	4.106 ± 0.1084	1654.9 ± 21.7	0.107 ± 0.002	1744.4 ± 34
5	0.178 ± 0.0035	1053.6 ± 19.3	3.498 ± 0.0968	1526.1 ± 22.1	0.136 ± 0.0021	2179.8 ± 27
8	0.243 ± 0.0052	1402.1 ± 27	3.766 ± 0.1028	1584.3 ± 22	0.107 ± 0.0013	1738.9 ± 23
9	0.271 ± 0.0047	1543.5 ± 23.8	4.9 ± 0.145	1801.2 ± 24.9	0.125 ± 0.0016	2020.1 ± 22.6
10	0.309 ± 0.0068	1734.1 ± 33.7	5.046 ± 0.1325	1826 ± 22.1	0.113 ± 0.0016	1852.3 ± 27.2
11	0.112 ± 0.0037	682.1 ± 21.8	1.925 ± 0.0632	1087.4 ± 22	0.122 ± 0.002	1977.9 ± 28.4
SFDD15-03						
1	0.307 ± 0.0042	1725.4 ± 20.9	4.416 ± 0.1185	1714 ± 22.3	0.102 ± 0.0016	1659.8 ± 28.2
2	0.22 ± 0.0042	1279.3 ± 22.1	3.281 ± 0.0975	1475.6 ± 22.7	0.106 ± 0.0021	1728.8 ± 35.8
3	0.305 ± 0.0042	1716 ± 20.8	4.363 ± 0.114	1704.2 ± 21.8	0.102 ± 0.0015	1657.3 ± 27.6
4	0.294 ± 0.0039	1662.2 ± 17.5	4.161 ± 0.1118	1665.2 ± 22.2	0.103 ± 0.0013	1687 ± 21.6
5	0.304 ± 0.0041	1712.5 ± 20.1	4.28 ± 0.1063	1688.7 ± 20.3	0.103 ± 0.0013	1666.4 ± 23.3
6	0.232 ± 0.0045	1344.9 ± 23.3	3.304 ± 0.0927	1481.4 ± 21.9	0.103 ± 0.0015	1677.1 ± 27.2
7	0.291 ± 0.0043	1644.8 ± 21.5	4.138 ± 0.109	1660.7 ± 21.8	0.104 ± 0.0011	1688.8 ± 19.2
8	0.202 ± 0.0034	1187.7 ± 18.4	2.968 ± 0.0773	1398.5 ± 19.7	0.107 ± 0.0013	1747.8 ± 22.4
9	0.3 ± 0.0043	1691.6 ± 21.2	4.175 ± 0.1139	1667.7 ± 22.3	0.101 ± 0.0014	1640.5 ± 24.9
10	0.299 ± 0.0037	1684.3 ± 18.4	4.172 ± 0.1074	1667.5 ± 21.1	0.102 ± 0.0014	1650.4 ± 24.7
11	0.267 ± 0.0045	1525.4 ± 22.9	3.716 ± 0.1047	1573.3 ± 22.6	0.101 ± 0.0011	1637.9 ± 20.5
12	0.273 ± 0.0037	1557.3 ± 18.9	3.926 ± 0.1005	1618.2 ± 20.8	0.104 ± 0.0013	1695.7 ± 22.8
13	0.292 ± 0.0039	1651.9 ± 19.7	4.008 ± 0.1043	1634.7 ± 21.4	0.1 ± 0.0012	1611.9 ± 22.8
14	0.295 ± 0.0037	1668.7 ± 18.4	4.236 ± 0.1042	1680.3 ± 20.3	0.104 ± 0.0011	1689.6 ± 18.8
15	0.271 ± 0.0046	1543.6 ± 23.2	3.977 ± 0.1217	1628.4 ± 24.9	0.106 ± 0.0022	1729 ± 36.9
17	0.29 ± 0.0037	1642.4 ± 18.6	4.073 ± 0.1084	1647.7 ± 21.8	0.102 ± 0.0015	1651.2 ± 28.6
18	0.298 ± 0.0045	1683.4 ± 22.5	4.238 ± 0.1035	1684.4 ± 20.3	0.104 ± 0.001	1686.7 ± 17.9
19	0.301 ± 0.0043	1696.9 ± 21.5	4.203 ± 0.1174	1673.3 ± 23.3	0.102 ± 0.0016	1657.9 ± 27.7
20	0.29 ± 0.0051	1638.6 ± 25.8	4.067 ± 0.1176	1645.7 ± 23.5	0.101 ± 0.0014	1637.9 ± 25.4
21	0.352 ± 0.0052	1943.8 ± 24.8	5.344 ± 0.1395	1875.2 ± 22.6	0.108 ± 0.0013	1761.6 ± 21.5
GJ						
1	0.097 ± 0.0018	598.7 ± 10.3	0.811 ± 0.0298	604.2 ± 17.6	0.06 ± 0.0019	595.1 ± 66.8
2	0.097 ± 0.0017	597.7 ± 10	0.813 ± 0.0264	602.9 ± 14.8	0.061 ± 0.0016	634.5 ± 53
3	0.098 ± 0.0014	604.1 ± 8.5	0.822 ± 0.0276	607.9 ± 15.4	0.061 ± 0.0016	610.1 ± 57.7

Sample	$^{206}Pb/^{238}U$	$^{206}Pb/^{238}U$ age	$^{207}Pb/^{235}U$	$^{207}Pb/^{235}U$ age	$^{207}Pb/^{206}Pb$	$^{207}Pb/^{206}Pb$ age
4	0.098 ± 0.0014	604.1 ± 8.2	0.814 ± 0.0279	603.3 ± 15.7	0.061 ± 0.0016	616.6 ± 56.8
5	0.097 ± 0.0015	596.4 ± 8.7	0.819 ± 0.0293	606.3 ± 16.3	0.061 ± 0.0016	627.2 ± 60.8
6	0.098 ± 0.0013	600.2 ± 7.6	0.802 ± 0.0308	596.5 ± 17.5	0.06 ± 0.0018	596.6 ± 61.7
7	0.099 ± 0.0013	606.6 ± 7.7	0.819 ± 0.0269	608.6 ± 14.1	0.061 ± 0.0015	607.1 ± 51.7
8	0.098 ± 0.0016	603.9 ± 9.6	0.822 ± 0.029	607.9 ± 16.1	0.06 ± 0.0017	617.2 ± 55.9
9	0.097 ± 0.0014	598.2 ± 8.4	0.807 ± 0.0292	599.3 ± 16.2	0.06 ± 0.0018	579.1 ± 61.7
10	0.098 ± 0.0014	601.6 ± 8.5	0.815 ± 0.0276	604.2 ± 15.3	0.06 ± 0.0015	577.8 ± 55.1
11	0.098 ± 0.0014	603.3 ± 8.3	0.817 ± 0.0287	605 ± 16.1	0.061 ± 0.002	632.8 ± 64.3
12	0.099 ± 0.0015	605.8 ± 8.8	0.81 ± 0.0286	601.3 ± 16	0.06 ± 0.0017	588.2 ± 59
13	0.097 ± 0.0014	599.5 ± 8.4	0.819 ± 0.0288	606 ± 16.2	0.061 ± 0.0018	626.2 ± 63.9
14	0.098 ± 0.0014	600.3 ± 8.2	0.807 ± 0.027	599.8 ± 15.1	0.059 ± 0.0015	554 ± 57.1
15	0.097 ± 0.0015	597.5 ± 9.1	0.826 ± 0.0308	609.5 ± 17.2	0.061 ± 0.002	645.6 ± 67.4
16	0.098 ± 0.0014	604.5 ± 8.5	0.816 ± 0.0288	604.2 ± 16.2	0.06 ± 0.0017	600.8 ± 58.5
17	0.097 ± 0.0014	599.2 ± 8.2	0.804 ± 0.0268	597.9 ± 15.1	0.06 ± 0.0016	613.7 ± 52.7
18	0.098 ± 0.0015	604.5 ± 8.6	0.825 ± 0.0269	609.9 ± 14.8	0.061 ± 0.0016	637.5 ± 53.7
19	0.098 ± 0.0013	603.3 ± 7.8	0.817 ± 0.0269	605.2 ± 15	0.061 ± 0.0016	625.1 ± 55
20	0.097 ± 0.0013	599.1 ± 7.7	0.803 ± 0.0301	596.8 ± 17	0.059 ± 0.0019	559.6 ± 64.2
21	0.098 ± 0.0016	604.6 ± 9.1	0.814 ± 0.028	603.7 ± 15.5	0.06 ± 0.0015	576.6 ± 56.2
22	0.098 ± 0.0014	602.4 ± 8.3	0.825 ± 0.0296	609.5 ± 16.5	0.062 ± 0.0019	678.8 ± 62.5
Plesovice						
1	0.053 ± 0.0007	334.6 ± 4.6	0.386 ± 0.0125	331.3 ± 9.1	0.053 ± 0.0013	373.2 ± 46
2	0.053 ± 0.0007	334.7 ± 4.4	0.379 ± 0.012	326 ± 8.8	0.052 ± 0.0012	328 ± 45
3	0.053 ± 0.0008	330.9 ± 4.9	0.4 ± 0.0121	341.1 ± 8.8	0.055 ± 0.0016	430.4 ± 55.9
4	0.054 ± 0.0007	336.1 ± 4.4	0.392 ± 0.0126	335.5 ± 9.2	0.053 ± 0.0014	395.5 ± 54.6
5	0.053 ± 0.0008	335.3 ± 5.2	0.396 ± 0.0137	337.9 ± 10	0.053 ± 0.0015	368.6 ± 58.7
6	0.054 ± 0.0007	340.1 ± 4.4	0.4 ± 0.0127	341.5 ± 9.2	0.053 ± 0.0012	349.9 ± 46.9
7	0.053 ± 0.0007	335.2 ± 4.6	0.403 ± 0.0138	343.3 ± 10	0.054 ± 0.0013	404.6 ± 48.5
8	0.053 ± 0.0008	333.3 ± 4.7	0.398 ± 0.0126	339.5 ± 9.1	0.054 ± 0.0011	395.3 ± 40.4
9	0.054 ± 0.0008	339.2 ± 4.6	0.387 ± 0.0147	331.4 ± 10.8	0.052 ± 0.0016	378.1 ± 57.8
10	0.054 ± 0.0007	339.8 ± 4.5	0.395 ± 0.0133	337.6 ± 9.7	0.053 ± 0.0014	383.2 ± 53
11	0.054 ± 0.0008	338.3 ± 4.9	0.402 ± 0.0136	342.5 ± 9.9	0.054 ± 0.0014	399.1 ± 53.3
12	0.053 ± 0.0008	332.2 ± 4.6	0.386 ± 0.0151	331 ± 11.1	0.053 ± 0.0016	394.8 ± 54.8
13	0.055 ± 0.0008	342.2 ± 5	0.373 ± 0.0134	321.4 ± 9.9	0.054 ± 0.0015	406 ± 52.8
14	0.054 ± 0.0008	336.4 ± 4.7	0.359 ± 0.0114	311.5 ± 8.5	0.054 ± 0.0013	369.4 ± 50.2
91500						
1	0.178 ± 0.0037	1058.1 ± 20.2	1.766 ± 0.0838	1026.5 ± 31.6	0.072 ± 0.0031	986 ± 79.9
2	0.177 ± 0.0038	1047.5 ± 20.8	1.758 ± 0.086	1028.3 ± 33.5	0.074 ± 0.0036	985.1 ± 98.1
3	0.178 ± 0.0033	1054.8 ± 18.2	1.824 ± 0.0922	1046.6 ± 33.4	0.074 ± 0.0031	1008.1 ± 88.7
4	0.177 ± 0.0033	1050 ± 17.9	1.807 ± 0.0736	1043.6 ± 26.9	0.074 ± 0.0027	1032.3 ± 71.3
5	0.177 ± 0.003	1050.4 ± 16.4	1.934 ± 0.075	1089 ± 26.2	0.079 ± 0.0026	1135 ± 68.4

Sample	$^{206}Pb/^{238}U$	$^{206}Pb/^{238}U$ age	$^{207}Pb/^{235}U$	$^{207}Pb/^{235}U$ age	$^{207}Pb/^{206}Pb$	$^{207}Pb/^{206}Pb$ age
6	0.178 ± 0.0033	1056.2 ± 17.9	1.861 ± 0.0714	1063.7 ± 25.8	0.075 ± 0.0026	1040.3 ± 72.7
7	0.18 ± 0.0039	1065.8 ± 21.2	1.86 ± 0.0881	1060.5 ± 30.7	0.075 ± 0.003	1046.8 ± 79.9
8	0.176 ± 0.0032	1044.1 ± 17.7	1.859 ± 0.0889	1059.9 ± 31.8	0.077 ± 0.0034	1067 ± 93
9	0.179 ± 0.0031	1063.7 ± 16.9	1.833 ± 0.0672	1054.1 ± 24	0.074 ± 0.0021	1026.2 ± 58.8
10	0.185 ± 0.0037	1094.2 ± 19.9	1.844 ± 0.0809	1056 ± 29.2	0.073 ± 0.0028	968.7 ± 82.1
11	0.177 ± 0.0034	1047.9 ± 18.4	1.759 ± 0.0724	1026 ± 26.7	0.073 ± 0.0025	998.1 ± 73.1
12	0.181 ± 0.004	1070.2 ± 21.8	1.839 ± 0.0884	1052.7 ± 31.6	0.075 ± 0.0034	1021.9 ± 93.4
13	0.177 ± 0.0038	1051.5 ± 21	1.816 ± 0.0788	1046.1 ± 28.7	0.078 ± 0.0033	1099 ± 87.1
14	0.179 ± 0.0042	1060.7 ± 22.7	1.744 ± 0.0843	1018.6 ± 30.9	0.075 ± 0.0036	1028.8 ± 93.3
Grain mounted monazite & standards						
SFDD01-03						
1	0.294 ± 0.0065	1659.3 ± 32.4	4.204 ± 0.098	1673.9 ± 19.2	0.103 ± 0.0017	1677.3 ± 30.5
2	0.295 ± 0.0059	1663.6 ± 29.5	4.217 ± 0.0923	1676.4 ± 18	0.103 ± 0.0015	1675.3 ± 24.5
3	0.289 ± 0.0062	1633.6 ± 31	4.069 ± 0.0933	1646.6 ± 18.6	0.102 ± 0.0014	1647.9 ± 26.3
4	0.292 ± 0.0058	1649.1 ± 28.7	4.142 ± 0.0916	1661.1 ± 18.1	0.102 ± 0.0012	1660.2 ± 21.3
5	0.292 ± 0.0057	1652.7 ± 26.2	4.214 ± 0.0997	1675.4 ± 19.4	0.104 ± 0.0014	1691.8 ± 24.5
6	0.291 ± 0.0057	1646.9 ± 28.2	4.16 ± 0.0948	1664.8 ± 18.6	0.103 ± 0.0014	1672.2 ± 26.4
7	0.295 ± 0.0054	1663.7 ± 26.7	4.15 ± 0.0878	1663 ± 17.2	0.101 ± 0.0012	1647.2 ± 21.5
8	0.295 ± 0.0053	1666.2 ± 26.5	4.208 ± 0.0894	1674.4 ± 17.5	0.103 ± 0.0014	1667.2 ± 24.9
9	0.3 ± 0.0078	1691.1 ± 38.5	4.196 ± 0.1322	1671 ± 25.7	0.101 ± 0.0018	1635.4 ± 33.7
10	0.289 ± 0.0063	1636.7 ± 31.3	4.176 ± 0.1146	1667.5 ± 22.5	0.104 ± 0.0019	1696.2 ± 33.9
11	0.286 ± 0.0052	1621.8 ± 25.9	4.154 ± 0.0856	1664.3 ± 16.8	0.105 ± 0.0009	1707.4 ± 15.4
12	0.289 ± 0.0052	1637.6 ± 26.3	4.12 ± 0.0812	1657.6 ± 16.1	0.103 ± 0.0009	1674.5 ± 16.4
13	0.291 ± 0.0053	1648.2 ± 26.4	4.123 ± 0.0762	1659.8 ± 16.1	0.102 ± 0.001	1666.1 ± 18.3
14	0.291 ± 0.0057	1644.9 ± 28.4	4.096 ± 0.0853	1652.6 ± 16.9	0.102 ± 0.0014	1655.6 ± 25.2
15	0.291 ± 0.0054	1647 ± 26.9	4.141 ± 0.092	1661.2 ± 18.2	0.103 ± 0.0015	1669.7 ± 26.2
16	0.296 ± 0.0057	1671.7 ± 28.3	4.166 ± 0.1004	1668.6 ± 18.4	0.102 ± 0.0016	1653.3 ± 29
17	0.299 ± 0.0059	1687.6 ± 29.3	4.23 ± 0.0957	1678.3 ± 18.6	0.102 ± 0.0011	1662.8 ± 20.6
18	0.297 ± 0.0057	1677 ± 28.2	4.209 ± 0.0923	1674.3 ± 18	0.103 ± 0.0014	1669.8 ± 25.4
19	0.295 ± 0.0054	1664 ± 26.7	4.214 ± 0.096	1675.4 ± 18.6	0.104 ± 0.0016	1684.1 ± 29.3
20	0.294 ± 0.0058	1661 ± 28.7	4.1 ± 0.0944	1655.1 ± 19.9	0.102 ± 0.0016	1653.1 ± 27.6
21	0.27 ± 0.006	1540.4 ± 30.2	3.688 ± 0.1049	1565.9 ± 22.3	0.099 ± 0.0023	1601.1 ± 44.2
22	0.269 ± 0.0061	1537.3 ± 30.7	3.645 ± 0.0893	1557.5 ± 19.5	0.098 ± 0.0013	1582.3 ± 25.7
23	0.29 ± 0.0057	1641.2 ± 28.6	4.07 ± 0.0975	1646.6 ± 19.6	0.102 ± 0.0013	1651.1 ± 23.1
24	0.291 ± 0.0057	1647.9 ± 28.4	4.115 ± 0.0917	1655.9 ± 18.3	0.102 ± 0.0013	1667.8 ± 24.2
25	0.285 ± 0.0055	1616.9 ± 27.6	4.024 ± 0.098	1637.7 ± 20	0.102 ± 0.0017	1664.2 ± 31
26	0.293 ± 0.0055	1658.4 ± 27.2	4.094 ± 0.095	1651.7 ± 18.9	0.102 ± 0.0018	1656.1 ± 32.9
27	0.299 ± 0.0058	1684.5 ± 28.9	4.217 ± 0.0961	1675.8 ± 18.8	0.103 ± 0.0014	1665.6 ± 25.2
28	0.3 ± 0.0056	1693.2 ± 27.9	4.224 ± 0.0918	1677.4 ± 17.8	0.102 ± 0.001	1655 ± 18.8
29	0.297 ± 0.0054	1674.3 ± 26.9	4.165 ± 0.0821	1666.6 ± 16.3	0.102 ± 0.001	1663.9 ± 18.5

Sample	$^{206}Pb/^{238}U$	$^{206}Pb/^{238}U$ age	$^{207}Pb/^{235}U$	$^{207}Pb/^{235}U$ age	$^{207}Pb/^{206}Pb$	$^{207}Pb/^{206}Pb$ age
30	0.298 ± 0.0056	1682 ± 27.5	4.213 ± 0.0874	1677.9 ± 18.1	0.103 ± 0.001	1673.6 ± 17.7
31	0.296 ± 0.0057	1672.9 ± 28.1	4.171 ± 0.0904	1667 ± 17.9	0.102 ± 0.0016	1659.7 ± 28.6
32	0.296 ± 0.0055	1671.4 ± 27.3	4.197 ± 0.0996	1671.7 ± 19.5	0.103 ± 0.0014	1672.7 ± 24.7
33	0.293 ± 0.0058	1657.5 ± 29	4.057 ± 0.0927	1644.2 ± 18.7	0.1 ± 0.0015	1627.2 ± 28.9
34	0.298 ± 0.0054	1682.6 ± 26.7	4.176 ± 0.0879	1668.4 ± 17.2	0.102 ± 0.0013	1654.2 ± 24
35	0.284 ± 0.0058	1609.8 ± 29	3.892 ± 0.1059	1609.1 ± 22.6	0.099 ± 0.0022	1608.6 ± 39.8
36	0.288 ± 0.0057	1633 ± 28.5	4.04 ± 0.1007	1640.3 ± 20.2	0.102 ± 0.0017	1649 ± 30.6
37	0.301 ± 0.0072	1696.3 ± 35.6	4.214 ± 0.1142	1675 ± 22	0.101 ± 0.0013	1640.7 ± 23.4
38	0.302 ± 0.0059	1699.6 ± 29.5	4.209 ± 0.0989	1674.2 ± 19.1	0.101 ± 0.0015	1646.7 ± 27
39	0.305 ± 0.0057	1714.7 ± 28	4.288 ± 0.0928	1689.8 ± 17.7	0.102 ± 0.0014	1657.7 ± 26
40	0.291 ± 0.0056	1647.6 ± 28.1	4.132 ± 0.0899	1659.4 ± 18	0.103 ± 0.0015	1672.8 ± 26.4
41	0.298 ± 0.0059	1682.5 ± 29.5	4.212 ± 0.0987	1674.9 ± 19.3	0.103 ± 0.0011	1670.9 ± 20.8
42	0.298 ± 0.0055	1680.5 ± 27.4	4.186 ± 0.0942	1669.8 ± 18.6	0.102 ± 0.0014	1654.5 ± 25.5
SFDD01-12						
1	0.288 ± 0.0059	1633.3 ± 29.4	3.932 ± 0.0849	1619.2 ± 17.4	0.099 ± 0.0012	1600.9 ± 21.8
2	0.295 ± 0.0054	1668 ± 27.1	4.246 ± 0.0938	1681.4 ± 18.2	0.104 ± 0.0014	1697.9 ± 24.8
3	0.292 ± 0.0056	1652.4 ± 28.1	4.185 ± 0.0985	1669.2 ± 19.4	0.104 ± 0.0015	1690.6 ± 27.3
4	0.294 ± 0.0055	1659.1 ± 27.4	4.18 ± 0.0994	1668.2 ± 19.5	0.103 ± 0.0018	1679.6 ± 32
5	0.293 ± 0.0056	1655.3 ± 27.7	4.086 ± 0.0958	1649.6 ± 19.2	0.101 ± 0.0014	1643.5 ± 26.5
6	0.299 ± 0.0061	1686.4 ± 30.1	4.187 ± 0.1115	1668.6 ± 22	0.102 ± 0.0021	1647.1 ± 38.2
7	0.297 ± 0.0056	1678.2 ± 27.7	4.153 ± 0.0993	1663 ± 19.7	0.102 ± 0.0017	1650.9 ± 33.7
8	0.278 ± 0.0061	1583.1 ± 30.8	3.974 ± 0.119	1625.3 ± 24.5	0.104 ± 0.0024	1680.5 ± 42.3
9	0.29 ± 0.0057	1641.6 ± 28.6	4.15 ± 0.1132	1661.5 ± 22.2	0.104 ± 0.0021	1682.6 ± 38.3
10	0.3 ± 0.0062	1690.6 ± 30.8	4.269 ± 0.113	1685.3 ± 22	0.103 ± 0.0018	1682.1 ± 35.8
11	0.289 ± 0.0055	1638.3 ± 27.6	4.073 ± 0.1009	1646.7 ± 20.2	0.102 ± 0.0018	1660.3 ± 32.4
12	0.292 ± 0.0062	1649.1 ± 30.8	4.098 ± 0.1006	1652.1 ± 20.1	0.102 ± 0.002	1660.2 ± 36.6
13	0.277 ± 0.006	1575.8 ± 30.3	3.756 ± 0.0908	1582.3 ± 19.3	0.099 ± 0.0012	1603.2 ± 23.2
14	0.291 ± 0.0059	1644.9 ± 29.5	4.083 ± 0.1046	1648.3 ± 20.7	0.102 ± 0.0018	1658 ± 32.4
15	0.274 ± 0.0055	1559.3 ± 27.6	3.673 ± 0.0798	1564.7 ± 17.2	0.098 ± 0.0013	1578.6 ± 24.9
16	0.295 ± 0.0063	1665.8 ± 31.5	4.164 ± 0.1192	1663.5 ± 23.4	0.103 ± 0.0022	1666.3 ± 39.1
17	0.287 ± 0.0054	1626.8 ± 27	3.954 ± 0.0875	1623.6 ± 17.8	0.1 ± 0.0015	1618.3 ± 28.5
18	0.293 ± 0.0058	1654.3 ± 28.7	4.12 ± 0.1045	1656.1 ± 20.6	0.103 ± 0.0018	1663.6 ± 32.3
19	0.271 ± 0.0049	1544.4 ± 24.6	3.6 ± 0.066	1549.2 ± 14.6	0.097 ± 0.0007	1568.3 ± 13.3
20	0.286 ± 0.0051	1621.9 ± 25.3	3.901 ± 0.0804	1612.8 ± 16.5	0.099 ± 0.0009	1611.4 ± 17.5
21	0.294 ± 0.0059	1660.4 ± 29.5	4.188 ± 0.1099	1669.6 ± 21.4	0.104 ± 0.0018	1689.6 ± 32.5
22	0.295 ± 0.0056	1666.9 ± 27.8	4.205 ± 0.1157	1671.7 ± 22.7	0.104 ± 0.002	1678.6 ± 36.8
23	0.292 ± 0.006	1650.8 ± 29.8	4.143 ± 0.1159	1660 ± 22.6	0.104 ± 0.0022	1680.6 ± 39.3
24	0.297 ± 0.0068	1675.8 ± 33.8	4.131 ± 0.1223	1657.7 ± 24.3	0.102 ± 0.0025	1654.5 ± 41.5
25	0.289 ± 0.0053	1635.1 ± 26.4	4.125 ± 0.0932	1657.7 ± 18.5	0.104 ± 0.0013	1696.8 ± 22.3
26	0.295 ± 0.0061	1668.2 ± 30.2	4.16 ± 0.1076	1666.3 ± 20.1	0.103 ± 0.0019	1668.6 ± 34.6

Sample	$^{206}Pb/^{238}U$	$^{206}Pb/^{238}U$ age	$^{207}Pb/^{235}U$	$^{207}Pb/^{235}U$ age	$^{207}Pb/^{206}Pb$	$^{207}Pb/^{206}Pb$ age
27	0.275 ± 0.0054	1567.9 ± 27.2	3.622 ± 0.0825	1553.2 ± 18.1	0.096 ± 0.0013	1545.8 ± 24.5
28	0.278 ± 0.0051	1580.1 ± 25.5	3.697 ± 0.0846	1569.2 ± 18.1	0.097 ± 0.0012	1558.2 ± 23.6
29	0.296 ± 0.0066	1670 ± 32.7	4.125 ± 0.1066	1656.7 ± 21	0.102 ± 0.0018	1652.4 ± 33.3
30	0.289 ± 0.0063	1637.8 ± 31.4	4.071 ± 0.1015	1646.2 ± 20.5	0.103 ± 0.0023	1670.1 ± 40.8
31	0.278 ± 0.0052	1579.9 ± 26.2	3.721 ± 0.0787	1575.1 ± 17	0.098 ± 0.001	1580.2 ± 18.4
32	0.298 ± 0.0068	1680.7 ± 33.7	4.196 ± 0.1166	1673.9 ± 20.9	0.103 ± 0.0016	1665.5 ± 28.4
33	0.301 ± 0.006	1694.2 ± 29.8	4.27 ± 0.1071	1685.4 ± 20.9	0.104 ± 0.0019	1680.7 ± 33.2
34	0.295 ± 0.0063	1664.3 ± 31.5	4.149 ± 0.1013	1664.3 ± 20.9	0.103 ± 0.0019	1678 ± 33.7
35	0.279 ± 0.0051	1583.6 ± 25.8	3.755 ± 0.0751	1582.5 ± 16	0.099 ± 0.001	1594.2 ± 19.2
36	0.307 ± 0.0063	1725.5 ± 30.8	4.215 ± 0.0981	1675.6 ± 19.2	0.101 ± 0.0017	1633.9 ± 31.7
37	0.301 ± 0.0069	1695.2 ± 34.1	4.097 ± 0.1106	1650.7 ± 22.3	0.1 ± 0.002	1607.7 ± 37.6
38	0.276 ± 0.0051	1571 ± 25.7	3.698 ± 0.079	1569.7 ± 17	0.098 ± 0.001	1581.4 ± 19.3
39	0.278 ± 0.0074	1582.5 ± 37.4	3.701 ± 0.1089	1570.5 ± 23.7	0.098 ± 0.0026	1571.7 ± 49.5
40	0.301 ± 0.0059	1698 ± 29.1	4.236 ± 0.0981	1679.2 ± 18.9	0.103 ± 0.0016	1669.4 ± 27.1
41	0.276 ± 0.0052	1569.2 ± 26.1	3.682 ± 0.074	1566.8 ± 15.9	0.097 ± 0.001	1573.2 ± 18.5
42	0.294 ± 0.006	1660.7 ± 30.1	4.156 ± 0.1018	1663.9 ± 20.1	0.104 ± 0.0022	1681.9 ± 39.1
SFDD15-01						
1	0.293 ± 0.0054	1657.8 ± 26.7	4.144 ± 0.0825	1662.1 ± 16.2	0.103 ± 0.0007	1669.3 ± 13
2	0.296 ± 0.0053	1672.4 ± 26.3	4.167 ± 0.0793	1667 ± 15.5	0.102 ± 0.0009	1661.8 ± 16.7
3	0.295 ± 0.0054	1666.5 ± 26.9	4.182 ± 0.081	1669.7 ± 15.9	0.103 ± 0.0008	1675.3 ± 13.9
4	0.303 ± 0.0065	1706.2 ± 32.3	4.347 ± 0.1499	1697.1 ± 28.2	0.104 ± 0.0026	1683.6 ± 50
5	0.316 ± 0.0084	1767.4 ± 40.8	5.378 ± 0.2724	1874.9 ± 43	0.125 ± 0.0053	2012.9 ± 73.5
6	0.269 ± 0.0057	1536.4 ± 29	3.709 ± 0.1258	1570.4 ± 27.1	0.1 ± 0.0028	1615.3 ± 52.3
7	0.28 ± 0.0063	1592.5 ± 31.8	3.917 ± 0.1246	1614.9 ± 25.7	0.101 ± 0.0026	1639.9 ± 46.6
8	0.284 ± 0.0051	1609.4 ± 25.8	3.826 ± 0.0962	1596.5 ± 20.3	0.098 ± 0.0015	1574.9 ± 28.9
9	0.281 ± 0.006	1602.1 ± 32.1	3.83 ± 0.1054	1596.4 ± 22.1	0.098 ± 0.0021	1586.1 ± 39.1
10	0.284 ± 0.0061	1609.7 ± 30.9	3.871 ± 0.1026	1605.3 ± 21.3	0.099 ± 0.002	1589.9 ± 38.7
11	0.276 ± 0.0078	1572.4 ± 39.3	3.781 ± 0.1656	1591.1 ± 31.2	0.1 ± 0.0035	1614.8 ± 62.6
12	0.283 ± 0.0055	1607.3 ± 27.6	3.844 ± 0.0829	1601 ± 17.4	0.098 ± 0.0013	1589.5 ± 24.2
13	0.29 ± 0.0059	1639.8 ± 29.4	3.971 ± 0.0991	1626.2 ± 20.2	0.099 ± 0.0015	1604.6 ± 29.5
14	0.276 ± 0.0053	1570.4 ± 26.6	3.708 ± 0.0817	1571.9 ± 17.6	0.097 ± 0.0013	1569.4 ± 24.8
15	0.287 ± 0.006	1624 ± 30.1	4.079 ± 0.1127	1647.6 ± 22.4	0.103 ± 0.0023	1673.1 ± 40.5
16	0.287 ± 0.0059	1628 ± 29.7	3.898 ± 0.1021	1611.1 ± 21.2	0.098 ± 0.0018	1580.9 ± 34.4
17	0.3 ± 0.0069	1692.2 ± 34.1	4.098 ± 0.1238	1651.4 ± 24.6	0.099 ± 0.0024	1590.6 ± 46.5
18	0.288 ± 0.0061	1632.1 ± 30.3	4.012 ± 0.0913	1635.4 ± 18.5	0.101 ± 0.0013	1632.7 ± 23.7
19	0.288 ± 0.0074	1631.4 ± 37	4.04 ± 0.1246	1640.8 ± 25	0.102 ± 0.0023	1649.9 ± 42.2
20	0.284 ± 0.0057	1612.6 ± 28.8	3.845 ± 0.0925	1600.4 ± 19.4	0.098 ± 0.0017	1582.3 ± 31.5
21	0.282 ± 0.007	1598.7 ± 35.3	3.766 ± 0.1	1584.3 ± 21	0.098 ± 0.0021	1571.1 ± 40.6
22	0.283 ± 0.0055	1608 ± 27.4	3.795 ± 0.0909	1589.9 ± 19.3	0.097 ± 0.0018	1555.9 ± 35.1
23	0.281 ± 0.0053	1596.3 ± 26.8	3.792 ± 0.0852	1591.8 ± 19.1	0.098 ± 0.0013	1575.7 ± 25.7

Sample	$^{206}Pb/^{238}U$	$^{206}Pb/^{238}U$ age	$^{207}Pb/^{235}U$	$^{207}Pb/^{235}U$ age	$^{207}Pb/^{206}Pb$	$^{207}Pb/^{206}Pb$ age
24	0.304 ± 0.0066	1711.5 ± 32.8	4.311 ± 0.1151	1693.9 ± 22.1	0.102 ± 0.0022	1663 ± 38.8
25	0.283 ± 0.0052	1608 ± 26	3.899 ± 0.078	1612.7 ± 16.1	0.099 ± 0.0009	1608.7 ± 18
26	0.288 ± 0.0052	1630.9 ± 26.1	3.99 ± 0.0806	1631.4 ± 16.6	0.1 ± 0.001	1621.8 ± 19.1
27	0.297 ± 0.0061	1675.9 ± 30.3	4.211 ± 0.0911	1674.9 ± 17.8	0.102 ± 0.0009	1663.6 ± 16.4
28	0.295 ± 0.0056	1667.8 ± 27.9	4.166 ± 0.0839	1666.7 ± 16.5	0.102 ± 0.0008	1655.1 ± 14.8
29	0.285 ± 0.0055	1617 ± 27.4	3.813 ± 0.0885	1594 ± 18.6	0.096 ± 0.0014	1552.2 ± 26.7
30	0.277 ± 0.0055	1576.5 ± 27.8	3.777 ± 0.0898	1586.3 ± 19.2	0.098 ± 0.0014	1588.7 ± 26.5
31	0.273 ± 0.0058	1555.5 ± 29.2	3.693 ± 0.1057	1566.9 ± 22.7	0.098 ± 0.0021	1570.4 ± 40
32	0.293 ± 0.0068	1656.3 ± 33.7	4.006 ± 0.1109	1632.6 ± 22.3	0.099 ± 0.0019	1598.6 ± 33.3
33	0.28 ± 0.0053	1591.2 ± 26.6	3.825 ± 0.0842	1596.7 ± 17.7	0.099 ± 0.0014	1592.6 ± 26.8
34	0.281 ± 0.0052	1594.2 ± 26	3.791 ± 0.0905	1589 ± 19.1	0.098 ± 0.0017	1570 ± 32
35	0.296 ± 0.0069	1668.6 ± 34.5	4.246 ± 0.1089	1681.7 ± 21.3	0.104 ± 0.0016	1689.1 ± 28.3
36	0.281 ± 0.005	1597.2 ± 25.1	3.771 ± 0.084	1585.3 ± 17.9	0.097 ± 0.0012	1562.4 ± 23.3
37	0.278 ± 0.0058	1586.7 ± 31.6	3.807 ± 0.1138	1590.9 ± 24.2	0.099 ± 0.0026	1581.8 ± 50.3
38	0.277 ± 0.0051	1573.9 ± 25.7	3.682 ± 0.0751	1566.6 ± 16.3	0.096 ± 0.0009	1551.9 ± 18.2
39	0.289 ± 0.0065	1636.7 ± 32.2	3.941 ± 0.1038	1619.8 ± 21.5	0.099 ± 0.0019	1593.6 ± 36.9
40	0.284 ± 0.0064	1611.3 ± 32.1	3.912 ± 0.1187	1613.7 ± 24.6	0.1 ± 0.0023	1613.8 ± 43.7
41	0.28 ± 0.0055	1592.4 ± 27.8	3.779 ± 0.0968	1586.1 ± 20.4	0.098 ± 0.0019	1581.5 ± 36.6
42	0.29 ± 0.0053	1642.5 ± 26.5	4.1 ± 0.0772	1653.9 ± 15.3	0.102 ± 0.001	1663.2 ± 17.8
43	0.284 ± 0.0055	1611.2 ± 27.4	3.777 ± 0.0899	1586.1 ± 19	0.097 ± 0.0017	1558.7 ± 32.2
44	0.291 ± 0.0063	1644.9 ± 31.3	3.97 ± 0.0976	1626.5 ± 20.1	0.099 ± 0.0015	1605.6 ± 27.6
45	0.299 ± 0.0063	1684.5 ± 31.1	4.013 ± 0.1069	1633.9 ± 21.6	0.098 ± 0.0019	1578.5 ± 37.2
SFDD15-03						
1	0.276 ± 0.0081	1569.8 ± 40.9	3.717 ± 0.114	1573.6 ± 24.7	0.098 ± 0.0017	1588.8 ± 32
2	0.287 ± 0.0056	1627.3 ± 28.2	4.058 ± 0.0895	1644.5 ± 17.8	0.103 ± 0.0012	1669 ± 21.6
3	0.29 ± 0.0053	1642.6 ± 26.5	4.054 ± 0.0882	1645.9 ± 16.7	0.102 ± 0.0012	1655 ± 21.3
4	0.292 ± 0.0053	1649.6 ± 26.6	4.132 ± 0.0884	1659.3 ± 17.5	0.103 ± 0.0012	1675.9 ± 22.3
5	0.287 ± 0.0052	1627.1 ± 25.9	4.044 ± 0.0793	1642.3 ± 16	0.102 ± 0.001	1665.2 ± 17.9
6	0.275 ± 0.0054	1565.5 ± 27.3	3.708 ± 0.0834	1572.5 ± 17.9	0.098 ± 0.0012	1576.4 ± 23.2
7	0.296 ± 0.0066	1670.6 ± 32.9	4.196 ± 0.1136	1670.9 ± 22.3	0.103 ± 0.0018	1673.4 ± 32.4
8	0.297 ± 0.0058	1675.5 ± 28.7	4.135 ± 0.0844	1660.8 ± 16.7	0.101 ± 0.0012	1641.5 ± 24.4
9	0.293 ± 0.0057	1655.4 ± 28.1	4.176 ± 0.0897	1668.1 ± 17.4	0.104 ± 0.0012	1684.4 ± 20.8
10	0.275 ± 0.005	1567.3 ± 25.2	3.703 ± 0.0736	1571.4 ± 16	0.098 ± 0.0008	1575.9 ± 15.3
11	0.295 ± 0.0058	1663.5 ± 29.1	4.163 ± 0.0945	1667.4 ± 19.7	0.103 ± 0.0015	1666.5 ± 27.6
12	0.296 ± 0.0054	1670.7 ± 26.8	4.186 ± 0.0894	1670 ± 17.5	0.102 ± 0.0011	1663.4 ± 20.1
13	0.292 ± 0.0057	1650.9 ± 28.2	4.09 ± 0.0907	1650.9 ± 18	0.102 ± 0.0014	1647.2 ± 25
14	0.287 ± 0.0054	1628.1 ± 27.2	4.09 ± 0.0895	1651.1 ± 17.7	0.103 ± 0.001	1672.6 ± 18.6
15	0.294 ± 0.0067	1660.9 ± 33.2	4.104 ± 0.1151	1652.7 ± 23.1	0.101 ± 0.002	1637.4 ± 39.7
16	0.289 ± 0.0059	1637.4 ± 29.2	4.104 ± 0.094	1656 ± 19.8	0.103 ± 0.0019	1674.3 ± 33.1
17	0.289 ± 0.006	1637.6 ± 30.1	4.092 ± 0.0895	1651.8 ± 17.8	0.102 ± 0.0011	1665.6 ± 19.6

Sample	$^{206}Pb/^{238}U$	$^{206}Pb/^{238}U$ age	$^{207}Pb/^{235}U$	$^{207}Pb/^{235}U$ age	$^{207}Pb/^{206}Pb$	$^{207}Pb/^{206}Pb$ age
18	0.288 ± 0.0055	1632.5 ± 27.4	4.09 ± 0.0842	1651.5 ± 16.8	0.102 ± 0.0012	1665.7 ± 22
19	0.288 ± 0.0053	1633 ± 26.7	4.108 ± 0.081	1655.3 ± 16.2	0.103 ± 0.0012	1668.7 ± 21.4
20	0.285 ± 0.0057	1615.3 ± 28.4	4.038 ± 0.084	1641.1 ± 17	0.102 ± 0.001	1665.4 ± 17.8
21	0.287 ± 0.0055	1628.1 ± 27.3	4.072 ± 0.088	1647.5 ± 17.4	0.102 ± 0.0011	1667.7 ± 18.8
22	0.27 ± 0.0049	1541.5 ± 25	3.69 ± 0.0858	1567.8 ± 18.5	0.099 ± 0.0016	1593.8 ± 29.8
23	0.292 ± 0.0062	1649.1 ± 31	4.115 ± 0.1068	1654.7 ± 21.3	0.102 ± 0.0021	1653.5 ± 37.8
24	0.29 ± 0.0057	1639 ± 28.2	4.09 ± 0.0866	1651.2 ± 17.4	0.102 ± 0.0014	1659.5 ± 25.5
25	0.288 ± 0.0054	1630 ± 27.1	4.085 ± 0.0883	1650.1 ± 17.5	0.103 ± 0.0013	1669.4 ± 23.3
26	0.285 ± 0.0057	1617.6 ± 28.6	4.038 ± 0.0906	1643.3 ± 19.5	0.103 ± 0.0014	1669.1 ± 25.5
27	0.29 ± 0.0052	1642.4 ± 26	4.154 ± 0.0821	1664.2 ± 16.1	0.104 ± 0.0012	1686.3 ± 21
28	0.289 ± 0.0059	1635.3 ± 29.7	4.132 ± 0.0969	1659.3 ± 19.2	0.103 ± 0.0013	1683.9 ± 23.4
29	0.27 ± 0.0059	1539.6 ± 29.8	3.712 ± 0.0969	1572.6 ± 20.8	0.1 ± 0.002	1614.2 ± 37.5
	0.294 ± 0.0072	1660.9 ± 36	4.176 ± 0.1557	1666.6 ± 30.3	0.103 ± 0.0027	1667.4 ± 48.7
30	0.291 ± 0.0055	1643.7 ± 27.2	4.141 ± 0.0864	1661.3 ± 17	0.104 ± 0.0012	1689.2 ± 20.2
31	0.286 ± 0.0051	1623.5 ± 25.5	4.058 ± 0.0801	1645.3 ± 16.1	0.102 ± 0.0011	1670.1 ± 18.9
32	0.287 ± 0.0052	1624.1 ± 26.3	4.04 ± 0.0821	1641.3 ± 16.6	0.102 ± 0.001	1662 ± 18.5
33	0.272 ± 0.0056	1550.9 ± 28.6	3.657 ± 0.0895	1560.6 ± 19.4	0.098 ± 0.0018	1573.4 ± 34.9
34	0.291 ± 0.006	1648.2 ± 29.8	4.111 ± 0.1071	1654.5 ± 21.2	0.102 ± 0.0015	1654.3 ± 27.3
35	0.274 ± 0.0052	1558.6 ± 26.3	3.743 ± 0.0954	1579.5 ± 20.3	0.099 ± 0.0018	1600.3 ± 33
	0.298 ± 0.0069	1681.4 ± 34.3	4.2 ± 0.126	1671.9 ± 24.6	0.102 ± 0.0024	1658 ± 42.9
36	0.289 ± 0.0057	1635 ± 28.8	4.074 ± 0.0925	1647.8 ± 18.4	0.102 ± 0.0013	1664.7 ± 23.1
37	0.273 ± 0.006	1557.1 ± 30.3	3.717 ± 0.1001	1574.1 ± 21.7	0.099 ± 0.0015	1601.6 ± 27.7
	0.291 ± 0.0057	1643.8 ± 28.4	4.044 ± 0.0956	1642 ± 19.2	0.101 ± 0.0015	1632.5 ± 27.6
38	0.288 ± 0.0052	1629.7 ± 26	4.072 ± 0.0881	1647.5 ± 17.5	0.103 ± 0.0012	1670.6 ± 21.3
39	0.291 ± 0.0057	1646.7 ± 28.3	4.16 ± 0.089	1665.1 ± 17.6	0.104 ± 0.0012	1690.5 ± 20.6
40	0.293 ± 0.0057	1656.9 ± 28.4	4.18 ± 0.0987	1668.2 ± 19.1	0.104 ± 0.0014	1685 ± 24.9
41	0.288 ± 0.0052	1631.8 ± 26.2	4.069 ± 0.0836	1647.3 ± 16.6	0.103 ± 0.001	1668.9 ± 18.6
42	0.27 ± 0.0056	1539.5 ± 28.3	3.629 ± 0.0897	1554.3 ± 19.6	0.098 ± 0.0015	1576.4 ± 28.2
43	0.291 ± 0.0056	1647.6 ± 27.9	4.089 ± 0.0928	1650.5 ± 18.5	0.102 ± 0.0017	1656 ± 31.3
44	0.292 ± 0.0056	1655.6 ± 25.9	4.11 ± 0.0882	1655.3 ± 17.5	0.102 ± 0.0011	1660.9 ± 20.8
45	0.291 ± 0.0051	1645.7 ± 25.4	4.103 ± 0.0837	1654 ± 16.7	0.102 ± 0.001	1665.9 ± 18.6
46	0.29 ± 0.0055	1643.6 ± 27.5	4.133 ± 0.0857	1659.9 ± 16.9	0.103 ± 0.001	1678.6 ± 18
MAdel1						
1	0.084 ± 0.0015	520.8 ± 8.9	0.659 ± 0.0154	513.6 ± 9.5	0.057 ± 0.001	473.9 ± 40.1
2	0.083 ± 0.0016	514.1 ± 9.3	0.658 ± 0.0158	513.1 ± 9.7	0.057 ± 0.0012	516.4 ± 43
3	0.083 ± 0.0016	513.5 ± 9.4	0.649 ± 0.0168	507.4 ± 10.3	0.057 ± 0.0011	472 ± 41.1
4	0.085 ± 0.0015	522.9 ± 9	0.663 ± 0.018	515.6 ± 11	0.056 ± 0.0012	470.6 ± 49
5	0.083 ± 0.0016	516.2 ± 9.4	0.661 ± 0.0154	515 ± 9.4	0.058 ± 0.001	506.8 ± 37.7
6	0.083 ± 0.0015	516.8 ± 9.1	0.658 ± 0.0159	512.6 ± 9.8	0.057 ± 0.001	493.2 ± 37
7	0.084 ± 0.0015	520.8 ± 9	0.656 ± 0.0161	511.5 ± 9.9	0.057 ± 0.001	467.6 ± 38.9

Sample	$^{206}Pb/^{238}U$	$^{206}Pb/^{238}U$ age	$^{207}Pb/^{235}U$	$^{207}Pb/^{235}U$ age	$^{207}Pb/^{206}Pb$	$^{207}Pb/^{206}Pb$ age
8	0.084 ± 0.0016	517.4 ± 9.2	0.659 ± 0.0161	513.4 ± 9.8	0.057 ± 0.0009	497.4 ± 36.2
9	0.084 ± 0.0015	518.5 ± 9	0.657 ± 0.0164	512.1 ± 10.1	0.057 ± 0.0009	468.4 ± 36.4
10	0.084 ± 0.0016	518.6 ± 9.5	0.653 ± 0.0156	509.7 ± 9.6	0.057 ± 0.001	476.6 ± 36.2
11	0.084 ± 0.0015	518.3 ± 8.7	0.655 ± 0.016	510.9 ± 9.8	0.057 ± 0.0011	478.4 ± 39.8
12	0.083 ± 0.0015	515.4 ± 8.8	0.66 ± 0.0172	514.1 ± 10.6	0.058 ± 0.0012	512.6 ± 44.3
13	0.085 ± 0.0018	526.3 ± 10.6	0.667 ± 0.0186	517.9 ± 11.3	0.057 ± 0.0012	483.6 ± 46.9
14	0.084 ± 0.0016	517.4 ± 9.5	0.665 ± 0.0189	517 ± 11.6	0.058 ± 0.0013	540.7 ± 46
15	0.084 ± 0.0016	519.5 ± 9.6	0.655 ± 0.0172	510.6 ± 10.5	0.057 ± 0.0012	487.9 ± 45.6
16	0.084 ± 0.0017	517.1 ± 9.8	0.643 ± 0.0222	502.4 ± 13.7	0.056 ± 0.0015	484.3 ± 54.3
17	0.083 ± 0.0015	516.9 ± 9.2	0.652 ± 0.016	509 ± 9.9	0.057 ± 0.001	471.4 ± 38.7
18	0.083 ± 0.0016	516.3 ± 9.5	0.66 ± 0.0168	514 ± 10.3	0.057 ± 0.0011	489.8 ± 41.7
19	0.084 ± 0.0015	521 ± 8.8	0.664 ± 0.0164	516.3 ± 10	0.057 ± 0.0012	493 ± 41.8
20	0.083 ± 0.0016	514.4 ± 9.7	0.65 ± 0.0193	507.3 ± 12	0.057 ± 0.0015	488.5 ± 53.6
21	0.084 ± 0.0016	522.6 ± 9.5	0.66 ± 0.0164	514.1 ± 10	0.057 ± 0.001	475.4 ± 42.1
22	0.084 ± 0.0015	517.2 ± 8.9	0.658 ± 0.0157	513.2 ± 9.6	0.057 ± 0.001	493.1 ± 40.4
23	0.084 ± 0.0015	518.8 ± 9.1	0.652 ± 0.0163	508.9 ± 10	0.057 ± 0.0011	460.7 ± 42.2
24	0.084 ± 0.0015	517.8 ± 9.1	0.669 ± 0.0175	519.7 ± 10.7	0.058 ± 0.0011	510.7 ± 43.5
25	0.084 ± 0.0016	518.6 ± 9.4	0.656 ± 0.0174	511.6 ± 10.6	0.057 ± 0.001	474.6 ± 41.6
26	0.083 ± 0.0015	513.3 ± 9	0.646 ± 0.0158	505.2 ± 9.7	0.056 ± 0.0009	451.3 ± 36.9
27	0.085 ± 0.0016	526 ± 9.5	0.664 ± 0.0156	516.9 ± 9.5	0.057 ± 0.0011	473.6 ± 40.9
28	0.083 ± 0.0016	516.6 ± 9.4	0.659 ± 0.0162	513.5 ± 10	0.057 ± 0.001	478.2 ± 37.8
29	0.084 ± 0.0016	518.6 ± 9.4	0.657 ± 0.0165	512.3 ± 10.1	0.057 ± 0.0011	490.6 ± 43.3
30	0.084 ± 0.0015	517.8 ± 8.8	0.652 ± 0.0168	509.1 ± 10.3	0.057 ± 0.0012	501.7 ± 42.2
31	0.084 ± 0.0016	518.7 ± 9.5	0.666 ± 0.0175	517.3 ± 10.6	0.058 ± 0.0011	514.3 ± 40.5
Ambat						
1	0.083 ± 0.0016	512.3 ± 9.5	0.666 ± 0.0188	517.3 ± 11.4	0.058 ± 0.0013	519.4 ± 50
2	0.083 ± 0.0015	513.6 ± 9.1	0.664 ± 0.0184	516.1 ± 11.3	0.058 ± 0.0014	520.3 ± 53.7
3	0.084 ± 0.0016	518.8 ± 9.7	0.662 ± 0.0177	515.4 ± 10.8	0.058 ± 0.0014	506.1 ± 50.8
4	0.083 ± 0.0015	513.6 ± 9.1	0.647 ± 0.0181	505.8 ± 11.2	0.057 ± 0.0012	493.5 ± 41.7
5	0.084 ± 0.0016	521.1 ± 9.6	0.652 ± 0.0185	508.6 ± 11.5	0.057 ± 0.0013	470.3 ± 47.5
6	0.082 ± 0.0016	508.7 ± 9.3	0.652 ± 0.0197	508.5 ± 12	0.057 ± 0.0014	502.5 ± 49.5
7	0.083 ± 0.0016	512.5 ± 9.5	0.655 ± 0.018	512.2 ± 10.5	0.057 ± 0.0012	506 ± 44.7
8	0.083 ± 0.0016	515.6 ± 9.3	0.661 ± 0.0176	514.8 ± 10.6	0.058 ± 0.0012	503.9 ± 45.1
9	0.082 ± 0.0015	510.2 ± 9.1	0.652 ± 0.0178	509.2 ± 10.9	0.057 ± 0.0013	497.7 ± 47.3
222						
1	0.071 ± 0.0013	442.4 ± 8.1	0.563 ± 0.0144	453 ± 9.3	0.057 ± 0.0011	498 ± 42.2
2	0.07 ± 0.0014	438.8 ± 8.6	0.552 ± 0.0141	445.9 ± 9.2	0.057 ± 0.0012	471.2 ± 45.6
3	0.071 ± 0.0013	444.5 ± 7.9	0.549 ± 0.014	443.6 ± 9.2	0.056 ± 0.0012	458.1 ± 43.3
4	0.071 ± 0.0014	444 ± 8.3	0.55 ± 0.014	444.7 ± 9.2	0.056 ± 0.001	446.8 ± 40.9
5	0.073 ± 0.0014	456.1 ± 8.2	0.561 ± 0.0166	451.1 ± 10.8	0.055 ± 0.0013	422 ± 46.1

Sample	$^{206}Pb/^{238}U$	$^{206}Pb/^{238}U$ age	$^{207}Pb/^{235}U$	$^{207}Pb/^{235}U$ age	$^{207}Pb/^{206}Pb$	$^{207}Pb/^{206}Pb$ age
6	0.072 ± 0.0014	446.4 ± 8.4	0.563 ± 0.0143	453.1 ± 9.4	0.057 ± 0.0013	501.9 ± 43.7
7	0.072 ± 0.0013	450.8 ± 8.1	0.552 ± 0.0155	445.5 ± 10.2	0.056 ± 0.0013	457.8 ± 46.7
8	0.072 ± 0.0013	445.5 ± 7.8	0.547 ± 0.012	442.4 ± 7.9	0.056 ± 0.0007	433.4 ± 28.8
9	0.072 ± 0.0014	449.5 ± 8.2	0.543 ± 0.0126	439.9 ± 8.3	0.055 ± 0.0009	395.5 ± 36.6
10	0.072 ± 0.0014	449.7 ± 8.6	0.556 ± 0.0144	448.3 ± 9.4	0.056 ± 0.0011	460.5 ± 42.9
11	0.071 ± 0.0013	444.7 ± 7.9	0.557 ± 0.0143	450.4 ± 9.8	0.057 ± 0.0012	461.6 ± 45.4
12	0.072 ± 0.0013	445.6 ± 7.9	0.558 ± 0.0156	449.4 ± 10.1	0.056 ± 0.0012	461.7 ± 44.2
13	0.072 ± 0.0013	447.5 ± 7.7	0.554 ± 0.0134	447.4 ± 8.7	0.056 ± 0.001	436.2 ± 39.5
14	0.067 ± 0.0018	419.2 ± 11.1	0.515 ± 0.0182	420.6 ± 12.2	0.056 ± 0.0013	462.6 ± 51.2
15	0.072 ± 0.0013	448 ± 8.1	0.553 ± 0.0151	448 ± 9.4	0.056 ± 0.0011	439.2 ± 41
16	0.072 ± 0.0013	446.7 ± 8.1	0.562 ± 0.0162	452.1 ± 10.5	0.056 ± 0.0013	471.9 ± 49.5
17	0.072 ± 0.0014	446.7 ± 8.3	0.553 ± 0.014	446.2 ± 9.2	0.056 ± 0.0011	434.3 ± 40.3
18	0.073 ± 0.0014	451.5 ± 8.2	0.572 ± 0.0146	458.5 ± 9.4	0.057 ± 0.0011	476.7 ± 42.3
19	0.072 ± 0.0014	450.9 ± 8.3	0.576 ± 0.0161	461.1 ± 10.3	0.058 ± 0.0013	522 ± 46.8
20	0.071 ± 0.0013	444.8 ± 7.8	0.55 ± 0.015	444.1 ± 9.9	0.056 ± 0.0013	473.3 ± 46.7
In situ monazite & standards						
SFDD01-04						
1	0.281 ± 0.0041	1594.7 ± 20.7	3.977 ± 0.0847	1629 ± 17.3	0.103 ± 0.0017	1669.6 ± 30.7
2	0.32 ± 0.0066	1789.9 ± 32.2	4.547 ± 0.1217	1736.9 ± 21.7	0.103 ± 0.0015	1668.2 ± 27.4
3	0.289 ± 0.0029	1638.6 ± 14.3	4.09 ± 0.0736	1651.8 ± 14.6	0.102 ± 0.0013	1664.4 ± 23.8
4	0.297 ± 0.0057	1675.6 ± 28	4.207 ± 0.0981	1674.8 ± 18.8	0.103 ± 0.0019	1670.2 ± 35
5	0.295 ± 0.0029	1668.2 ± 14.4	4.161 ± 0.0745	1665.9 ± 14.7	0.102 ± 0.0014	1662 ± 25.3
6	0.295 ± 0.0044	1668.7 ± 21.8	4.222 ± 0.0807	1678.1 ± 15.6	0.103 ± 0.0016	1684.4 ± 27.9
7	0.299 ± 0.0055	1683.4 ± 26.9	4.213 ± 0.0985	1674.8 ± 18.9	0.102 ± 0.0012	1660.4 ± 22.6
8	0.303 ± 0.0033	1705.1 ± 16.1	4.243 ± 0.0787	1681.7 ± 15.2	0.101 ± 0.0015	1641.4 ± 26.6
9	0.296 ± 0.0026	1670.3 ± 13	4.193 ± 0.0729	1672.2 ± 14.3	0.103 ± 0.0014	1667.8 ± 25.5
10	0.288 ± 0.0035	1632.2 ± 17.5	4.035 ± 0.0722	1640.8 ± 14.5	0.101 ± 0.0014	1645.4 ± 24.8
11	0.295 ± 0.0036	1666.2 ± 18.1	4.136 ± 0.0787	1661 ± 15.7	0.101 ± 0.0013	1646.7 ± 23.1
12	0.307 ± 0.0108	1723.4 ± 53.2	4.303 ± 0.148	1691.5 ± 28.2	0.101 ± 0.0017	1648.8 ± 30.6
13	0.355 ± 0.0055	1958.3 ± 26.4	5.01 ± 0.1101	1820 ± 18.5	0.102 ± 0.0014	1661.6 ± 23
15	0.304 ± 0.0038	1709.7 ± 18.7	4.281 ± 0.0789	1689 ± 15.1	0.102 ± 0.0014	1656.1 ± 25.6
16	0.306 ± 0.0039	1719.9 ± 19.3	4.35 ± 0.0857	1702 ± 16.3	0.103 ± 0.0014	1672.8 ± 24.7
18	0.303 ± 0.0045	1704.7 ± 22.3	4.187 ± 0.1019	1669.3 ± 20.2	0.1 ± 0.0016	1618 ± 29.1
19	0.285 ± 0.0047	1614 ± 23.3	4.014 ± 0.0901	1636.1 ± 18.2	0.102 ± 0.0013	1658.2 ± 24.2
20	0.288 ± 0.0054	1632.7 ± 26.9	4.075 ± 0.0858	1648.7 ± 17.3	0.102 ± 0.0016	1667.7 ± 24.8
21	0.305 ± 0.0045	1716.9 ± 22.3	4.349 ± 0.0941	1701.4 ± 17.6	0.103 ± 0.0015	1682.3 ± 26.3
22	0.293 ± 0.0037	1657.4 ± 18.4	4.106 ± 0.0754	1654.8 ± 14.9	0.102 ± 0.0013	1657.4 ± 24.4
23	0.31 ± 0.0037	1746.1 ± 17	4.337 ± 0.0908	1699.2 ± 17.3	0.101 ± 0.0017	1646.5 ± 31.5
24	0.303 ± 0.0038	1706.4 ± 18.9	4.255 ± 0.0884	1683.5 ± 17	0.102 ± 0.0015	1652.3 ± 28
25	0.283 ± 0.0029	1606.9 ± 14.6	3.929 ± 0.0724	1619 ± 14.8	0.101 ± 0.0014	1637.4 ± 23.8

Sample	$^{206}Pb/^{238}U$	$^{206}Pb/^{238}U$ age	$^{207}Pb/^{235}U$	$^{207}Pb/^{235}U$ age	$^{207}Pb/^{206}Pb$	$^{207}Pb/^{206}Pb$ age
26	0.294 ± 0.0031	1662.7 ± 15.5	4.16 ± 0.0753	1665.5 ± 14.8	0.103 ± 0.0014	1668.6 ± 24.7
27	0.311 ± 0.0046	1746.6 ± 22.6	4.313 ± 0.0892	1694.7 ± 16.9	0.1 ± 0.0015	1626.5 ± 28.4
28	0.307 ± 0.0032	1723.7 ± 15.8	4.288 ± 0.0847	1690 ± 16.2	0.102 ± 0.0016	1653.4 ± 28.6
29	0.302 ± 0.0033	1700.9 ± 16.6	4.244 ± 0.0836	1683.7 ± 17.2	0.103 ± 0.0017	1668.1 ± 30.5
30	0.313 ± 0.0044	1752.8 ± 21.4	4.386 ± 0.0931	1708.3 ± 17.5	0.102 ± 0.0016	1665.5 ± 26.5
31	0.28 ± 0.0038	1591 ± 19.1	3.769 ± 0.0736	1585.2 ± 15.8	0.098 ± 0.0016	1585.6 ± 31.5
SFDD01-09						
2	0.269 ± 0.003	1537.9 ± 15.2	3.599 ± 0.0761	1548.1 ± 16.8	0.096 ± 0.0016	1552.4 ± 31.2
3	0.272 ± 0.0036	1549.3 ± 18.2	3.607 ± 0.0841	1549.3 ± 18.5	0.096 ± 0.0018	1540.1 ± 35.6
4	0.276 ± 0.0029	1573.3 ± 14.7	3.679 ± 0.071	1566.1 ± 15.4	0.096 ± 0.0015	1547.7 ± 29.5
5	0.272 ± 0.0048	1550.6 ± 24.3	3.577 ± 0.0965	1543.4 ± 21.7	0.095 ± 0.0022	1525 ± 43.5
6	0.277 ± 0.005	1576.8 ± 25.5	3.705 ± 0.083	1571.6 ± 17.8	0.097 ± 0.0017	1567.5 ± 33.7
7	0.277 ± 0.0043	1577.2 ± 21.8	3.759 ± 0.1094	1582.5 ± 23.4	0.098 ± 0.0023	1580.8 ± 44.6
8	0.278 ± 0.004	1580.2 ± 20.4	3.774 ± 0.0952	1585.5 ± 20.4	0.098 ± 0.0022	1592.9 ± 37.8
9	0.278 ± 0.0034	1578.4 ± 17	3.676 ± 0.0741	1567.2 ± 15.2	0.096 ± 0.0015	1546.4 ± 30
10	0.264 ± 0.0043	1508.5 ± 21.8	3.5 ± 0.0962	1529.6 ± 23.3	0.096 ± 0.0023	1544.1 ± 44.9
13	0.273 ± 0.0042	1556.6 ± 21.2	3.663 ± 0.097	1562.5 ± 21.1	0.097 ± 0.0024	1563.5 ± 46.8
15	0.277 ± 0.0052	1573.6 ± 26.4	3.634 ± 0.108	1555.8 ± 23.7	0.095 ± 0.0027	1528.3 ± 53.5
16	0.274 ± 0.0079	1560.1 ± 39.8	3.71 ± 0.1613	1571.2 ± 35.1	0.098 ± 0.0035	1586.5 ± 67.1
18	0.277 ± 0.0079	1574.5 ± 39.6	3.723 ± 0.1071	1575.3 ± 23.1	0.098 ± 0.0022	1578.5 ± 41.5
19	0.278 ± 0.0102	1580.9 ± 51.4	3.672 ± 0.169	1562.8 ± 36.5	0.096 ± 0.0029	1545 ± 56.9
SFDD01-12						
2	0.29 ± 0.0046	1640.5 ± 22.9	3.952 ± 0.0956	1622.6 ± 19.3	0.099 ± 0.0015	1608.7 ± 28.4
3	0.307 ± 0.0055	1725 ± 27.1	4.448 ± 0.1266	1718.4 ± 23.7	0.105 ± 0.002	1711.4 ± 35.2
4	0.284 ± 0.0042	1612.2 ± 21	4.048 ± 0.0869	1642.5 ± 17.3	0.103 ± 0.0016	1682.8 ± 28.7
5	0.277 ± 0.0044	1576.6 ± 22.1	3.934 ± 0.0764	1619.7 ± 15.8	0.103 ± 0.0015	1677.7 ± 27
6	0.298 ± 0.004	1679 ± 19.9	4.256 ± 0.0969	1683.2 ± 18.7	0.104 ± 0.0019	1688.4 ± 33.4
7	0.305 ± 0.0032	1715.2 ± 15.8	4.349 ± 0.088	1703.8 ± 15.7	0.104 ± 0.0016	1688 ± 28.5
8	0.284 ± 0.0032	1612 ± 16	4.014 ± 0.0744	1636.3 ± 15.1	0.102 ± 0.0014	1667.3 ± 24.5
9	0.317 ± 0.0055	1774.6 ± 26.6	4.482 ± 0.0993	1726 ± 18.3	0.102 ± 0.0015	1664.6 ± 26.3
10	0.292 ± 0.0039	1652.8 ± 19.7	4.098 ± 0.0848	1654.8 ± 17.9	0.102 ± 0.0015	1660.4 ± 25.7
11	0.277 ± 0.0027	1577.7 ± 13.5	3.707 ± 0.0665	1572.3 ± 14.4	0.097 ± 0.0013	1563.5 ± 24.7
12	0.277 ± 0.0024	1575.9 ± 12	3.738 ± 0.0678	1578.9 ± 14.5	0.098 ± 0.0013	1577.4 ± 25.3
13	0.276 ± 0.0025	1572.7 ± 12.7	3.708 ± 0.0636	1572.6 ± 13.7	0.097 ± 0.0013	1570.2 ± 26.6
14	0.294 ± 0.003	1663.4 ± 14.9	4.171 ± 0.0825	1667.3 ± 16.3	0.103 ± 0.0017	1669.3 ± 30.4
15	0.321 ± 0.0047	1796.3 ± 22.8	4.54 ± 0.1024	1736.7 ± 18.8	0.102 ± 0.0016	1663.2 ± 28.7
16	0.298 ± 0.0026	1683 ± 13	4.213 ± 0.0828	1675.6 ± 16.2	0.102 ± 0.0017	1662.8 ± 31.3
17	0.278 ± 0.0032	1580.3 ± 16.2	3.71 ± 0.0684	1572.9 ± 14.7	0.097 ± 0.0014	1560.1 ± 27.8
18	0.278 ± 0.0061	1578.9 ± 30.8	3.77 ± 0.1006	1585.5 ± 21.3	0.098 ± 0.002	1590.5 ± 38.8
19	0.279 ± 0.0048	1583.7 ± 23.9	3.757 ± 0.0913	1582.8 ± 19.4	0.098 ± 0.0021	1577.4 ± 39.5

Sample	$^{206}Pb/^{238}U$	$^{206}Pb/^{238}U$ age	$^{207}Pb/^{235}U$	$^{207}Pb/^{235}U$ age	$^{207}Pb/^{206}Pb$	$^{207}Pb/^{206}Pb$ age
20	0.289 ± 0.0037	1638.5 ± 18.4	4.017 ± 0.0871	1636.1 ± 17.8	0.1 ± 0.0015	1628.8 ± 28.7
21	0.278 ± 0.003	1582.5 ± 15.3	3.699 ± 0.0741	1570.1 ± 15.9	0.096 ± 0.0015	1549 ± 29.6
22	0.281 ± 0.0025	1595.4 ± 12.8	3.774 ± 0.0697	1586.6 ± 14.8	0.097 ± 0.0014	1569.8 ± 26.8
23	0.277 ± 0.0031	1573.8 ± 15.7	3.718 ± 0.0675	1574.6 ± 14.6	0.097 ± 0.0013	1571.9 ± 25.3
24	0.294 ± 0.0039	1660.4 ± 19.3	4.158 ± 0.1068	1664.5 ± 21	0.102 ± 0.0018	1657.5 ± 33.6
25	0.276 ± 0.0028	1571.4 ± 14	3.669 ± 0.0695	1565.8 ± 14.1	0.096 ± 0.0013	1551.6 ± 24.2
26	0.279 ± 0.0042	1585.1 ± 21.3	3.682 ± 0.0776	1566.7 ± 16.8	0.096 ± 0.0015	1537.9 ± 30.4
27	0.273 ± 0.0034	1555.5 ± 17.1	3.652 ± 0.0737	1560.3 ± 16.1	0.097 ± 0.0014	1563.9 ± 27.4
28	0.279 ± 0.0032	1584.4 ± 15.9	3.737 ± 0.0668	1578.8 ± 14.3	0.097 ± 0.0013	1567.9 ± 25.7
29	0.274 ± 0.0034	1559.8 ± 17.3	3.608 ± 0.0655	1552.8 ± 15.7	0.096 ± 0.0013	1539.6 ± 26.5
30	0.277 ± 0.0032	1576.7 ± 16	3.744 ± 0.069	1580.3 ± 14.8	0.098 ± 0.0014	1580.5 ± 26.8
31	0.309 ± 0.0051	1736 ± 24.9	4.312 ± 0.1226	1693.9 ± 23.7	0.101 ± 0.0022	1638.1 ± 40.8
32	0.298 ± 0.0034	1682.7 ± 16.9	4.282 ± 0.088	1688.7 ± 16.8	0.104 ± 0.002	1692.2 ± 35.2
33	0.288 ± 0.0027	1632.7 ± 13.3	3.936 ± 0.0691	1620.5 ± 14.3	0.099 ± 0.0014	1601.2 ± 25.5
34	0.291 ± 0.0032	1646.3 ± 15.8	4.103 ± 0.0763	1655.8 ± 16.2	0.102 ± 0.0013	1661 ± 24
35	0.276 ± 0.0035	1572.6 ± 17.6	3.713 ± 0.074	1576.3 ± 17.6	0.098 ± 0.0014	1578.4 ± 27.2
36	0.286 ± 0.0029	1618.9 ± 14.8	3.787 ± 0.0743	1589 ± 15.9	0.096 ± 0.0015	1546.6 ± 29.4
37	0.275 ± 0.0026	1565.4 ± 13.2	3.718 ± 0.0633	1574.9 ± 13.6	0.098 ± 0.0013	1578.9 ± 24.3
38	0.288 ± 0.0035	1632.8 ± 17.6	4.029 ± 0.0691	1639.6 ± 13.9	0.102 ± 0.0014	1655.7 ± 25.6
40	0.271 ± 0.005	1546.4 ± 25.1	3.589 ± 0.0946	1546.3 ± 20.7	0.096 ± 0.0018	1551 ± 35.9
41	0.301 ± 0.0039	1697.7 ± 19.4	4.264 ± 0.0867	1685.8 ± 16.7	0.103 ± 0.0014	1675.6 ± 24.6
42	0.292 ± 0.0026	1652.9 ± 13	4.055 ± 0.0764	1644.6 ± 15.4	0.101 ± 0.0015	1637.7 ± 27.7
43	0.288 ± 0.0053	1632.7 ± 26.6	3.97 ± 0.1011	1627.1 ± 20.7	0.1 ± 0.0022	1625.1 ± 42.4
44	0.299 ± 0.003	1686.5 ± 14.7	4.221 ± 0.0785	1677.3 ± 15.2	0.103 ± 0.0016	1672.1 ± 28.9
46	0.297 ± 0.0027	1675.2 ± 13.6	4.17 ± 0.0743	1667.6 ± 14.7	0.102 ± 0.0014	1665.5 ± 25.3
47	0.301 ± 0.003	1694.9 ± 14.9	4.28 ± 0.0802	1688.8 ± 15.4	0.103 ± 0.0015	1684.9 ± 26.8
48	0.281 ± 0.0028	1596.8 ± 14	3.834 ± 0.0739	1599.1 ± 15.4	0.099 ± 0.0014	1606.3 ± 25.8
49	0.281 ± 0.0029	1596 ± 14.7	3.812 ± 0.0666	1594.8 ± 14	0.099 ± 0.0012	1601.9 ± 23.4
50	0.275 ± 0.004	1567.9 ± 20.1	3.682 ± 0.0831	1566.7 ± 17.8	0.097 ± 0.0015	1574.8 ± 28.2
51	0.286 ± 0.0038	1622.4 ± 19	3.98 ± 0.0837	1629.5 ± 16.9	0.101 ± 0.0018	1647.2 ± 32.2
52	0.29 ± 0.0059	1640.6 ± 29.5	4.106 ± 0.1143	1654 ± 22.7	0.103 ± 0.002	1682.2 ± 40.7
53	0.301 ± 0.0051	1698.2 ± 25.2	4.276 ± 0.1061	1687.9 ± 20.4	0.103 ± 0.0018	1684.6 ± 31.8
54	0.285 ± 0.004	1617.7 ± 19.9	3.909 ± 0.0817	1614.4 ± 16.7	0.1 ± 0.0015	1622.4 ± 28
55	0.296 ± 0.005	1671.1 ± 24.8	4.229 ± 0.1087	1677.8 ± 21.2	0.104 ± 0.002	1699.3 ± 35.8
56	0.281 ± 0.0022	1594.3 ± 11.2	3.766 ± 0.0645	1586.3 ± 12.9	0.098 ± 0.0013	1585.3 ± 24.1
SFDD01-17						
1	0.276 ± 0.0029	1573.2 ± 14.8	3.724 ± 0.0677	1575.9 ± 14.5	0.098 ± 0.0013	1588.8 ± 23.9
2	0.291 ± 0.0031	1646.6 ± 15.3	4.071 ± 0.0701	1648 ± 14	0.102 ± 0.0013	1659.8 ± 23.3
5	0.296 ± 0.0032	1668.7 ± 15.8	4.14 ± 0.0746	1661.6 ± 14.8	0.102 ± 0.0014	1664.1 ± 24.8
6	0.293 ± 0.0029	1658.4 ± 14.7	4.116 ± 0.0736	1656.9 ± 14.7	0.102 ± 0.0013	1667.1 ± 23

Sample	$^{206}Pb/^{238}U$	$^{206}Pb/^{238}U$ age	$^{207}Pb/^{235}U$	$^{207}Pb/^{235}U$ age	$^{207}Pb/^{206}Pb$	$^{207}Pb/^{206}Pb$ age
8	0.272 ± 0.0026	1552.9 ± 13.1	3.651 ± 0.0618	1560.3 ± 13.6	0.098 ± 0.0012	1580.9 ± 23
9	0.279 ± 0.0027	1587.9 ± 13.6	3.801 ± 0.0673	1592.5 ± 14.2	0.099 ± 0.0012	1611.8 ± 22.8
10	0.273 ± 0.0047	1557.2 ± 24	3.675 ± 0.0776	1565.3 ± 17	0.098 ± 0.0016	1586.4 ± 31.3
11	0.291 ± 0.0046	1646.2 ± 23.2	4.117 ± 0.0844	1657.1 ± 16.6	0.103 ± 0.0015	1680.6 ± 26.7
14	0.296 ± 0.0032	1669.1 ± 15.8	4.158 ± 0.0741	1665.2 ± 14.6	0.102 ± 0.0013	1663 ± 22.8
15	0.294 ± 0.0028	1658.9 ± 14	4.14 ± 0.0687	1661.8 ± 13.6	0.103 ± 0.0013	1671 ± 23.2
17	0.293 ± 0.0026	1654.9 ± 12.8	4.1 ± 0.0686	1653.9 ± 13.6	0.102 ± 0.0013	1656.4 ± 23.1
18	0.308 ± 0.004	1730.9 ± 19.8	4.319 ± 0.0885	1696.1 ± 16.8	0.102 ± 0.0015	1656.5 ± 27
19	0.294 ± 0.0029	1663.3 ± 14.5	4.13 ± 0.0683	1661.1 ± 14.4	0.102 ± 0.0013	1660.3 ± 25.6
20	0.27 ± 0.0026	1543 ± 12.9	3.623 ± 0.0639	1554 ± 14	0.097 ± 0.0012	1570.2 ± 22.6
21	0.289 ± 0.003	1634.5 ± 14.9	4.038 ± 0.0745	1641.1 ± 15.1	0.102 ± 0.0013	1650.4 ± 23.9
24	0.299 ± 0.0028	1686.1 ± 13.7	4.214 ± 0.0711	1676.4 ± 13.8	0.102 ± 0.0013	1658.9 ± 23.5
25	0.28 ± 0.0029	1590 ± 14.5	3.829 ± 0.0726	1598.1 ± 15.1	0.099 ± 0.0013	1602.3 ± 24.1
26	0.29 ± 0.0028	1642.4 ± 13.9	4.082 ± 0.0717	1650.1 ± 14.3	0.102 ± 0.0013	1652.7 ± 24.1
27	0.311 ± 0.0068	1746.2 ± 33.3	4.344 ± 0.122	1698.5 ± 22.6	0.101 ± 0.0014	1638.2 ± 26.4
28	0.315 ± 0.0056	1765.4 ± 27.6	4.454 ± 0.1042	1721 ± 19.5	0.102 ± 0.0015	1662.8 ± 26.3
MAdel						
2	0.084 ± 0.0008	519.6 ± 4.9	0.66 ± 0.0151	514.2 ± 9.2	0.057 ± 0.0013	494.3 ± 47.8
3	0.084 ± 0.0011	522.2 ± 6.7	0.655 ± 0.0145	511.1 ± 8.9	0.057 ± 0.0011	477.9 ± 40.4
4	0.083 ± 0.0008	516.1 ± 4.9	0.655 ± 0.0158	511.3 ± 9.6	0.057 ± 0.0012	483.6 ± 45.1
5	0.083 ± 0.001	513.4 ± 5.9	0.65 ± 0.0164	508.1 ± 10	0.057 ± 0.0013	470.4 ± 50.2
6	0.084 ± 0.0009	520 ± 5.4	0.672 ± 0.0159	521.7 ± 9.6	0.058 ± 0.0013	516.2 ± 49
7	0.083 ± 0.0009	515.5 ± 5.5	0.646 ± 0.0154	505.7 ± 9.6	0.057 ± 0.0012	471.5 ± 47.6
8	0.084 ± 0.0009	517.7 ± 5.1	0.649 ± 0.0156	507.3 ± 9.6	0.057 ± 0.0011	470.6 ± 45.1
9	0.084 ± 0.0011	521 ± 6.6	0.656 ± 0.0158	511.7 ± 9.7	0.057 ± 0.0012	481.2 ± 45.2
10	0.084 ± 0.0009	518.6 ± 5.4	0.651 ± 0.0149	508.7 ± 9.1	0.056 ± 0.0011	465.7 ± 40.7
11	0.084 ± 0.0009	520.2 ± 5.2	0.672 ± 0.0144	521.6 ± 8.7	0.058 ± 0.0011	515.3 ± 43.3
12	0.083 ± 0.001	514.6 ± 5.7	0.66 ± 0.0168	514.2 ± 10.3	0.057 ± 0.0013	505 ± 47
13	0.084 ± 0.0009	520.4 ± 5.5	0.667 ± 0.0168	518.4 ± 10.2	0.058 ± 0.0014	509.7 ± 50.5
14	0.084 ± 0.0008	519.4 ± 4.9	0.657 ± 0.0166	512.2 ± 10.1	0.057 ± 0.0013	473.7 ± 49.9
15	0.084 ± 0.0009	519.7 ± 5.5	0.654 ± 0.016	510.5 ± 9.8	0.056 ± 0.0012	471.4 ± 47.1
16	0.084 ± 0.0008	519.2 ± 4.9	0.664 ± 0.0154	518.1 ± 8.8	0.058 ± 0.0013	508.7 ± 47.6
17	0.084 ± 0.0009	519 ± 5.4	0.653 ± 0.0148	511.1 ± 9.7	0.056 ± 0.0012	466.8 ± 48.8
18	0.084 ± 0.0009	517.6 ± 5.1	0.661 ± 0.0153	514.5 ± 9.3	0.057 ± 0.0012	491.4 ± 48.1
19	0.083 ± 0.0009	514.4 ± 5.2	0.653 ± 0.0159	511.1 ± 10.4	0.057 ± 0.0013	498.8 ± 45.6
20	0.084 ± 0.001	519.8 ± 5.7	0.663 ± 0.0157	516.2 ± 9.6	0.057 ± 0.0011	493.5 ± 43.8
21	0.084 ± 0.0008	519.8 ± 4.7	0.658 ± 0.016	512.7 ± 9.8	0.057 ± 0.0011	469.7 ± 45.9
22	0.084 ± 0.0009	519.2 ± 5.2	0.657 ± 0.0149	512.5 ± 9.1	0.057 ± 0.0011	494.1 ± 45.6
23	0.083 ± 0.0007	514.8 ± 4.4	0.652 ± 0.0157	509 ± 9.6	0.057 ± 0.0012	490 ± 46.6
24	0.084 ± 0.001	522.5 ± 5.8	0.657 ± 0.0142	512.2 ± 8.7	0.057 ± 0.0011	480.7 ± 43.6

Sample	$^{206}Pb/^{238}U$	$^{206}Pb/^{238}U$ age	$^{207}Pb/^{235}U$	$^{207}Pb/^{235}U$ age	$^{207}Pb/^{206}Pb$	$^{207}Pb/^{206}Pb$ age
Ambat						
1	0.097 ± 0.0011	601 ± 7.1	2.201 ± 0.0778	1177.2 ± 23.3	0.162 ± 0.004	2465.6 ± 39.3
2	0.083 ± 0.0009	515.4 ± 5.4	0.646 ± 0.0159	505.6 ± 9.7	0.056 ± 0.0014	452.8 ± 53.2
3	0.083 ± 0.0009	511.3 ± 5.4	0.651 ± 0.0166	508.5 ± 10.2	0.057 ± 0.0013	499.5 ± 47.4
4	0.084 ± 0.0009	521.7 ± 5.3	0.661 ± 0.0164	514.4 ± 10.1	0.057 ± 0.0013	486.4 ± 47.3
5	0.083 ± 0.0009	514.2 ± 5.2	0.652 ± 0.0171	508.9 ± 10.5	0.057 ± 0.0014	491.6 ± 55.4
6	0.084 ± 0.0011	517.8 ± 6.7	0.656 ± 0.0159	513 ± 10.4	0.058 ± 0.0014	509.9 ± 52
7	0.082 ± 0.001	510.6 ± 5.9	0.643 ± 0.0161	503.9 ± 10	0.056 ± 0.0014	465.2 ± 52.9
8	0.084 ± 0.001	517.9 ± 6.1	0.66 ± 0.0199	514 ± 12	0.057 ± 0.0015	475.9 ± 59
9	0.084 ± 0.0009	519.1 ± 5.6	0.664 ± 0.0162	516.5 ± 9.8	0.058 ± 0.0012	502 ± 46
10	0.083 ± 0.0008	516.5 ± 4.7	0.66 ± 0.0165	514.1 ± 10.1	0.057 ± 0.0012	494.7 ± 46.9
11	0.085 ± 0.0009	526.3 ± 5.4	0.661 ± 0.0168	514.6 ± 10.3	0.056 ± 0.0014	458.3 ± 52.6
12	0.085 ± 0.001	525.8 ± 5.7	0.665 ± 0.0163	518.3 ± 10.6	0.057 ± 0.0013	473.2 ± 51.3
13	0.089 ± 0.0012	551.4 ± 7.4	1.181 ± 0.1128	767.5 ± 53.9	0.095 ± 0.0083	1338.7 ± 185.2
14	0.085 ± 0.001	528 ± 6.1	0.661 ± 0.0162	515 ± 9.8	0.056 ± 0.0012	451.9 ± 49
15	0.086 ± 0.001	529.2 ± 6.2	0.673 ± 0.0174	522.2 ± 10.6	0.058 ± 0.0014	512 ± 51.6
16	0.084 ± 0.001	522.5 ± 5.7	0.666 ± 0.0161	517.7 ± 9.8	0.058 ± 0.0012	513 ± 46.9
222						
1	0.072 ± 0.0008	447.9 ± 4.7	0.556 ± 0.0145	448.7 ± 9.4	0.056 ± 0.0013	463.9 ± 48.4
2	0.073 ± 0.0009	453.6 ± 5.2	0.556 ± 0.0134	448.4 ± 8.7	0.055 ± 0.0013	422.5 ± 48.9
3	0.073 ± 0.0008	453.9 ± 4.8	0.566 ± 0.0162	455 ± 10.6	0.056 ± 0.0015	470.5 ± 55.2
4	0.073 ± 0.0008	453.2 ± 4.6	0.569 ± 0.0141	456.9 ± 9.1	0.057 ± 0.0013	469 ± 51.3
5	0.072 ± 0.0008	446.9 ± 4.9	0.551 ± 0.014	445.1 ± 9.2	0.056 ± 0.0013	444.2 ± 50.7
6	0.072 ± 0.0008	447.5 ± 5.1	0.549 ± 0.0147	444 ± 9.7	0.056 ± 0.0014	448.9 ± 51.1
7	0.072 ± 0.0008	447.7 ± 4.9	0.544 ± 0.0146	440.7 ± 9.7	0.055 ± 0.0015	409.9 ± 53.9
8	0.071 ± 0.0007	444.6 ± 4.4	0.561 ± 0.0145	451.6 ± 9.5	0.057 ± 0.0014	482.6 ± 51.6
9	0.074 ± 0.0009	459.4 ± 5.5	0.57 ± 0.0143	457.9 ± 9.2	0.056 ± 0.0015	452.5 ± 56
10	0.072 ± 0.0009	450.6 ± 5.3	0.553 ± 0.0144	446.5 ± 9.4	0.055 ± 0.0012	419.8 ± 49.9
11	0.073 ± 0.0009	456.3 ± 5.6	0.567 ± 0.0136	455.4 ± 8.8	0.056 ± 0.0012	452.3 ± 43.3
12	0.072 ± 0.0009	447.2 ± 5.2	0.548 ± 0.0151	443 ± 9.9	0.055 ± 0.0014	417.3 ± 52.7
13	0.073 ± 0.0008	453 ± 4.5	0.555 ± 0.0153	447.6 ± 10	0.055 ± 0.0014	411.7 ± 55.1
14	0.073 ± 0.0008	453.8 ± 4.9	0.566 ± 0.0149	454.6 ± 9.6	0.056 ± 0.0013	450.7 ± 50.1
15	0.073 ± 0.0007	453.2 ± 4.2	0.577 ± 0.014	462.2 ± 9	0.058 ± 0.0014	526.3 ± 49.9
16	0.073 ± 0.0008	454 ± 5	0.557 ± 0.0146	449 ± 9.5	0.056 ± 0.0012	450.2 ± 45.2

APPENDIX D: TRACE ELEMENT LA-ICP-MS RESULTS

Sample	Y89 (ppm)	La139 (ppm)	Ce140 (ppm)	Pr141 (ppm)	Nd146 (ppm)	Sm147 (ppm)	Eu153 (ppm)	Gd157 (ppm)	Tb159 (ppm)	Dy163 (ppm)	Ho165 (ppm)	Er166 (ppm)	Tm169 (ppm)	Yb172 (ppm)	Lu175 (ppm)
Grain mounted zircon and standards															
SFDD01-03															
1	1525.9	0.0	18.5	0.2	4.4	8.2	1.7	41.3	12.6	146.2	52.4	241.1	46.2	399.2	77.8
2	3945.1	24.7	392.6	70.2	498.1	316.7	63.3	467.8	83.5	589.6	128.3	417.4	66.5	520.1	93.3
3	1227.8	35.9	155.6	21.1	104.9	39.9	9.2	62.8	12.8	124.1	39.6	188.6	42.6	472.5	99.4
4	647.6	1.0	22.4	1.6	11.0	8.7	1.7	16.8	4.2	51.2	20.1	108.9	28.8	329.1	72.4
5	1308.6	0.9	66.6	2.8	23.7	19.1	5.1	50.9	12.6	127.5	43.7	195.5	39.8	364.1	71.8
6	4117.8	18.1	334.4	52.7	420.5	283.1	57.7	422.8	65.4	476.3	116.8	477.0	102.6	1033.6	217.4
7	3878.4	24.0	366.9	48.2	345.3	227.7	55.4	365.3	69.3	513.9	124.1	434.5	73.3	588.6	106.1
8	1939.9	1.8	74.0	4.9	38.7	35.5	8.1	86.2	21.0	201.4	64.2	277.4	52.5	457.7	88.1
9	3768.1	21.6	264.5	45.1	312.9	213.4	42.9	354.6	64.5	514.0	129.8	458.8	79.0	608.0	108.5
11	875.6	3.2	22.3	1.7	9.1	6.0	0.8	16.7	5.5	70.3	27.2	140.6	30.9	287.3	60.2
12	902.6	0.6	15.1	0.9	6.7	4.8	0.9	14.7	4.9	67.2	27.6	151.8	34.5	345.6	74.4
13	1689.3	6.4	118.8	16.4	116.6	91.1	18.8	146.5	27.2	208.3	52.4	196.0	36.7	325.5	65.6
14	1961.8	16.3	102.5	6.8	32.3	19.8	3.4	56.4	15.2	171.4	61.4	297.5	63.9	585.6	117.2
15	938.3	1.4	62.4	3.6	28.8	21.5	5.0	46.2	10.2	91.0	29.3	129.9	26.7	240.4	48.1
16	1452.8	10.0	158.7	10.3	67.9	48.7	12.9	92.2	19.1	169.7	49.0	188.0	35.6	308.3	60.7
17	1767.1	1.1	64.2	4.1	36.6	29.1	4.9	77.7	18.2	181.0	59.0	259.1	49.1	429.4	84.8
18	2589.4	18.8	211.8	28.6	195.4	122.8	24.2	204.4	38.6	336.8	84.4	331.5	60.0	494.6	94.8
19	7103.3	47.1	655.6	103.2	750.8	532.0	115.9	847.5	144.7	1005.8	216.9	660.2	104.9	801.4	140.8
20	1525.1	4.8	107.9	14.3	101.0	76.8	15.6	118.1	23.5	185.6	50.6	192.8	35.9	317.4	64.0
21	9131.4	69.4	981.9	163.5	1123.7	768.8	167.5	1146.0	211.3	1454.1	301.7	910.5	130.3	901.9	144.6

Sample	Y89 (ppm)	La139 (ppm)	Ce140 (ppm)	Pr141 (ppm)	Nd146 (ppm)	Sm147 (ppm)	Eu153 (ppm)	Gd157 (ppm)	Tb159 (ppm)	Dy163 (ppm)	Ho165 (ppm)	Er166 (ppm)	Tm169 (ppm)	Yb172 (ppm)	Lu175 (ppm)
22	1366.3	0.1	34.2	0.5	7.8	11.7	3.0	47.5	12.7	135.6	45.6	204.4	39.5	337.1	65.3
24	1533.3	4.9	107.1	12.8	93.3	65.6	16.3	117.8	24.9	200.3	49.5	185.5	32.9	290.4	57.7
25	1191.7	2.2	56.1	3.2	19.5	17.7	3.8	44.6	10.6	112.4	38.4	176.2	35.7	324.5	66.7
26	1657.5	14.1	101.1	13.4	78.1	47.4	12.6	74.1	15.8	149.5	50.4	256.0	65.4	731.3	157.9
27	2118.5	13.6	123.6	12.4	72.2	45.8	10.9	90.7	21.4	219.2	70.3	312.4	62.3	570.4	110.2
28	1837.0	26.4	206.9	21.2	116.2	73.6	15.1	126.5	26.2	228.9	62.3	253.7	47.1	411.7	78.6
29	741.6	6.0	44.3	5.2	33.4	24.3	4.6	57.0	12.0	97.0	25.0	87.8	15.2	122.7	22.2
30	1002.7	13.3	53.6	8.9	47.2	14.0	2.8	20.3	4.5	63.2	28.6	184.4	52.2	634.2	138.9
31	1180.3	2.2	46.9	3.9	30.4	17.9	2.9	44.9	10.0	109.2	37.1	169.7	35.8	319.0	65.7
32	1867.0	10.5	112.2	8.0	48.9	37.1	12.8	84.5	20.9	195.4	61.4	263.9	52.2	473.4	91.4
33	2320.3	16.0	205.4	17.6	108.3	68.6	19.1	135.3	28.3	251.0	70.7	316.9	65.2	612.2	125.8
34	2379.2	0.6	17.5	1.9	13.5	12.1	2.7	48.0	16.6	210.8	79.6	379.4	75.6	689.6	133.5
SFDD01-12															
1	388.7	2.7	32.0	6.6	44.9	27.3	10.8	47.8	8.2	59.3	12.8	32.8	4.3	29.0	3.8
2	601.6	78.4	485.4	88.9	488.5	127.5	50.8	128.1	16.1	91.6	15.6	39.3	4.7	25.3	3.3
4	559.0	1.8	18.8	3.3	21.2	20.0	7.3	40.6	10.1	81.1	20.5	61.5	9.0	60.9	9.0
	247.5	0.6	6.5	1.1	8.5	7.3	2.7	18.0	4.4	36.3	7.7	26.0	4.2	30.7	5.3
5	31.6	0.0	0.6	0.0	0.2	0.7	0.3	3.2	0.7	4.4	0.9	2.4	0.3	1.7	0.3
6	557.5	0.2	3.1	0.3	2.5	2.5	0.9	9.9	3.3	43.8	17.4	99.9	25.0	285.0	62.6
8	1014.8	22.2	167.7	34.3	198.6	84.6	28.9	124.5	27.1	190.1	37.8	113.1	15.4	90.7	13.2
9	498.3	3.5	24.2	4.2	25.6	18.8	7.0	36.6	8.5	71.5	16.2	52.2	7.1	50.9	7.3
10	1166.2	5.4	65.1	11.0	77.2	53.9	20.4	90.5	17.5	126.9	32.4	128.0	24.3	238.1	47.3
SFDD15-01															
1	852.6	0.5	18.9	0.8	6.5	9.4	1.8	26.6	8.1	87.1	29.4	131.7	25.9	228.3	44.6
2	1522.5	37.6	106.5	11.5	56.1	29.7	5.6	67.8	18.5	176.9	54.0	218.9	40.9	338.0	61.0

Sample	Y89 (ppm)	La139 (ppm)	Ce140 (ppm)	Pr141 (ppm)	Nd146 (ppm)	Sm147 (ppm)	Eu153 (ppm)	Gd157 (ppm)	Tb159 (ppm)	Dy163 (ppm)	Ho165 (ppm)	Er166 (ppm)	Tm169 (ppm)	Yb172 (ppm)	Lu175 (ppm)
3	1773.9	0.2	15.6	0.3	2.1	2.5	1.1	14.2	6.6	109.0	51.9	323.0	84.5	912.2	199.1
4	3175.0	8.1	92.9	16.0	105.5	77.3	30.7	151.8	35.1	312.0	90.4	404.4	85.6	848.9	170.4
5	7894.1	29.5	264.1	52.7	338.1	242.7	78.3	468.2	106.2	912.6	233.3	871.8	158.0	1325.0	230.6
8	3454.1	12.6	114.7	20.0	127.2	88.2	33.9	170.1	39.3	344.4	104.3	463.1	97.1	949.9	194.0
9	2693.4	19.9	138.3	18.9	105.8	61.5	17.9	124.1	27.6	257.3	79.4	358.0	76.2	741.3	153.5
10	2624.2	8.5	90.1	11.2	72.9	50.4	20.7	105.1	21.7	207.0	71.2	332.1	75.5	735.0	151.3
11	2820.5	58.1	207.9	32.0	147.8	93.8	21.7	164.7	42.8	384.8	103.7	433.7	92.2	904.8	177.5
SFDD15-03															
1	227.3	0.0	1.0	0.0	0.4	1.8	0.5	12.5	3.6	29.2	7.0	19.9	2.7	16.6	2.2
2	544.3	2.1	12.7	2.0	11.8	7.4	2.4	20.1	5.3	55.7	17.7	76.3	14.0	115.1	21.1
3	81.5	0.1	0.8	0.0	0.3	0.9	0.6	6.8	1.9	13.7	2.6	7.4	1.0	7.6	1.6
4	430.3	1.6	22.0	3.9	24.2	11.2	3.3	20.0	5.0	48.7	13.1	47.4	8.0	64.7	11.7
5	482.0	0.0	1.5	0.0	0.6	2.7	0.7	18.3	5.3	53.3	15.2	60.3	10.1	79.4	14.7
6	438.0	1.0	11.3	1.8	11.8	8.0	2.4	17.5	4.4	44.6	13.0	58.3	12.4	109.0	22.7
7	314.0	0.7	9.1	1.4	8.9	4.7	2.3	9.0	2.8	28.7	9.2	39.0	7.8	72.4	13.7
8	1583.8	11.9	123.5	29.3	194.5	100.9	50.6	136.6	27.6	208.4	52.3	195.7	36.0	285.6	43.5
9	87.8	0.0	0.5	0.0	0.1	0.8	0.4	5.9	1.6	12.1	2.6	6.5	0.8	5.2	0.7
10	335.6	0.0	0.5	0.0	0.2	0.7	0.3	5.1	1.7	23.9	9.1	47.6	10.3	91.5	16.5
11	282.1	0.3	3.1	0.4	2.2	2.0	1.0	10.0	3.2	30.6	7.8	29.5	5.3	44.9	7.7
12	641.4	4.2	48.7	10.3	64.1	24.4	7.4	38.2	8.8	76.6	19.1	63.6	10.2	76.8	13.0
13	98.7	0.1	1.4	0.3	1.8	1.9	1.2	8.8	2.3	17.3	3.1	8.2	1.1	6.9	1.0
14	443.4	0.3	3.3	0.6	4.2	3.3	1.4	15.4	5.2	51.7	12.0	38.6	6.2	46.1	6.8
15	526.4	11.4	141.9	34.8	227.1	74.7	22.3	70.1	11.7	78.0	17.9	57.4	9.4	71.5	10.6
17	235.8	0.2	2.3	0.3	1.5	1.8	0.7	7.9	2.7	25.2	6.5	23.7	4.2	31.3	5.1
18	462.4	4.4	46.9	10.7	63.3	23.4	7.5	34.6	7.1	58.6	13.7	44.5	7.0	44.4	6.6

Sample	Y89 (ppm)	La139 (ppm)	Ce140 (ppm)	Pr141 (ppm)	Nd146 (ppm)	Sm147 (ppm)	Eu153 (ppm)	Gd157 (ppm)	Tb159 (ppm)	Dy163 (ppm)	Ho165 (ppm)	Er166 (ppm)	Tm169 (ppm)	Yb172 (ppm)	Lu175 (ppm)
19	91.4	0.0	0.5	0.1	0.4	0.6	0.6	5.4	1.8	12.9	2.8	7.5	1.1	7.2	1.2
20	132.6	0.7	10.8	1.8	13.4	5.2	3.8	13.1	3.0	21.2	4.0	11.6	1.6	10.7	1.6
21	523.4	2.4	7.5	1.1	5.7	5.2	1.0	15.9	5.1	51.2	15.5	61.8	12.1	98.7	17.8
NIST610															
1	462.2	439.7	452.4	447.8	428.7	455.7	446.4	448.2	436.0	437.8	448.7	452.7	434.2	449.7	438.9
2	462.2	438.6	451.9	446.7	430.5	450.1	446.0	448.7	436.9	434.8	448.0	456.5	435.0	448.5	437.7
3	459.8	438.1	450.6	445.8	428.5	449.8	445.8	447.0	434.6	434.7	445.8	452.8	432.5	448.4	435.2
4	465.0	445.7	458.7	452.2	433.0	457.1	451.9	453.1	441.6	442.6	453.8	458.6	438.8	453.9	445.8
5	457.1	435.2	448.8	444.9	426.3	452.7	442.8	445.8	434.4	432.3	445.9	452.3	433.3	447.1	436.7
6	465.6	444.4	458.3	452.9	436.3	457.6	452.0	454.5	440.8	441.0	454.2	459.4	439.3	455.4	442.9
7	459.8	437.7	450.0	445.5	428.3	448.9	443.7	445.6	434.6	434.4	445.2	453.6	431.3	445.7	434.5
8	464.7	441.1	454.3	448.8	429.8	454.7	449.5	450.5	438.2	439.4	450.4	455.1	436.8	452.7	441.5
NIST612															
1	38.9	36.2	38.4	38.0	35.3	37.7	35.6	38.1	37.8	35.9	37.7	38.4	37.3	38.4	36.9
2	40.0	37.3	39.9	39.2	37.2	38.8	36.8	39.5	38.5	37.3	38.9	39.9	38.3	39.8	37.8
3	37.4	35.4	37.5	37.6	35.1	37.3	34.9	37.8	36.3	34.7	37.1	37.9	37.0	37.9	36.4
4	38.6	36.1	38.4	38.0	35.5	37.6	35.7	38.1	37.6	36.5	37.9	39.1	37.0	38.8	37.1
5	39.1	36.3	38.5	38.0	35.8	37.7	36.3	38.8	37.5	36.4	38.3	39.0	37.5	39.5	36.8
Grain mounted monazite and standards															
SFDD01-03															
1	20014.2	103689.5		21273.5	71189.7	11526.9	1227.4	8054.4	944.5	4603.5	725.9	1523.9	143.5	583.5	57.4
2	20171.9	103647.3		21514.9	71261.6	11593.8	1255.1	8167.6	948.1	4674.0	733.9	1535.5	142.8	593.3	58.1
3	18259.2	101740.3		21698.3	75343.1	12350.7	1352.4	8440.3	985.8	4804.1	705.0	1441.5	133.7	560.0	52.5
4	19687.9	100522.2		21914.3	75755.4	12538.1	1236.3	8587.8	987.1	4845.9	743.9	1527.3	140.0	582.4	56.5
5	24108.0	100491.9		21788.8	75050.9	12637.9	1469.5	9308.0	1106.4	5551.0	870.8	1839.6	172.3	725.2	71.7

Sample	Y89 (ppm)	La139 (ppm)	Ce140 (ppm)	Pr141 (ppm)	Nd146 (ppm)	Sm147 (ppm)	Eu153 (ppm)	Gd157 (ppm)	Tb159 (ppm)	Dy163 (ppm)	Ho165 (ppm)	Er166 (ppm)	Tm169 (ppm)	Yb172 (ppm)	Lu175 (ppm)
6	23056.4	98978.9		21663.3	75130.4	12520.8	1411.3	9134.2	1060.9	5222.9	838.8	1753.8	161.6	696.1	67.2
7	25539.8	99930.8		21920.7	76045.3	13023.9	1469.5	9602.5	1148.9	5873.3	925.0	1964.2	183.9	775.9	75.2
8	21263.7	100775.4		21658.9	75406.8	12266.6	1355.7	8758.9	1026.0	5066.1	793.2	1645.9	153.5	644.2	64.5
9	18738.8	103593.8		21864.1	72307.2	11745.9	1373.9	8205.0	939.6	4634.9	701.8	1465.3	138.6	620.1	62.3
10	19170.8	102735.3		21965.2	74433.9	12178.3	1278.1	8377.4	956.5	4624.3	713.2	1471.7	135.1	571.8	55.0
11	21280.9	97779.7		21964.3	76301.5	13579.9	1182.5	9682.0	1183.3	5747.8	833.6	1680.7	156.9	648.9	60.8
12	20544.2	98735.8		21932.8	75899.4	13099.9	1174.1	9364.8	1145.7	5535.8	791.5	1593.3	147.4	616.3	57.9
13	20370.4	98100.2		21835.0	76755.0	13420.2	1174.5	9491.7	1154.8	5595.2	810.5	1609.8	148.9	615.4	58.1
14	20125.9	103436.9		21517.7	72575.4	11726.4	1327.1	8377.8	970.0	4770.5	736.2	1551.2	144.3	602.2	59.3
15	22247.9	99359.2		21689.5	74639.2	12404.1	1428.8	8882.0	1040.9	5182.4	803.0	1701.7	154.4	647.0	61.6
16	21891.4	100422.3		21782.5	75334.5	12606.3	1410.7	9004.1	1053.6	5117.0	800.2	1680.7	155.7	641.0	63.3
17	21977.1	100126.6		21688.6	73676.7	12442.6	1433.8	8943.1	1047.6	5150.4	794.4	1667.1	153.6	648.6	63.4
18	17585.5	106898.3		20715.7	69367.8	10769.4	1096.9	7423.6	833.9	4168.3	642.2	1365.4	131.8	560.3	54.4
19	20804.9	101314.7		21403.7	74944.5	12105.3	1253.5	8629.5	981.0	4877.2	765.0	1596.7	145.7	618.3	60.0
20	21348.6	102184.3		21533.9	75252.8	12416.4	1284.0	8916.8	1020.1	5036.3	776.8	1655.5	153.5	652.8	64.1
21	15827.3	100921.7		21630.4	73331.9	11472.0	1046.9	7573.1	822.4	3866.4	587.4	1187.5	108.3	444.1	43.6
22	16300.6	100800.5		21762.3	73464.5	11752.3	1032.1	7938.1	885.1	4186.7	625.1	1252.4	114.8	474.8	44.7
23	21523.6	100400.9		21698.9	75697.0	12502.0	1335.1	8943.7	1031.7	5075.0	794.1	1646.1	152.9	648.7	62.0
24	23183.5	99346.4		21542.0	74726.4	12642.8	1424.3	9244.9	1080.5	5382.0	851.3	1774.2	164.8	692.8	69.0
25	20304.1	101931.3		21700.4	72499.9	11986.2	1293.7	8586.2	984.1	4742.1	750.6	1561.6	141.2	611.7	59.4
26	21623.1	101334.3		21748.9	73930.6	12033.4	1341.1	8486.1	1012.2	5041.6	793.7	1653.6	154.0	662.7	63.1
27	21405.7	101468.8		21417.6	73317.8	12158.6	1365.4	8593.2	1019.4	5041.4	792.7	1656.1	153.5	647.8	63.4
28	21249.9	106317.6		20680.0	69523.1	11783.2	1759.3	8303.2	1018.7	5121.6	775.6	1672.8	166.8	752.7	73.9

Sample	Y89 (ppm)	La139 (ppm)	Ce140 (ppm)	Pr141 (ppm)	Nd146 (ppm)	Sm147 (ppm)	Eu153 (ppm)	Gd157 (ppm)	Tb159 (ppm)	Dy163 (ppm)	Ho165 (ppm)	Er166 (ppm)	Tm169 (ppm)	Yb172 (ppm)	Lu175 (ppm)
29	20823.5	98094.8		22300.2	76468.6	13503.4	1198.9	9582.7	1168.6	5679.1	831.3	1617.4	149.7	638.1	58.0
30	20750.9	99820.6		22115.2	76058.9	13170.5	1181.9	9360.2	1129.4	5505.6	805.9	1594.5	145.7	616.8	57.9
31	19551.0	103306.0		21307.7	71405.3	11543.8	1289.1	8091.2	935.8	4599.1	715.7	1500.5	143.6	583.6	58.7
32	20030.2	104691.4		21407.5	72557.9	11691.8	1300.2	8127.0	953.2	4739.9	725.0	1532.2	142.1	606.6	59.9
33	20844.8	101774.0		21792.2	74418.3	12127.9	1354.8	8361.5	986.3	4860.5	763.1	1598.7	147.2	633.4	60.7
34	22129.5	100275.1		21641.9	74860.8	12617.2	1314.3	8951.0	1040.0	5169.7	805.6	1681.2	154.5	660.7	64.4
35	16536.6	102489.0		21242.0	73803.4	11421.4	1058.0	7707.6	848.7	4007.1	613.2	1261.0	112.7	469.1	44.9
36	20013.8	100149.5		21191.2	72946.6	12068.3	1243.5	8614.8	976.6	4730.2	738.7	1531.4	141.0	598.8	58.4
37	20830.9	101832.2		21737.0	74306.0	12363.1	1634.4	8718.4	1038.5	5055.1	771.0	1591.0	145.4	622.9	59.2
38	22271.6	103687.4		21725.0	75209.1	12388.2	1295.7	8779.7	1028.0	5112.3	796.4	1676.2	155.3	639.6	63.4
39	21968.5	101366.1		21873.0	75827.6	12536.9	1380.8	8833.5	1035.3	5115.7	788.7	1659.6	154.5	644.5	63.3
40	23346.7	100319.2		21650.5	74365.5	12601.2	1439.6	8901.9	1069.5	5330.7	845.1	1762.8	167.7	705.3	67.0
41	19377.3	100274.2		22054.3	76014.7	12357.6	1310.2	8680.9	1011.3	4961.4	752.6	1503.1	131.3	542.3	50.1
42	20347.8	102087.9		20872.9	70733.2	11690.0	1309.5	8175.0	944.9	4658.7	728.1	1538.2	141.8	599.2	57.6
SFDD01-12															
1	51.8	107286.8		21029.2	71099.0	7209.8	686.6	1111.7	30.3	43.7	2.4	2.5	0.1	0.1	0.0
2	368.0	105149.9		20964.7	72812.2	9446.8	795.6	3111.5	136.9	237.6	13.6	12.0	0.5	1.4	0.1
3	342.3	105979.5		21252.3	72118.5	9250.3	776.2	3012.6	127.8	225.1	12.7	11.5	0.5	1.0	0.1
4	326.1	104891.5		21101.8	73993.1	9546.9	843.9	3025.2	126.8	216.4	11.7	10.5	0.4	1.1	0.1
5	296.8	105089.6		21238.2	73456.1	9532.7	963.1	3036.7	125.0	208.1	11.3	10.0	0.5	1.1	0.1
6	327.7	107828.9		20678.6	71604.0	8781.0	485.8	2670.3	115.4	205.2	12.2	10.6	0.5	1.5	0.1
7	272.7	103873.2		20618.5	71692.2	9247.7	820.7	2934.1	117.3	184.6	9.7	8.3	0.4	0.6	0.0
8	298.3	105507.2		21414.7	72387.7	9459.9	808.8	3029.0	124.6	202.3	11.0	9.7	0.4	1.0	0.0
9	374.4	107589.6		21020.1	71100.4	8316.8	446.8	2538.3	113.3	217.2	13.2	12.8	0.6	1.6	0.1
10	397.6	106842.5		21035.4	72138.3	8618.9	631.8	2588.6	115.8	218.0	15.6	17.9	0.8	2.0	0.2

Sample	Y89 (ppm)	La139 (ppm)	Ce140 (ppm)	Pr141 (ppm)	Nd146 (ppm)	Sm147 (ppm)	Eu153 (ppm)	Gd157 (ppm)	Tb159 (ppm)	Dy163 (ppm)	Ho165 (ppm)	Er166 (ppm)	Tm169 (ppm)	Yb172 (ppm)	Lu175 (ppm)
11	425.4	104177.0		21197.0	72503.2	9231.5	656.6	2941.1	132.8	253.1	15.7	14.7	0.6	1.7	0.1
12	399.7	106951.6		20899.9	70735.4	9007.9	634.1	2963.5	134.0	247.7	14.8	13.1	0.5	1.3	0.1
13	448.8	104028.1		21350.1	73429.8	9716.9	924.9	3309.0	143.0	271.7	17.9	18.4	1.0	2.6	0.1
14	434.8	106017.6		20677.4	71879.1	9040.9	549.2	2834.5	126.4	247.5	16.2	17.3	0.9	2.3	0.1
15	374.2	106207.6		20955.3	71124.7	9476.7	826.7	3200.1	141.5	242.7	14.8	13.6	0.7	1.6	0.1
16	360.9	108166.9		21260.3	72370.2	8593.3	498.5	2651.9	115.4	212.6	13.6	14.3	0.7	2.0	0.1
17	242.1	103338.7		20826.9	71350.6	9225.3	976.0	2521.0	91.8	152.6	8.3	7.6	0.4	1.0	0.1
18	473.6	105333.7		20909.6	72106.3	9039.3	578.8	2943.8	140.3	272.5	17.3	16.9	0.8	1.8	0.1
19	472.5	107826.8		20653.0	68425.3	9533.5	877.1	3878.7	173.8	298.3	18.2	16.6	0.7	1.7	0.1
20	296.7	106551.8		20811.6	70010.3	9617.3	904.9	3184.1	130.4	211.2	11.4	10.3	0.4	0.7	0.0
21	376.3	105635.0		21218.4	71244.1	8827.4	608.1	2781.5	123.2	233.9	13.8	13.2	0.8	1.3	0.1
22	452.7	107045.2		21004.0	70461.4	8427.7	509.1	2647.7	123.4	245.5	16.8	18.5	0.9	2.2	0.2
23	420.5	106322.3		21772.0	73274.1	9265.8	603.7	2910.4	131.8	246.7	15.9	14.8	0.6	1.6	0.1
24	304.9	106421.5		21336.7	72828.6	8927.1	476.0	2761.2	114.8	197.6	11.4	9.3	0.4	0.9	0.1
25	126.4	105524.2		21021.3	72695.6	9197.4	955.2	2566.9	87.2	109.3	4.7	4.4	0.1	0.4	0.0
26	347.8	107372.9		20647.4	72065.6	8819.6	682.0	2749.2	119.3	215.1	12.7	12.2	0.5	1.3	0.0
27	2530.3	108862.8		21023.2	69776.3	9318.9	477.0	4745.7	339.1	1045.4	103.1	136.0	8.1	23.8	1.8
28	1799.6	110538.5		20114.0	66390.0	8491.0	654.5	3947.2	261.8	757.9	75.3	104.3	6.6	20.4	1.5
29	2146.8	106115.5		20898.2	70583.8	9248.7	452.3	3702.3	247.1	792.6	88.1	132.5	9.4	30.0	2.7
30	268.7	107646.4		20976.4	71311.4	8302.4	432.0	2472.4	96.3	161.3	9.9	8.8	0.5	1.1	0.1
31	772.2	104290.5		20986.9	70185.3	9826.9	983.1	4215.7	227.3	473.1	31.2	31.3	1.3	3.1	0.2
32	347.9	107020.1		21125.8	71837.5	9237.8	759.0	3013.0	133.7	236.6	13.1	11.6	0.4	1.0	0.1
33	417.5	102346.5		20956.0	73145.2	9372.0	690.1	3114.4	142.4	262.4	15.4	14.2	0.6	1.5	0.0
34	509.9	102877.9		20811.1	72183.0	9211.3	709.8	3092.1	145.7	297.3	20.3	20.1	1.0	2.8	0.2
35	882.9	104654.5		21081.7	72021.2	9574.6	852.5	3679.9	196.8	437.2	35.1	40.8	2.2	5.8	0.4

Sample	Y89 (ppm)	La139 (ppm)	Ce140 (ppm)	Pr141 (ppm)	Nd146 (ppm)	Sm147 (ppm)	Eu153 (ppm)	Gd157 (ppm)	Tb159 (ppm)	Dy163 (ppm)	Ho165 (ppm)	Er166 (ppm)	Tm169 (ppm)	Yb172 (ppm)	Lu175 (ppm)
36	286.0	106453.3		21674.0	74330.2	9282.1	723.9	2802.2	111.3	184.4	9.7	9.8	0.4	1.1	0.1
37	405.4	104067.5		21013.2	70985.1	8647.2	492.1	2697.7	118.3	232.6	14.8	14.5	0.7	1.7	0.1
38	635.4	106652.8		20874.9	71239.1	9432.6	920.5	3649.6	181.0	363.9	26.1	26.5	1.2	3.7	0.3
39	424.7	109513.1		21104.1	74262.2	9350.9	738.0	3181.0	147.2	266.6	16.0	15.0	0.8	2.6	0.1
40	523.3	104847.8		20900.9	72148.1	9589.5	789.1	3249.4	154.1	300.5	19.7	18.9	0.9	2.4	0.2
41	658.8	105367.0		21243.4	72373.3	9657.6	968.3	3890.7	197.9	390.3	26.5	26.2	1.1	3.1	0.3
42	357.2	109085.4		20889.2	69747.6	9054.0	745.3	2884.5	128.6	222.2	12.4	10.3	0.5	1.0	0.1
SFDD15-01															
1	20754.1	98101.1		22512.1	80369.0	14985.8	1321.5	10989.5	1361.7	6376.1	858.1	1626.6	142.3	594.4	52.3
2	16972.2	106331.5		21570.2	75136.7	12916.0	1231.4	9276.1	1119.9	5247.7	719.5	1326.9	115.7	463.6	42.7
3	19686.5	101787.1		22404.7	80266.8	14373.5	1344.6	10488.8	1285.8	6000.1	816.5	1537.0	132.2	533.2	48.3
4	13981.6	107196.8		21159.4	69264.6	10723.4	780.7	7134.9	783.1	3590.7	532.1	1028.1	86.0	332.4	31.0
5	14909.0	104545.4		21304.1	73653.8	11295.7	827.5	7558.8	816.2	3763.4	561.3	1093.2	93.2	360.2	33.0
6	15939.4	103856.7		21903.2	77761.9	12230.5	423.2	8507.1	896.0	4159.7	623.0	1207.8	100.3	392.1	34.9
7	10285.5	104393.3		21403.2	70113.0	10637.9	646.0	6679.9	671.6	2847.4	395.4	729.6	58.8	224.0	20.3
8	16069.8	104584.0		21251.7	73120.2	11643.9	594.0	7938.5	858.0	3990.0	611.9	1230.8	106.5	429.4	39.5
9	12937.9	106310.6		21695.0	72936.3	11337.8	761.0	7373.7	788.7	3488.4	500.4	949.7	77.7	298.2	25.7
10	14853.5	105476.7		21805.2	76460.9	12056.2	738.8	8073.7	875.9	3994.8	580.6	1107.0	91.9	354.2	30.5
11	10663.6	105223.2		21914.3	73829.2	10994.3	296.1	7204.0	710.7	3002.9	415.2	740.9	57.4	201.4	16.8
12	17214.8	105500.7		22027.6	79584.8	12804.2	744.5	8929.3	982.2	4458.2	643.5	1236.7	109.7	449.4	41.4
13	13819.8	106345.4		21874.8	77606.0	12325.0	734.2	8289.9	846.6	3778.3	530.5	990.1	83.2	321.2	30.2
14	17538.2	105377.6		22103.7	76784.8	12635.7	655.7	8970.4	958.3	4399.1	643.3	1259.9	104.8	423.9	37.6
15	9902.5	104121.5		21359.4	73175.5	10762.9	729.2	6912.9	668.5	2846.0	394.2	710.8	55.7	208.6	18.4
16	12594.4	107952.4		21395.5	74270.2	11066.6	752.0	7309.5	772.9	3404.5	487.4	925.4	75.3	287.9	25.6
17	16965.3	106633.9		22183.5	76311.8	12326.2	1015.1	8607.4	943.2	4358.6	647.1	1282.5	109.1	437.9	40.4

Sample	Y89 (ppm)	La139 (ppm)	Ce140 (ppm)	Pr141 (ppm)	Nd146 (ppm)	Sm147 (ppm)	Eu153 (ppm)	Gd157 (ppm)	Tb159 (ppm)	Dy163 (ppm)	Ho165 (ppm)	Er166 (ppm)	Tm169 (ppm)	Yb172 (ppm)	Lu175 (ppm)
18	15588.4	108277.2		21696.2	72946.4	11810.2	1382.7	8218.5	919.2	4309.1	596.7	1170.5	101.1	433.7	40.4
19	17644.1	110546.4		22428.2	75641.1	12351.4	927.6	8746.1	1000.5	4724.4	684.4	1352.9	117.1	460.2	39.9
20	17250.5	103392.9		21768.8	74781.3	12208.8	850.7	8662.1	967.6	4477.2	668.5	1315.6	108.8	419.5	38.4
21	16272.5	107577.5		21877.5	73260.9	11765.9	685.2	7861.4	878.8	4093.0	615.8	1245.2	106.9	424.3	39.2
22	12645.0	107433.7		21479.7	72303.8	11145.4	750.4	7309.9	773.5	3428.3	493.2	925.3	73.8	284.5	25.7
23	15995.3	104081.5		21366.4	74650.8	11802.0	712.3	7992.3	891.1	4130.5	621.6	1247.2	107.9	433.5	41.3
24	20319.8	102232.2		21867.7	77627.9	12843.1	1104.2	9184.2	1042.4	5019.0	770.2	1512.0	133.7	529.7	49.5
25	17585.1	102276.0		22773.8	77947.4	14095.6	1886.4	9890.5	1174.0	5429.0	722.5	1346.0	116.4	466.5	41.1
26	18947.7	102020.7		22503.0	77898.8	14091.1	1976.5	9890.1	1212.3	5598.8	768.7	1505.1	133.9	569.8	50.2
27	18253.1	100973.2		22349.0	76811.9	14502.0	1294.2	10446.7	1273.3	5815.9	768.5	1417.2	124.7	518.1	46.8
28	20617.7	101728.9		22949.6	80146.0	14724.8	1375.9	10837.2	1333.3	6221.0	841.7	1584.2	139.6	597.8	53.4
29	23780.1	103200.1		22207.9	78012.6	13190.4	578.9	9333.1	1142.1	5760.6	893.2	1842.3	167.4	679.7	63.6
30	20247.4	102049.0		22183.2	78327.0	12957.1	405.9	9064.4	1060.3	5110.2	770.7	1549.7	138.3	555.1	51.7
31	12035.6	105382.2		21230.8	73089.1	11089.8	357.7	7375.1	755.9	3297.4	471.6	868.9	67.1	246.9	22.0
32	13486.8	104505.2		21453.1	73538.1	11485.9	710.4	7469.1	798.1	3584.8	520.1	1003.1	83.2	327.8	29.8
33	17474.5	104714.0		21632.4	73724.1	11679.9	667.6	8024.7	891.6	4228.5	655.6	1351.8	121.7	485.4	45.6
34	14496.0	105753.8		21588.0	73934.9	11650.5	689.8	7740.8	818.7	3740.6	556.5	1112.0	98.9	391.7	35.5
35	12675.0	104549.1		22637.4	79671.9	13656.7	1838.5	9300.7	999.2	4194.8	539.6	983.5	87.5	363.7	31.9
36	22592.0	103261.6		21932.4	76673.8	12421.2	749.6	8672.8	1060.2	5341.2	839.1	1806.8	168.9	703.3	67.6
37	13594.4	103184.3		21775.2	75188.2	11667.7	554.1	7887.2	827.1	3691.9	533.0	999.4	83.1	314.2	27.4
38	17731.7	104563.1		21897.8	75672.7	11722.4	685.1	7881.9	907.5	4455.9	688.4	1462.0	140.3	600.3	56.3
39	10782.9	105573.3		21147.6	71484.5	10624.1	713.7	6768.8	687.6	3018.3	433.4	803.9	64.3	242.6	22.1
40	12016.7	105343.5		21838.8	72593.2	10961.9	732.1	7074.1	740.6	3311.3	481.2	909.3	74.7	277.1	25.9
41	13720.2	108657.8		21959.6	74923.0	11415.7	739.9	7503.4	802.1	3653.1	529.7	1037.1	86.0	341.9	31.4
42	21266.2	100854.6		22408.7	80678.1	14295.0	1164.6	10541.0	1300.0	6250.3	859.6	1632.8	143.9	596.0	54.2

Sample	Y89 (ppm)	La139 (ppm)	Ce140 (ppm)	Pr141 (ppm)	Nd146 (ppm)	Sm147 (ppm)	Eu153 (ppm)	Gd157 (ppm)	Tb159 (ppm)	Dy163 (ppm)	Ho165 (ppm)	Er166 (ppm)	Tm169 (ppm)	Yb172 (ppm)	Lu175 (ppm)
43	15112.3	105500.5		21697.1	73586.3	11352.2	735.1	7717.2	843.0	3989.8	586.3	1142.8	94.3	363.2	33.0
44	12912.3	105760.7		21697.4	74466.0	11135.6	788.2	7353.2	805.0	3587.0	509.1	972.0	79.6	301.6	27.6
45	17712.5	104491.1		22120.3	80131.5	13787.3	999.2	9569.9	1045.6	4751.4	680.2	1306.7	107.4	409.7	36.0
SFDD15-03															
1	8777.9	106411.4		22549.3	79366.3	11729.0	1108.8	7249.4	701.2	2812.3	356.5	639.4	46.9	163.0	13.7
2	4934.9	104481.3		21958.8	78165.0	12516.2	782.4	7809.2	674.2	2100.9	193.1	220.6	11.0	30.8	2.1
3	1132.0	103635.6		22063.0	78085.8	12012.7	989.3	5444.5	302.7	646.2	43.8	41.4	1.9	4.3	0.2
4	1382.0	102685.3		21734.4	76036.7	11999.9	948.6	5792.7	341.9	770.6	53.6	51.5	2.4	5.3	0.4
5	942.5	102803.2		22199.4	79015.7	12845.9	993.7	5581.6	290.0	569.4	36.6	32.1	1.5	3.3	0.2
6	2399.4	108964.5		20781.8	72590.1	9835.6	1040.8	5184.7	389.0	1116.6	88.6	93.0	4.5	11.2	0.5
7	4758.1	106282.6		22018.9	75200.6	10620.5	560.1	5751.1	471.0	1638.3	189.0	279.6	18.5	56.6	4.5
8	1680.1	97801.7		22660.3	78871.1	14513.8	1104.3	7220.1	437.8	928.5	60.1	60.9	3.2	6.8	0.8
9	1441.3	100344.1		22183.6	78950.5	13977.4	1042.6	6903.2	407.5	835.4	53.6	48.8	2.3	5.8	0.4
10	4381.3	105022.3		22109.5	77088.7	12032.8	1982.8	7338.0	584.0	1809.9	170.3	208.8	10.9	29.4	2.0
11	1076.2	103320.3		21845.5	77474.7	11762.8	867.2	5296.1	286.8	615.7	41.3	38.7	1.7	3.9	0.3
12	1306.0	102994.8		21985.1	76895.1	12043.7	954.7	5711.7	334.9	748.4	51.7	48.3	2.4	5.7	0.3
13	1102.2	104391.2		21909.5	74200.4	11493.7	895.1	5205.4	292.4	641.7	43.4	40.6	1.8	3.9	0.3
14	1076.9	103410.0		22180.6	77181.4	12223.6	974.9	5346.9	295.4	636.0	42.5	38.2	1.7	3.8	0.3
15	2436.7	102316.7		22014.3	77442.3	11403.3	601.8	5575.7	377.6	1054.9	101.5	131.7	7.6	22.9	1.7
16	2109.6	104829.1		22239.7	77309.0	11579.3	569.5	5581.7	359.6	973.1	89.0	108.7	6.1	17.8	1.4
17	1361.0	98272.1		22350.4	79570.7	13929.1	1129.6	7063.6	397.0	795.5	50.6	47.1	2.3	5.8	0.5
18	1447.2	97866.8		22712.6	78804.6	14461.4	1033.6	7060.8	409.9	843.7	52.0	48.5	2.4	5.8	0.4
19	1500.9	99351.1		22777.6	79216.2	14010.6	1089.7	7064.1	417.5	869.1	54.4	47.2	2.1	5.7	0.5
20	1386.5	101324.5		22247.3	77917.0	13625.6	1037.1	6775.5	395.6	822.2	51.6	46.3	2.3	5.4	0.4
21	1478.5	98748.4		22581.1	79490.3	14448.3	1115.7	7146.9	417.7	864.7	53.9	51.3	2.7	7.1	0.4

22	6854.8	105754.8	22163.4	80714.1	12305.5	1611.1	7008.5	598.1	2211.1	278.5	481.3	35.0	114.2	9.4
23	1222.6	105210.0	22443.4	79784.5	11756.1	570.2	5348.1	296.2	659.9	48.4	50.2	2.6	6.1	0.4
24	1016.6	101193.1	22323.7	79503.3	12824.6	885.3	5881.3	327.3	632.6	39.4	33.0	1.4	3.4	0.2
25	953.3	100979.0	22558.7	78492.3	12985.7	919.0	5974.6	320.7	606.9	35.1	29.0	1.4	2.4	0.2
26	641.7	99610.9	21996.2	76109.2	12087.5	865.9	5090.8	244.2	431.5	23.7	23.3	0.8	1.9	0.1
27	672.5	102224.1	21851.5	77621.5	12502.5	887.6	5308.3	253.7	443.1	25.0	21.5	1.0	2.3	0.1
28	2415.0	106219.8	22074.7	76295.0	11218.2	851.0	5779.5	394.4	1106.6	103.2	130.0	7.5	22.9	2.1
29	10232.9	103519.7	21810.8	75939.8	11179.8	725.6	6939.1	680.9	2864.1	396.4	689.3	47.2	157.1	12.7
	3511.7	107035.7	21047.9	73445.3	11018.2	779.9	6022.1	434.6	1354.4	144.4	205.6	13.8	37.2	3.6
30	1123.8	100535.9	22072.0	77669.3	13292.2	1038.3	6396.9	350.0	682.3	42.0	36.0	1.7	4.1	0.3
31	1379.5	100922.6	22556.3	79503.4	13810.9	1092.0	7024.7	399.0	816.6	52.3	48.2	2.7	6.2	0.4
32	840.0	105831.5	20754.1	70592.6	10449.7	867.4	5251.2	317.2	603.1	25.7	15.3	0.5	0.9	0.1
33	13414.6	104960.8	22406.1	77305.2	12241.1	1458.1	7804.1	780.6	3568.2	539.5	1068.7	86.2	314.6	27.7
34	4187.7	101690.5	21865.1	78772.7	12108.0	379.7	6974.1	541.5	1690.2	172.9	232.5	13.6	42.0	3.7
35	12684.4	105444.0	22198.8	78520.2	12075.9	1542.2	7046.1	684.2	3105.6	487.5	1101.9	105.1	418.9	38.0
	3704.6	104793.5	22124.1	78473.2	12415.4	512.1	6544.8	469.2	1453.1	154.9	222.8	13.4	45.6	3.3
36	2289.7	106940.0	22229.2	76764.6	11446.8	699.5	5672.9	379.7	1036.5	93.3	118.2	6.7	19.6	1.5
37	5129.5	104366.7	22143.7	81831.1	12359.8	1842.5	7041.9	568.3	1868.6	210.0	315.6	21.5	65.2	5.3
	2259.0	107055.4	21673.6	74342.3	11308.4	855.0	5577.8	374.6	1002.9	92.9	119.1	7.3	20.3	1.6
38	961.4	102418.5	21615.7	74592.2	12170.4	929.5	5561.3	306.9	613.6	36.6	28.9	1.2	2.9	0.2
39	10929.2	108605.7	21868.6	75710.0	11292.8	928.3	7487.7	759.1	3264.3	419.4	716.3	53.6	190.5	15.7
40	2306.5	104657.9	22236.6	78067.9	12020.3	626.0	5907.8	392.4	1054.3	95.3	118.1	6.3	18.0	1.4
41	1279.6	100499.2	22487.9	79673.2	13681.0	1065.3	6699.3	373.6	757.4	46.4	43.9	2.2	5.6	0.4
42	13463.8	105237.5	22493.4	79994.4	12214.1	1493.2	7478.5	761.7	3475.6	529.2	1107.9	92.5	343.4	30.9
43	1603.8	102221.4	22453.9	80077.5	12877.9	455.0	6126.9	405.0	915.1	57.6	45.1	1.7	3.9	0.3
44	1503.7	98889.0	22118.5	77834.2	13724.8	1011.8	6702.4	403.8	849.3	55.6	55.2	3.0	8.2	0.6

Sample	Y89 (ppm)	La139 (ppm)	Ce140 (ppm)	Pr141 (ppm)	Nd146 (ppm)	Sm147 (ppm)	Eu153 (ppm)	Gd157 (ppm)	Tb159 (ppm)	Dy163 (ppm)	Ho165 (ppm)	Er166 (ppm)	Tm169 (ppm)	Yb172 (ppm)	Lu175 (ppm)
45	1579.0	100180.8		22841.0	81426.8	14604.2	1085.7	7238.0	431.3	920.9	59.7	57.0	2.9	7.9	0.6
46	1407.3	99243.8		22794.9	81256.3	14175.3	1022.5	6770.0	392.8	811.5	52.0	48.9	2.1	5.8	0.4
NIST610															
1	463.8	439.7		446.8	431.2	451.6	445.7	449.3	436.1	435.3	447.6	454.6	433.6	448.2	437.9
2	461.2	441.0		447.7	430.1	456.7	447.3	447.2	435.9	437.2	449.0	454.7	434.6	450.8	439.4
3	458.3	437.2		448.7	429.4	453.1	447.0	448.2	437.5	436.5	450.5	456.4	437.5	451.5	440.1
5	464.3	441.6		449.3	427.2	452.1	448.8	451.0	438.8	440.8	450.1	455.4	435.3	450.7	440.3
7	461.2	440.0		449.6	431.9	452.4	448.2	449.3	437.9	437.3	449.6	455.0	434.7	448.7	437.8
9	462.0	440.0		448.5	430.5	452.6	445.2	448.3	435.8	437.3	447.0	453.4	434.5	450.6	437.8
11	463.6	439.7		446.4	429.6	452.3	447.3	449.6	436.6	436.4	449.9	455.5	435.2	448.8	439.3
13	463.7	441.8		447.7	427.4	453.2	447.4	449.3	439.4	438.0	450.7	455.7	436.2	451.2	439.8
15	461.7	438.0		447.2	429.3	452.9	445.8	450.6	435.0	435.2	447.5	454.5	434.6	449.3	438.5
17	462.6	441.3		449.7	430.0	451.9	448.0	451.7	438.3	437.8	450.2	455.1	434.5	449.8	438.9
19	461.1	440.0		449.0	429.5	455.1	448.7	444.7	436.4	437.4	448.8	458.0	435.9	453.6	440.0
20	461.2	439.2		446.3	433.0	453.2	445.4	449.3	436.9	436.8	448.0	452.8	433.9	447.7	438.0
XNIST															
4	447.2	435.1		442.2	416.9	454.6	437.1	423.9	422.4	426.4	432.5	433.1	414.9	428.4	420.9
6	452.7	442.6		451.5	429.9	448.3	437.5	460.0	430.3	433.7	438.5	435.6	425.3	444.1	430.1
8	452.5	427.2		441.9	418.5	441.3	437.5	441.6	424.2	422.2	435.5	447.4	419.1	431.8	422.0
10	457.8	442.5		450.6	420.1	455.6	440.4	442.0	427.4	433.0	437.6	438.4	426.9	435.5	420.3
12	459.2	444.1		445.2	434.1	438.4	433.8	447.2	426.4	425.4	436.6	443.7	418.3	432.4	423.1
14	463.8	446.1		453.9	423.0	460.7	449.8	450.8	434.6	427.3	443.8	454.5	427.5	441.2	431.1
16	450.8	434.0		443.1	432.4	452.2	433.8	440.5	419.5	419.8	436.1	442.7	422.2	429.3	422.2
18	444.3	428.2		438.8	439.1	444.6	438.7	443.5	421.1	418.6	429.3	437.5	417.1	439.7	417.9
Sample	**Y89 (ppm)**	**La139 (ppm)**	**Ce140 (ppm)**	**Pr141 (ppm)**	**Nd146 (ppm)**	**Sm147 (ppm)**	**Eu153 (ppm)**	**Gd157 (ppm)**	**Tb159 (ppm)**	**Dy163 (ppm)**	**Ho165 (ppm)**	**Er166 (ppm)**	**Tm169 (ppm)**	**Yb172 (ppm)**	**Lu175 (ppm)**

In situ monazite and standards

SFDD01-04

Sample	Y89 (ppm)	La139 (ppm)	Ce140 (ppm)	Pr141 (ppm)	Nd146 (ppm)	Sm147 (ppm)	Eu153 (ppm)	Gd157 (ppm)	Tb159 (ppm)	Dy163 (ppm)	Ho165 (ppm)	Er166 (ppm)	Tm169 (ppm)	Yb172 (ppm)	Lu175 (ppm)
1	20210.8	101541.6		22689.9	79809.0	13833.6	1587.8	9596.6	1159.1	5516.3	776.1	1530.2	136.5	581.3	51.3
2	22344.5	100176.9		22224.7	81779.9	13395.5	1522.7	9688.5	1100.8	5334.2	813.3	1669.3	150.0	636.1	60.0
3	19556.1	99611.1		22239.6	78758.5	13698.4	1674.0	9492.8	1159.3	5452.9	754.4	1444.5	129.5	544.6	48.3
4	23436.9	99894.0		22469.6	80827.3	13860.3	1443.7	10055.6	1190.8	5789.8	866.1	1781.8	159.8	686.8	60.7
5	20253.0	99501.0		22494.6	79458.0	13710.2	1460.8	9625.1	1137.3	5430.3	773.4	1523.0	137.3	585.2	53.6
6	20972.2	100328.3		22250.6	80462.8	14046.0	1817.7	10230.7	1242.8	5807.4	821.6	1551.1	137.0	581.0	50.7
7	17945.1	97663.1		22796.0	83782.0	15552.6	1831.1	11260.4	1296.2	5617.2	713.2	1262.4	106.7	427.8	36.0
8	23337.2	98981.4		22584.1	80500.0	13936.3	1423.9	10171.2	1209.3	5880.1	879.7	1768.4	164.0	688.3	65.9
9	23271.4	100173.8		22685.0	81836.0	14191.1	1417.1	10204.2	1216.0	5852.5	869.1	1762.1	163.7	692.4	63.2
10	19096.9	101453.6		23214.6	86548.4	15693.8	2774.1	11284.9	1212.7	5188.5	675.2	1241.1	102.9	408.1	35.5
11	18189.6	98838.8		23041.0	86602.9	19043.5	2957.5	13826.4	1499.0	5977.3	682.0	1148.0	94.7	390.5	32.3
12	21182.2	100895.2		22870.4	83446.1	14914.1	1858.2	10675.7	1241.1	5533.8	787.5	1551.7	135.5	564.4	51.4
13	12101.1	116952.0		21962.0	81360.8	14677.9	2009.7	10253.3	1044.7	3839.2	421.7	664.6	49.6	174.3	14.7
15	19081.9	102189.5		22068.1	78726.8	13209.3	1361.4	9217.1	1060.5	5072.8	718.3	1426.8	130.2	539.0	49.3
16	15557.2	103945.8		22181.0	79445.8	13574.6	1559.2	9292.7	1056.0	4550.0	587.3	1090.4	94.9	388.8	33.2
18	25610.6	101020.0		22242.6	80776.2	13634.4	1571.4	9943.0	1178.4	5798.7	904.0	1939.0	177.2	766.8	74.1
19	17625.5	103263.0		22186.8	79036.4	13411.5	1547.2	9526.2	1098.2	4838.1	654.9	1224.8	105.2	424.2	38.3
20	18264.8	100636.3		22592.8	78811.5	13706.8	1486.5	9456.6	1103.5	5029.2	678.2	1308.6	117.1	482.3	43.2
21	24180.4	100804.1		22220.6	79774.2	13830.3	1539.1	10086.5	1229.7	5991.5	884.0	1824.5	169.4	717.9	68.2
22	18201.4	100954.8		22457.9	79750.8	14201.9	1615.9	10143.7	1175.5	5268.9	689.3	1277.0	110.5	450.4	39.7
23	23182.4	100211.2		22235.8	80933.7	13393.2	1498.4	9635.2	1106.5	5384.8	835.9	1751.5	157.2	661.6	63.0
24	25469.7	99723.6		22692.7	81350.4	13907.8	1556.3	10196.0	1200.9	5905.1	909.7	1910.5	175.8	751.8	71.9
25	23757.6	101672.8		21868.0	77215.0	12999.8	1688.5	9407.5	1129.1	5578.0	849.5	1812.0	172.6	779.1	75.2

26	17313.2	102862.4		22088.0	78074.8	13828.9	1889.9	9718.3	1100.5	4905.4	650.5	1222.5	106.7	448.0	39.6
27	22646.9	101434.2		22530.5	80923.2	13909.7	1651.7	10053.9	1160.6	5555.8	836.8	1669.6	151.8	642.1	61.7
28	23360.1	100166.6		22459.0	81440.8	13869.7	1423.3	10193.7	1174.8	5738.8	870.7	1775.8	159.5	664.8	60.8
29	25349.9	101054.3		22446.4	80897.6	13562.9	1528.7	10014.3	1168.9	5831.0	904.7	1904.5	175.1	745.0	73.0
30	23492.1	101984.5		21941.2	78423.4	13118.5	1553.2	9296.3	1109.0	5459.3	856.1	1793.1	166.8	727.2	69.3
31	22729.6	99510.9		22053.3	78770.5	13090.1	1453.8	9298.0	1099.7	5433.2	825.2	1702.8	153.7	648.1	61.5
SFDD01-09															
2	1522.9	108040.7		21432.3	73436.5	9269.4	1037.6	4334.3	280.5	720.0	59.0	65.2	3.5	9.1	0.7
3	862.6	114199.7		21208.6	72646.0	8198.3	739.8	3333.5	192.2	442.5	32.5	34.6	1.9	5.3	0.3
4	850.0	109830.9		21026.0	72726.2	8219.2	887.7	3005.1	165.1	388.9	34.0	47.4	3.7	14.5	1.4
5	1799.6	107711.9		21196.8	72653.8	8727.4	947.0	3886.6	273.1	791.9	70.9	81.2	4.1	10.4	0.8
6	2500.5	106740.1		22032.7	76921.6	9600.0	1088.4	4631.5	342.8	1049.3	99.9	112.2	5.4	16.3	1.0
7	1524.5	101961.2		22066.2	77282.9	9709.2	1158.8	4177.2	256.4	646.1	56.9	78.0	4.6	12.9	1.1
8	2862.0	107545.2		21814.9	76307.0	10343.5	1041.1	5481.0	381.6	1137.9	110.9	146.3	8.4	24.6	1.9
9	1348.4	108960.1		21533.8	73677.9	8827.9	764.1	3513.1	214.5	560.4	53.5	80.6	5.5	17.3	1.5
10	2254.8	108285.7		20966.8	74299.8	8560.0	1247.5	3622.5	239.9	763.2	86.8	140.6	8.5	20.2	1.3
13	2124.1	113943.7		21390.3	74710.7	9263.2	764.0	4695.7	314.9	902.6	85.4	111.7	6.4	19.1	1.8
15	1947.4	106843.1		22139.4	76361.0	9407.2	889.2	4362.9	277.6	801.9	77.1	104.6	6.9	21.3	1.8
16	2523.7	107717.2		21848.1	76605.6	9498.4	800.9	4773.6	331.6	994.6	100.8	127.8	7.4	19.9	1.7
18	1728.8	111767.7		21168.1	72118.1	8890.5	828.0	4636.1	301.7	807.2	69.8	80.0	4.1	9.8	0.9
19	1468.4	112098.0		21904.3	77429.5	9468.4	985.4	4502.5	279.2	710.2	57.9	67.4	3.3	8.1	0.8
SFDD01-12															
2	2081.8	103773.4		21584.5	77133.7	11251.4	985.8	5290.4	324.0	881.7	85.4	113.6	7.1	21.3	1.6
3	2755.1	104840.3		21721.1	78044.8	10770.6	1157.2	4618.9	332.7	1076.4	119.3	190.2	14.3	53.6	4.3
4	4360.4	103576.1		22124.1	79413.5	11026.5	958.1	4925.7	381.2	1420.0	180.0	312.9	23.9	90.8	7.2
Sample	**Y89 (ppm)**	**La139 (ppm)**	**Ce140 (ppm)**	**Pr141 (ppm)**	**Nd146 (ppm)**	**Sm147 (ppm)**	**Eu153 (ppm)**	**Gd157 (ppm)**	**Tb159 (ppm)**	**Dy163 (ppm)**	**Ho165 (ppm)**	**Er166 (ppm)**	**Tm169 (ppm)**	**Yb172 (ppm)**	**Lu175 (ppm)**

5	6543.9	101777.2		22278.1	82545.7	12503.6	1575.3	6499.1	589.9	2342.7	281.9	471.4	36.9	138.7	11.9
6	8126.4	101645.3		22232.7	81057.2	13338.7	2141.2	8541.2	841.7	3185.4	356.6	565.9	42.4	155.8	11.9
7	7583.6	105243.9		21943.7	80369.9	12745.8	1822.4	7467.4	720.4	2793.5	327.0	539.8	42.5	158.9	12.8
8	13687.6	100311.9		22260.2	82830.7	13630.1	1681.8	9357.2	1036.0	4472.7	568.8	1012.4	83.6	325.7	27.9
9	7839.0	102193.2		21779.4	79689.4	11265.5	707.5	6280.4	581.6	2448.1	329.5	580.2	44.7	166.6	14.1
10	5468.4	105755.1		22206.0	79669.4	10237.2	818.1	4411.8	390.3	1626.9	217.1	396.2	32.3	129.4	10.8
11	359.3	106929.6		21154.1	73530.1	9438.1	1094.1	3071.9	133.0	229.0	13.7	12.7	0.6	1.3	0.1
12	263.1	106887.5		21332.8	74028.7	9381.9	1130.2	2849.2	109.4	176.4	9.7	9.3	0.4	0.8	0.1
13	245.6	104874.7		21218.4	73725.7	9342.3	1084.2	2786.4	106.4	167.2	9.4	8.6	0.3	0.6	0.1
14	208.4	102751.5		21642.7	77168.6	10334.7	1213.1	3077.7	112.3	168.4	8.0	6.6	0.3	0.6	0.0
15	8372.3	104014.4		21943.5	79464.6	13220.0	2048.2	8221.1	816.8	3168.4	368.8	615.1	50.0	186.4	15.4
16	204.9	103530.3		21777.7	78997.6	10437.0	1253.6	3111.0	111.3	165.6	7.7	6.7	0.3	0.4	0.1
17	1032.3	105502.2		20989.0	73878.1	9836.2	1062.8	4154.3	242.2	564.1	41.5	43.6	2.1	5.9	0.4
18	854.9	108680.2		20970.3	70031.1	8772.9	550.3	3460.7	182.4	430.3	34.4	40.8	1.8	5.5	0.4
19	981.4	110588.5		21243.5	74959.0	9076.6	520.5	3578.4	195.0	455.5	39.1	48.1	2.5	7.7	0.7
20	1394.1	104263.8		22022.9	79444.0	11115.0	1037.2	4362.2	238.1	608.8	56.2	84.3	5.7	21.0	1.6
21	908.0	107461.4		21028.3	73152.6	9006.7	503.7	3447.2	186.2	441.3	36.8	44.5	2.2	6.0	0.5
22	396.6	104033.1		22085.5	77720.3	11002.6	1156.3	4065.7	190.2	322.7	15.8	11.7	0.5	1.1	0.1
23	376.3	103423.9		21747.8	77437.3	10809.0	1147.9	3996.3	183.0	312.7	15.5	11.2	0.4	1.1	0.1
24	295.6	103338.8		21853.4	77835.0	10253.3	1077.4	3131.9	114.8	186.3	11.0	14.3	0.8	2.9	0.1
25	950.3	103050.5		21503.7	79803.8	10928.5	1117.8	4246.3	220.7	506.4	39.5	44.2	2.1	5.7	0.4
26	874.1	104376.9		21717.7	77290.2	10114.4	522.6	3716.6	187.2	450.5	37.0	42.9	2.1	5.4	0.5
27	562.4	103636.5		21748.8	78041.8	10744.0	980.3	4026.0	186.5	354.0	22.1	20.5	0.8	2.1	0.2
28	951.8	103465.7		21810.9	78916.7	10843.2	1435.3	4388.6	252.0	563.0	37.2	36.0	1.5	4.4	0.2
29	996.5	102908.7		21393.8	77469.9	10910.5	1417.3	4449.2	259.6	582.7	39.1	35.0	1.6	3.7	0.2
Sample	**Y89 (ppm)**	**La139 (ppm)**	**Ce140 (ppm)**	**Pr141 (ppm)**	**Nd146 (ppm)**	**Sm147 (ppm)**	**Eu153 (ppm)**	**Gd157 (ppm)**	**Tb159 (ppm)**	**Dy163 (ppm)**	**Ho165 (ppm)**	**Er166 (ppm)**	**Tm169 (ppm)**	**Yb172 (ppm)**	**Lu175 (ppm)**

30	367.9	103635.5		21805.2	78316.9	10513.4	1127.9	3738.3	160.2	275.9	14.6	11.3	0.5	1.3	0.1
31	242.2	103715.6		21905.3	76993.1	10330.0	1127.2	3246.0	122.8	188.6	9.8	8.6	0.4	0.8	0.0
32	361.5	102528.0		21741.7	78205.9	10303.3	1038.6	3504.3	146.0	250.0	13.8	12.2	0.5	1.1	0.1
33	672.0	103129.4		21691.0	77792.5	11386.4	1197.7	4704.5	241.5	458.8	28.0	24.8	0.9	2.4	0.2
34	8495.0	100935.6		21876.1	80159.9	12338.7	1234.7	6985.6	652.1	2630.6	333.2	580.3	45.6	169.3	14.8
35	301.4	101643.5		21296.1	76642.9	10528.9	1078.6	3583.2	148.0	237.3	11.8	9.1	0.4	1.0	0.1
36	934.2	106970.5		20806.7	70869.9	8611.9	562.6	3306.5	181.9	441.2	38.3	50.8	2.8	9.4	0.8
37	382.6	104642.7		21442.9	74798.9	9772.2	1075.3	3260.4	138.0	250.8	15.0	15.0	0.7	1.9	0.1
38	11540.6	100472.3		22191.0	81680.5	13054.4	1130.0	8149.3	821.4	3431.2	454.4	796.1	62.6	237.0	20.8
40	1558.0	107383.8		22034.5	78653.8	11668.6	1715.8	5599.7	381.4	890.0	61.8	57.9	2.6	6.5	0.4
41	8204.0	98448.1		21648.8	81263.1	13096.1	1460.5	8109.5	765.3	2972.5	350.8	557.9	41.8	153.4	12.7
42	231.9	103101.7		21809.2	77232.7	10456.2	1192.9	3204.2	124.8	189.9	9.7	7.9	0.3	0.7	0.1
43	324.5	102653.1		21596.6	75170.6	10336.4	1151.1	3262.5	132.9	228.9	12.9	10.7	0.4	1.1	0.1
44	176.8	103027.5		22217.9	80369.6	10915.5	1355.0	3128.2	105.0	145.2	6.9	5.3	0.2	0.4	0.0
46	4948.6	103822.8		21796.1	77862.1	11756.8	671.5	6080.8	477.5	1725.1	210.6	315.6	19.4	56.3	4.6
47	9254.0	102071.8		21624.3	78087.3	12503.2	770.2	7544.6	701.9	2797.2	361.1	595.3	45.2	156.7	12.9
48	579.0	99956.3		22099.7	79768.7	11170.0	1169.9	3616.1	146.7	271.9	22.3	31.7	2.0	7.3	0.6
49	353.8	101864.5		21655.2	77540.7	11101.4	1148.6	4253.8	183.6	293.3	15.0	11.0	0.4	0.8	0.1
50	619.5	108428.4		22221.9	77760.2	10949.2	1312.2	4307.1	208.8	410.5	24.8	21.7	1.1	2.6	0.2
51	307.1	104836.7		21868.8	78551.1	10802.0	1136.9	3383.1	143.7	233.4	12.3	10.2	0.4	1.3	0.1
52	1480.4	102895.4		21218.1	78335.7	10784.2	991.4	3820.1	216.4	603.4	60.7	90.8	7.2	26.1	2.1
53	6381.3	99451.0		22060.2	80413.5	13076.3	1130.2	7899.8	684.3	2377.2	261.5	395.8	31.0	110.3	8.9
54	408.9	103210.1		21654.9	77673.4	10932.8	1167.2	3909.8	173.5	293.4	16.5	14.1	0.5	1.4	0.1
55	3290.8	102975.5		21774.6	78631.5	11242.9	1368.0	4967.2	367.5	1236.3	141.9	219.9	17.4	57.2	4.9
56	885.3	106836.5		21254.8	73959.7	10012.5	1006.8	3869.4	207.3	468.9	35.6	38.2	1.9	4.4	0.3
Sample	**Y89 (ppm)**	**La139 (ppm)**	**Ce140 (ppm)**	**Pr141 (ppm)**	**Nd146 (ppm)**	**Sm147 (ppm)**	**Eu153 (ppm)**	**Gd157 (ppm)**	**Tb159 (ppm)**	**Dy163 (ppm)**	**Ho165 (ppm)**	**Er166 (ppm)**	**Tm169 (ppm)**	**Yb172 (ppm)**	**Lu175 (ppm)**

Sample	Y89 (ppm)	La139 (ppm)	Ce140 (ppm)	Pr141 (ppm)	Nd146 (ppm)	Sm147 (ppm)	Eu153 (ppm)	Gd157 (ppm)	Tb159 (ppm)	Dy163 (ppm)	Ho165 (ppm)	Er166 (ppm)	Tm169 (ppm)	Yb172 (ppm)	Lu175 (ppm)
SFDD01-17															
1	23655.1	95021.7		22907.2	83703.1	15384.5	647.5	11896.2	1500.2	7475.0	1084.1	2043.1	168.9	633.9	51.5
2	20751.8	97527.5		22736.2	81874.7	14695.8	445.5	11198.0	1404.4	6776.2	956.2	1764.3	143.7	538.1	42.2
5	17157.7	96126.9		22002.2	79842.9	13917.9	394.9	10104.5	1237.7	5866.6	801.9	1421.9	111.2	412.4	32.1
6	25504.8	98661.6		22627.3	83366.1	15019.2	441.5	11771.8	1551.6	7896.3	1172.4	2247.8	188.7	725.8	59.1
8	28242.6	95423.8		22655.0	81769.3	15191.5	881.1	11778.7	1588.3	8271.9	1247.2	2551.1	225.3	905.6	73.8
9	24149.8	97388.0		22529.1	81847.9	14975.8	980.4	11341.8	1509.8	7654.5	1107.6	2138.5	184.0	722.2	60.2
10	22710.4	98167.7		23280.2	84097.5	14879.6	704.4	11207.9	1466.7	7285.9	1036.1	1972.7	169.5	654.7	53.9
11	22885.9	95597.5		22245.4	81591.8	14482.1	413.5	11355.3	1429.6	7170.4	1049.2	1987.0	164.6	624.7	49.9
14	19220.1	96714.6		22309.5	81516.4	15137.9	359.5	11273.3	1398.1	6732.5	914.4	1589.6	121.7	414.8	30.7
15	19155.2	96189.1		22117.2	81647.6	15010.1	346.0	11308.1	1411.1	6692.8	913.1	1582.2	119.9	415.2	31.5
17	23077.6	97111.2		22346.8	81272.7	14508.9	715.5	10947.3	1412.1	7100.2	1036.9	2018.5	172.1	674.9	55.5
18	14653.6	98208.9		21694.6	77644.0	12809.0	343.4	9325.2	1101.8	5135.2	687.6	1177.2	87.7	289.3	22.0
19	18086.8	97546.6		22216.9	79420.9	14260.2	357.1	10415.2	1297.4	6130.6	828.4	1482.2	112.4	406.0	31.4
20	26312.2	96441.7		21989.1	81547.6	14650.3	846.5	11053.7	1476.5	7732.5	1177.3	2452.0	218.0	881.8	73.2
21	19959.2	96693.6		22009.7	80639.8	13953.3	519.4	10206.3	1285.1	6299.6	911.9	1769.6	151.4	593.1	48.8
24	19416.0	98673.9		21845.5	78913.7	13948.7	400.2	10279.2	1325.8	6390.8	877.5	1627.7	128.8	491.0	39.0
25	20818.6	96866.2		22233.9	80693.2	14357.5	818.6	10700.2	1365.3	6784.3	952.0	1819.8	151.2	586.1	47.5
26	19981.5	95192.5		22290.5	81079.5	14161.2	399.6	10276.3	1315.7	6368.0	900.9	1707.7	139.1	528.0	42.2
27	10504.1	96843.5		22188.3	78567.0	13514.6	358.5	8871.3	979.4	4155.4	500.5	838.2	62.0	209.6	16.0
28	11909.7	97928.0		22150.2	78371.4	13339.9	450.1	9222.6	1085.5	4754.0	579.1	908.8	62.1	202.8	14.3
NIST610															
1	463.8	441.7		448.7	429.4	451.7	447.2	448.9	437.5	437.0	449.9	455.3	435.1	451.9	439.5
2	460.9	440.0		447.9	430.8	454.1	446.9	449.9	436.3	437.2	447.8	454.6	434.9	448.8	439.1
3	461.9	438.0		448.0	430.9	453.2	447.7	447.9	437.1	438.4	450.9	455.0	436.6	450.8	439.5

4	460.8	440.3	447.4	427.7	455.2	445.9	447.8	437.2	434.8	447.7	455.0	434.5	449.9	438.7
5	462.0	440.4	446.6	429.2	452.7	446.4	448.5	437.0	437.0	448.6	453.9	435.5	449.5	438.7
6	463.9	440.8	451.3	432.1	453.8	448.7	450.7	438.7	438.4	450.4	456.2	435.3	449.3	440.2
7	459.9	438.7	446.8	428.8	449.0	445.4	449.2	435.4	435.7	447.9	453.6	432.5	445.2	436.6
8	463.4	440.2	450.2	429.6	452.8	448.3	446.4	436.5	437.0	449.3	457.1	434.9	451.8	438.7
9	462.1	438.6	447.3	429.2	455.6	448.1	447.4	437.0	436.9	448.9	455.1	436.2	449.6	439.5
10	462.3	441.9	448.4	431.7	453.0	446.8	451.3	439.3	438.5	450.3	454.8	435.9	451.7	440.2
11	461.4	440.0	446.4	430.1	451.7	446.6	449.6	436.3	436.6	448.5	455.0	434.0	450.2	438.9
12	463.1	438.0	448.7	428.8	450.1	446.8	449.6	435.9	436.9	447.0	455.1	434.0	450.0	438.1
13	459.9	439.1	446.0	430.7	451.3	445.9	447.2	435.3	436.3	447.7	454.5	434.3	447.2	438.0
14	464.1	441.8	448.4	429.4	452.9	447.6	451.6	437.7	437.0	449.0	455.3	435.6	451.3	439.3
15	465.2	441.9	450.3	432.4	458.5	449.6	451.9	440.5	440.4	451.9	456.1	438.5	456.2	441.3
16	460.0	439.7	447.8	428.1	452.9	445.2	445.2	435.1	434.5	448.4	454.3	434.1	447.6	438.7
XNIST														
1	444.8	428.7	445.5	422.2	441.4	433.2	435.3	421.7	421.0	424.7	433.4	408.0	429.6	413.1
2	453.9	438.9	441.6	430.1	447.6	438.9	437.5	423.9	426.2	431.5	438.3	414.9	432.4	419.4
3	440.2	429.6	436.5	414.1	441.8	421.9	433.2	417.1	420.7	428.4	424.2	409.6	416.7	410.2
4	451.9	430.6	446.8	424.5	440.0	444.7	432.7	420.1	419.0	429.6	428.8	416.9	428.4	421.0
5	442.7	434.2	437.1	425.5	440.1	431.8	430.8	419.3	419.2	430.3	432.5	415.5	428.7	415.3
6	448.3	432.4	444.4	417.4	453.9	438.7	427.7	425.0	422.7	433.9	445.5	421.9	425.2	421.6
7	444.3	429.7	439.1	425.6	453.4	432.9	437.9	415.3	416.9	427.5	434.7	417.5	431.2	416.6
8	442.9	430.2	436.6	414.5	440.0	430.6	424.2	416.5	421.1	420.8	434.0	414.5	425.9	407.6

APPENDIX E: WHOLE-ROCK GEOCHEMICAL DATA

Sample	Al_2O_3	Fe_2O_3	Na_2O	SiO_2	La	Ce	Pr	Nd	Sm	Eu	Gd	Tb	Dy	Ho	Er	Tm	Yb	Lu
Unit	%	%	%	%	ppm	ppm	ppm	ppm	ppm	ppm	ppm	ppm	ppm	ppm	ppm	ppm	ppm	ppm
SFD015-03A	9.6	37.5	0.12	47.9	30.8	60.8	6.85	24	4.4	0.65	4.4	0.7	5.15	1.18	3.75	0.65	4.25	0.66
SFD015-03B	9.49	45.2	0.13	42.1	36.4	69.8	8.2	31.9	5.8	0.8	5	0.7	4.55	1.02	2.85	0.4	2.6	0.38
SFD015-03B_Rpt	9.47	44.8	0.12	42.1	38.1	73.1	8.7	29.3	5.35	0.85	5.4	0.76	5	0.94	2.85	0.45	2.65	0.4
SFDD01-09	6.99	44.9	0.07	44.7	20.9	47.4	5.8	22.1	4.35	0.8	4.6	0.64	4.25	0.88	2.7	0.4	2.45	0.36
SFDD01-12	14.9	32.9	0.32	44.9	58.7	117	13.2	47	8.2	1.3	8	1.16	6.45	1.18	3.2	0.45	2.6	0.4
SFDD01-13	17.4	29.3	0.18	44.5	63.8	128	15	53.3	9.3	1.4	8.6	1.24	7.9	1.56	4.45	0.65	4.1	0.58
SFDD01-14A	2.53	58.5	0.07	37	18.4	44.4	5.1	19.8	3.95	0.6	3.8	0.44	2.3	0.46	1.35	0.2	1.15	0.16
SFDD01-17A	17.1	2.9	4.26	71.2	74.7	172	17.7	62.8	11.3	1.25	9.4	1.18	5.9	0.9	2.05	0.25	1.35	0.2
SFDD01-17 B	11.1	2.93	1.83	78.1	42	83.9	9.6	33.8	6.1	0.7	5	0.64	3.4	0.58	1.5	0.2	1.2	0.2
STD 1					14.7	44.5	5.65	23.8	5.45	1.7	6.2	0.88	5.35	1.04	2.9	0.45	2.55	0.4
STD 1	5.56	41.5	0.26	27														
STD 2					10.9	22.9	2.95	12.2	3.1	1.15	3.8	0.56	3.45	0.7	2	0.3	1.85	0.28
STD 2	10.1	16	0.07	61.4														
STD 3					19.6	45.5	5.45	20.4	4	1.1	3	0.46	2.5	0.44	1.2	0.15	1.05	0.18
STD 3	14.7	6.09	0.74	67.4														
STD 4					169	152	10.6	29.2	4.1	2.3	4	0.52	3.15	0.62	1.85	0.3	1.85	0.3
STD 4	8.84	2.35	0.34	81.9														
STD 5					34.2	66.6	7.8	29.4	5.65	1.3	5.4	0.82	4.7	0.92	2.65	0.35	2.55	0.36
STD 5	8.48	6.64	0.85	72.1														